STUDIES OF STRIATED IMPULSE CORONAS IN HELIUM/NEON GAS MIXTURES AND AIR

by

Idalino J.A. Franco

B.Sc.(Hons)CNAA M.Sc. London

A thesis submitted for the degree of Doctor of Philosophy in the University of London

London 1978

Physics Department

Bedford College

University of London

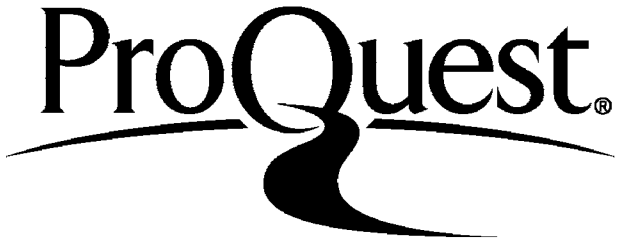

ESTA TESE É AOS MEUS PAIS DEDICADA

SEM CUJA ASSISTÊNCIA NÃO TINHA SIDO ACABADA

ABSTRACT

Some aspects of gas discharges have been studied with a streamer chamber. Specifically the origin of striations superimposed on Lichtenberg figures has been investigated.

It was observed that such effects could be seen in a columnar corona with a point-to-plane geometry.

The basic gas used was He/Ne, but some studies have also been carried out for atmospheric air. A variety of observations has been made at different voltages of both signs, pressures and gap widths.

It has been possible to gain some understanding of the mechanism of the initial creation of the striations, and some of the observations have resulted in quantitative estimates of the velocities of the advancing discharge wavefronts.

CONTENTS

CHAPTER 1

Electrical Discharges in Gases

1.1 Introduction

A great deal of theoretical and experimental work has been done on the manifold aspects of gas discharges over the past 70 years, and it is now 60 years since Sir J.S. Townsend wrote his monograph "The Theory of Ionization of Gases by Collision". In that time, the subject has been widely studied, and much progress has been made in understanding many aspects of the problem. The advances in knowledge that have been made have often come as a result of a number of good papers from various authors rather than a single outstanding piece of work. Such a form of progress is very understandable in a subject as complex and diverse as the electrical breakdown of gases, and it is often difficult, therefore, to determine which particular investigator first suggested the correct explanation for a particular phenomenon.

A quantitative theory of the initial avalanche phase at low pressures was developed by Townsend based on his earlier investigations into the phenomena accompanying the electrical breakdown of gases (Townsend 1910).

The Townsend theory accounted for most of the phenomena involved in the electrical discharge of a gas between parallel plates and it was not until 14 years later that some evidence emerged which put in doubt the breakdown mechanisms assumed by Townsend.

It was the work of Rogowski (1928) on the time lags for breakdown that struck the first blow on Townsend's theory of breakdown. The general conclusion of the work of Rogowski and others was that the Townsend theory as it was then expressed was unable to account for the short time lags observed, the rapid rate of rise of current in the discharge, or the large currents that were seen to accompany breakdown. This was particularly the case when the secondary ionization was assumed to be due to ionization of the gas by positive ions, since the time lags were orders of magnitude shorter than the time taken by positive ions to cross the discharge gap.

Raether (1937) and his co-workers using a cloud chamber as a technique for studying gas discharges attacked the problem experimentally. They observed the development in space and time of a low current pre-breakdown electron avalanche whose initial spatial growth was described by the Townsend equation $n = N\exp(\alpha x)$ into a high current spark. Investigations using impulse discharges rather than static d.c. discharges were able to clarify the difficulties previously encountered.

Raether interpreted the results of his experiments as showing that at a critical amplification the electron avalanche becomes unstable and a spark track starts developing towards the anode at a high velocity (8×10^7 cm/s) from the head of the avalanche. A little later a track started developing towards the cathode also. The high speed of the development of the tracks was attributed to the high space-charge fields at the tips of the tracks along with the production of gas-ionizing radiation. When the cathode directed track or 'kanal' reached the cathode, a narrow track bridged the two electrodes. This was faintly luminous at first, but the current increased rapidly and the light output reached that of a 'spark'.

The results of this work appeared to be difficult to explain on the basis of the ideas set out by Townsend and others, and were one reason for the attempts of Raether, Loeb, Meek (1940) and others to formulate alternative mechanisms for the development of spark breakdown. The theory was developed by Raether independently of that proposed by Meek. The two theories have much in common and have come to be known as the 'Streamer Theory' of spark breakdown. They are based on considerations of individual electron avalanches, the transition from an avalanche into a streamer and the subsequent behaviour of the streamer. The theory involved ionization by electrons and photons in the gas and space charge fields.

Meek's theory given in his paper of 1940 followed earlier papers by Loeb and Leigh (1937) and by Loeb and Kip (1939) in which a qualitative picture of breakdown involving the formation of 'streamers' was given. Loeb's earlier work was stimulated by his observations and those of Kip of the streamers produced in corona discharges. Loeb and his succession of students threw a great deal of light onto the initial mechanisms of gas breakdown which helped enormously in the understanding of several thereto unconnected phenomena. The work of Nasser (1963) on impulse coronas using the Lichtenberg figure technique allowed streamer propogation to be studied and tip velocities to be accurately measured.

In 1969 Lozanskii devised a theory of streamers based on the concept of the streamer as an expanding plasma and soon after confirmation of his prediction was published in a paper by Rudenko and Smetanin (1972, 1973).

1.2 Avalanche Formation

Early work in this field was mainly carried out at the Cavendish Laboratory, Cambridge, by J.J. Thomson (1928, 1933) and J.S. Townsend (1910,1915), who investigated how ionization in a gas develops to lead finally to the breakdown of the insulating properties of a gas. When a potential difference is established between electrodes in a gas, the gas behaves as

an insulator unless the potential exceeds a certain definite value, which is called the sparking or breakdown potential. In practice, this potential V_s is sharply defined; the gas insulates well at a potential only a few volts less than V_s. When the applied potential V is greater than V_s, even if only by a small amount, the insulator breaks down, and a large current can pass if the circuit conditions permit, i.e. if the source of potential has low impedence. The physical problem is to account for the development of the ionization in an electric field from a small number of initiatory electrons up to any specified final current, in terms of any fundamental electronic, atomic and ionic collision processes in the gas, and at electrode surfaces.

Townsend studied the variation of the current in a plane parallel gap as a function of an applied electric field.

An electron starting at the cathode at x = 0 will be accelerated towards the anode by the electric field E = V/d where V is the voltage between the two planes and d is their separation. If the electron causes ionization by colliding with the gas molecules, the total number of electrons available will increase. The newly liberated electrons will similarly gain kinetic energy from the field and are able to ionize further. The number of electrons will increase

continuously from cathode to anode; for instance, after the first ionizing collision one electron is liberated which moves with the initial electron. These two electrons collide and ionize, liberating another two electrons. The total of four electrons again ionize four atoms, yielding a new total of eight electrons. This process is called an Electron Avalanche because of the fast increase of electron number.

To determine the number of electrons in a quantitative way, one considers a slab at a distance x from the cathode and having a thickness dx. If n electrons are entering this slab, after a distance dx, dn new electrons are produced where dn must be proportional to n and to dx. The constant of proportionality is the number of ionizations per unit length, α. Hence

$$dn = \alpha n dx \qquad 1.2.1$$

If, at x = 0, n = N, the number of electrons emitted from the cathode (preferably by irradiation which can be made very uniform), one obtains

$$\ln(n/N) = \int_0^x \alpha dx \qquad 1.2.2$$

In the special case of a uniform field, α is independent of x and the right hand side of Eq. 1.2.2 is equal to

$$\alpha \int_0^x dx = \alpha x \qquad 1.2.3$$

Eq. 1.2.2 becomes

$$n = N\exp(\alpha x) \qquad 1.2.4$$

and the number of electrons, and also positive ions, increases exponentially from cathode to anode.

Multiplying both side of Eq. 1.2.4 by the electronic charge e, one obtains

$$en = eN\exp(\alpha x) \qquad 1.2.5$$

Since the drift velocity depends only on E and is therefore independent of x, i, the current measured by placing the anode at various distances from the cathode, is

$$i = I\exp(\alpha x) \qquad 1.2.6$$

Since the electron drift velocity is constant, I is a result of the primary electrons emitted from the cathode and is called the photocurrent. In some cases, especially under low pressure, the primary electrons cannot ionize in the vicinity of the cathode because of their low kinetic energy. Only when they have acquired enough kinetic energy to equal the ionization energy V_i does the above expression become valid. The distance δ from the cathode in which no ionization takes place, is given by

$$\delta = V_i/E \qquad 1.2.7$$

At high fields δ is therefore negligible, but at low fields, or low pressure, it is appreciable and must be taken into account in Eq. 1.2.6, which becomes

$$i = I\exp\alpha(x - \delta) \qquad 1.2.8$$

By measuring i and I and using either Eq. 1.2.6 or Eq. 1.2.8 one can determine α. This is usually done by changing d, the electrode separation, and measuring the current i at each d. Plotting the ratios of i to I on a logarithmic scale versus d on a linear scale should yield linear relationships, since from Eq. 1.2.6 at $d = d_1$ (cf. Fig. 1.2.1)

$$\alpha d_1 = \ln(i_1/I) \qquad 1.2.9$$

and

$$\alpha_1 = (1/d_1)\ln(i_1/I) \qquad 1.2.10$$

The photocurrent I can be determined from two readings at d_1 and d_2 , for instance, at $d = d_2$

$$\alpha_2 = (1/d_2)\ln(i_2/I) \qquad 1.2.11$$

and if the ratio E/p is maintained constant,

$$\alpha_1 = \alpha_2 \qquad 1.2.12$$

and

$$(1/d_1)(\ln i_1 - \ln I) = (1/d_2)(\ln i_2 - \ln I) \qquad 1.2.13$$

from which it follows that

$$\ln(I) = (d_2 \ln i_1 - d_1 \ln i_2)/(d_2 - d_1) \qquad 1.2.14$$

The current I is produced by the radiation incident on the cathode and is therefore termed total current. The use of thermionic sources for I is theoretically possible, but practically not recommended because of the non-uniformity of the electron density.

Evaluating the total current from Eq. 1.2.14 rather than from the point of intersection of the straight lines with the ordinate gives more accurate results that those obtained by the graphical method. In all experimental work, great care is required to keep I constant by holding the radiation intensity on the cathode constant. However, some cathodes show signs of fatigue and it is always desirable to check and evaluate I several times while taking the data.

The principle of actually measuring α is based on the above linearities and is thus exceedingly simple. It utilises Eq. 1.2.6 and sometimes Eq. 1.2.8 when a correction is needed at very low pressures. The current i is measured at constant E and constant P. Since i cannot be measured at any distance x from the cathode, the anode current is

Curve	E(KV/cm)
1	36
2	32
3	30
4	28
5	26
6	24
7	22
8	20

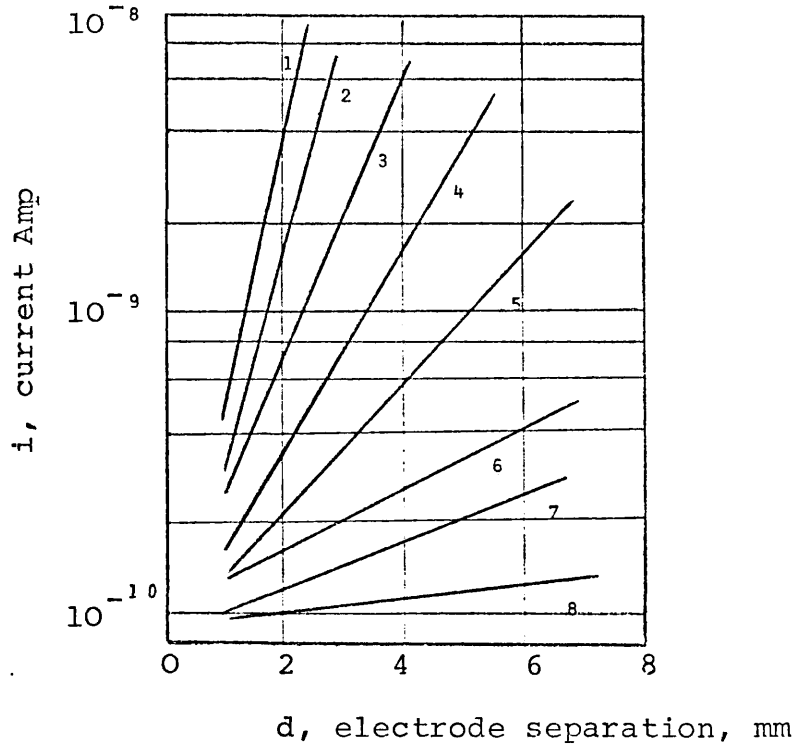

FIG. 1.2.1

The current i as a function of gap distance d at different values of E/p in contaminated air at p = 747torr(Chanin 1963).

measured and x is equal to t. By changing d while keeping E and p constant, α will not change. It is equivalent to the slope of the straight lines, obtained by plotting i/I against d on a semi-logarithmic base, as shown in Fig. 1.2.1. The abscissa represents d in centimetres, and also the applied voltage V, since V = Ed and E is kept constant for each curve.

Increasing the distance and/or voltage between the plates will lead to an overexponential rise in current that is used in measuring the second Townsend ionization coefficient.

α represents the number of new electrons and positive ions created by a single electron traversing one centimetre of path in the field direction in a gas at appropriately high E/p. It is called the first Townsend coefficient. Its reciprocal $1/\alpha$ represents the average distance required to be traversed by an electron to make a new ion pair in a field of appropriately high E/p, i.e. the ionization free path. The $\exp(\alpha x)$ electrons created by one electron in advancing x centimetres in a uniform field direction are termed an electron avalanche.

If the field E is not uniform along x, α will vary with the field E, and thus with distance x traversed along E. In this case, the avalanche must be computed from

$$\exp\left(\int_a^b \alpha dx\right) \qquad 1.2.15$$

In almost all gas discharge work, it is of vital interest to know the exact numerical values of the first Townsend coefficient. In general, since α/p is what is sought after in tables and curves of data, it is natural to express α/p against E/p to a linear scale in values of α/p. This shows the functional shape of the curve. For extended ranges, such as those observed, these plots are impractical. For use, curves of sections of α/p values against E/p in regions are best. Thus it is advisable to present the data for α/p as a $f(E/p)$ in tables, with E/p expressed in volts per centimetre per millimetre Hg pressure of gas. In plotting results for α/p as a function of E/p there is another notation which has certain useful properties, and which leads to valuable interpretations, especially in regard to breakdown. In this, α is replaced by a quantity which is α divided by E, namely

$$\eta = \alpha/E \qquad 1.2.16$$

That is, in place of setting $di = i\alpha dx$, one sets $di = i\eta dV$. Accordingly, on integration, in place of $i = I\exp(\alpha x)$ one writes

$$i = I\exp(\eta V) \qquad 1.2.17$$

This expression is extensively used by von Engel and Steenbeck (1932,1955). They use, not $\eta = \alpha/E$, but $1/\eta = E/\alpha$. This gives a chance to calculate the volts per ion pair in Townsend's ionization for comparison with that by ionization by fast electrons. Where ionizing efficiency is of importance, this is the function to use. Where number of ions is required, the α/p function of Townsend is most convenient.

Thus, $\eta V = \alpha x$, and for a plane parallel gap where the field $E = V/x$, $\eta = \alpha/E$. In order to evaluate α from η the latter is merely multiplied by the field strength E.

The quantity

$$\eta = \alpha/E = (\alpha/p)/(E/p) \qquad 1.2.18$$

represents the ions per centimetre created per unit energy available from the electric field.

The α/p-E/p curves have a characteristic "S" shape, rising from an asymptote, then passing through a point of inflexion to an apparent "saturation" value Fig. 1.2.2a). In contrast, the quantity η plotted on a log-log scale has generally a uniform shape, rising steeply at low E/p, reaching a peak and then declining.

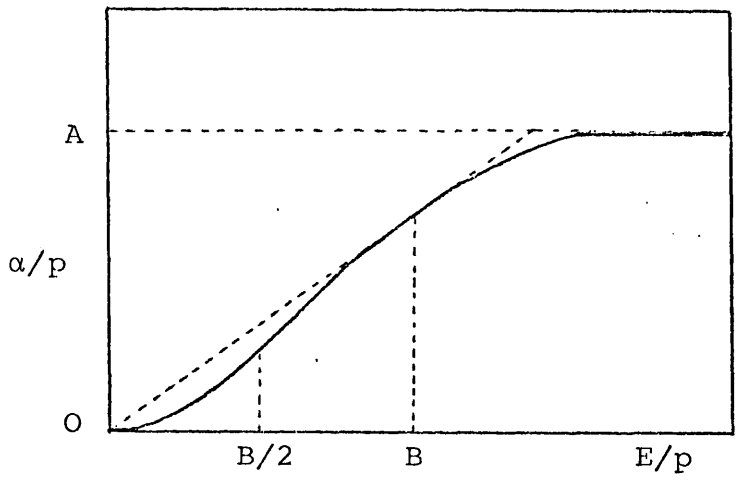

a)

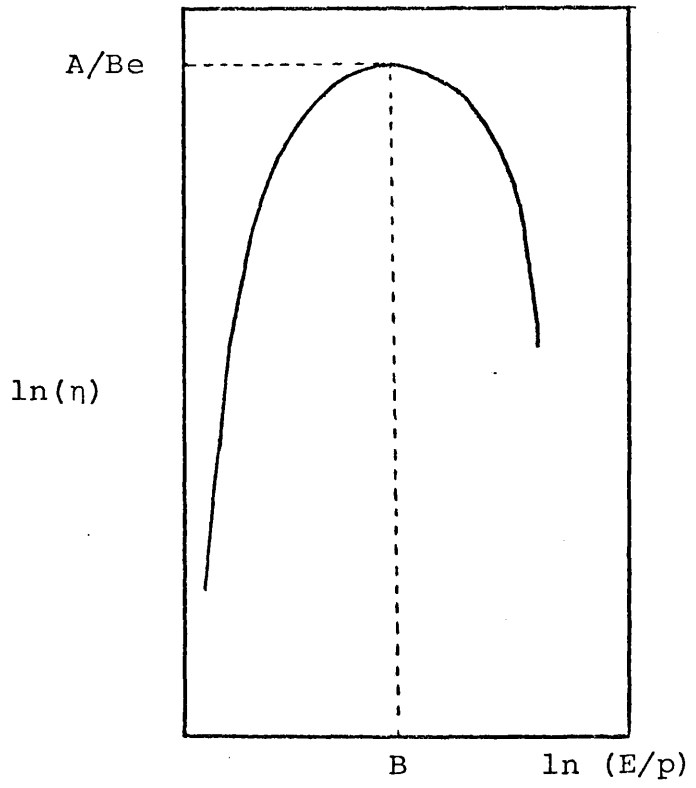

b)

FIG. 1.2.2

Characteristic curves for α/p and $\ln(\eta)$ plotted against E/p and $\ln(E/p)$ respectively.

In actuality, owing to the change of electron energy distributions with E/p, there is really no single or unique functional relation covering the whole range of the α/p-E/p curves for any gas. There does exist a semi-empirical, single functional relation which simulates observed forms. This was originally deduced by Townsend (cf. Loeb 1955, Nasser 1971) on inaccurate and primitive theory before the ionization potentials were discovered. The relation has been justified in some correct, modern approximations for limited ranges of E/p, as by von Engel and Steenbeck (1932) for high E/p, and by Druyvesteyn and Penning (1940) for inert gases at a low range of E/p. While this expression, because of its general form, can be made to approximate sections of the α/p-E/p curve by judicious choice of constants, it is not generally applicable over the whole curve for any gas. It is, however, a single, continuous function over the E/p range that has the general "S" shape and other superficial properties of the observed curve, and serves as a convenient guide in discussing the effects of the α/p-E/p curves on sparking and otherwise. The expression reads

$$\alpha/p = A\exp(-Bp/E) \qquad 1.2.19$$

This starts at zero, when E/p = 0, rises asymptotically and more slowly to a point of inflexion at B/2, and then

slowly approaches A as E/p increases indefinitely (Fig. 1.2.2a)). The expression in terms of η, is

$$\eta = \alpha/E = (Ap/E)\exp(-Bp/E) \qquad 1.2.20$$

At low E/p, η is small and increases until E/p = B, at which point η = A/Be. Thereafter, η declines with E/p. This is shown in Fig. 1.2.2b). The peak at E/p = B is flat, but rapidly decreases beyond E/p = 2B.

These properties apply to pure gases and to some mixed gases, provided that they do not include gases of low excitation or metastable potential. The α/p-E/p curve starts at an E/p value depending upon the ionization energy of the gas. As the field is increased, the electrons gain more energy and are capable of causing more ionization. Thus α/p rises quickly with E/p and then slows down. There is a connection between α and the ionization cross-sections, whose dependence upon electron energy may be used to explain qualitatively the above behaviour.

It can be shown that the probability of ionization does not increase indefinitely with electron energy, but declines after reaching a maximum. Therefore, by increasing E/p further, the increase in α/p begins to slow down. This decline is due to the fact that very high energy electrons do not use their total energy for ionization any longer. This excessive

kinetic energy is ultimately delivered to the anode when these fast electrons reach it. A rigorous theoretical derivation of α in terms of the cross-section can be obtained. (Brown 1966, Loeb 1955).

After the onset of ionization by electron collision, the current increases exponentially with electrode separation at a constant E and constant E/p following the relation 1.2.6 i.e.

$$i = I\exp(\alpha x) \qquad 1.2.6$$

The plotting of i/I on a logarithmic scale against x on a linear scale, therefore yields straight lines as shown in Fig. 1.2.1. The slopes of the straight lines are α. If x, and consequently V, are increased while E is kept constant, the current i will continue to increase, satisfying the above relation.

This current depends on the magnitude of radiation incident on the cathode which governs the values of N and I. If the radiation is cut off, N and I will be zero and so will i. For this reason this current is termed nonself-sustaining. Increasing the voltage leads to the development of an ionized channel in the form of a spark at high pressure or glow at low pressure. This transition, which is termed breakdown, is an irreversible process. It means that

lowering the voltage will not lead to the reduction of current and the redevelopment of the Townsend discharge. It will cause coronas, or partial breakdown, to develop (cf. Section 1.4).

When breakdown occurs, a current will flow whose magnitude is governed by the external circuit only; that is, this current is totally independent of any external ionization and will continue to flow if radiation is cut off. For this reason this current is known as self-sustained.

It was found, in air, that at starting values of E/p = 110V/cm-torr an over-exponential current increase, shown by an upward curvature in the curve ln(i/I) v. x, begins to appear. This curvature increases with x until breakdown occurs. The breakdown current is independent of the external ionizer and continues to flow even with the external ionization cut off. This current therefore becomes a self-sustained current.

The cause of this over-exponential increase in current can be sought in various processes which take place either within the gas or at the cathode. In the gas the positive ions can ionize further atoms by collision. At the cathode, they may, by means of their potential and kinetic energy, liberate secondary electrons. In the gas ionization by

electron collision may be enhanced by the high local fields of the ionic space charges as small increases in E result in large increases in α because of the exponential relation between α and E (cf. 1.2.19). Collisions of the second kind with excited particles or metastables can augment the ionization. Finally, the radiation from excited states, metastables, and ionized particles on recombination may either ionize further atoms of the main gas or of any admixtures present or it may augment the number of electrons emitted by incidence on the cathode.

All these processes can be classified in two main categories:

1. Gas processes in which ionization by ion collision is effective are termed β-processes, β being Townsend's second coefficient of ionization or the coefficient of ionization by ion collision.

2. Cathode processes usually referred to as secondary or γ- processes, in which electrons are liberated from the cathode by the action in the gas.

Townsend first attempted to explain the over-exponential current increase of an avalanche by considering that a secondary process due to positive ion collision was at play.

The coefficient of ionization by positive ion collisions, Townsend's second coefficient, β, is defined as the number of electrons an ion produces by collision with gas atoms per unit length in the field direction.

A general expression, which includes the β mechanism, can be derived for the number of electrons at any distance x in the uniform field gap. This is

$$n = N\{(\alpha-\beta)\exp(\alpha-\beta)d\}/\{\alpha-\beta\exp(\alpha-\beta)d\} \qquad 1.2.21$$

This equation gives the total number of electrons arriving at the anode per unit cross-sectional area per second, when both electrons and ions ionize by collision and where α and β are their coefficients of ionization respectively.

The correctness of this equation can be tested by setting $\beta = 0$ and obtaining $n = N\exp(\alpha d)$, as it should.

From Eq. 1.2.21 the current can be evaluated by multiplying both sides by the electron charge since all particles are singly ionized. Since the drift velocities are constant,

$$i/I = \{(\alpha-\beta)\exp(\alpha-\beta)d\}/\{\alpha -\beta \exp(\alpha-\beta)d\} \qquad 1.2.22$$

The current i becomes infinite when the denominator in Eq. 1.2.22 approaches zero, which is the criterion for the

occurrence of a transition to a self-sustained current. When this is reached, I or N does not affect i or n any longer. If the external ionizer is then shut off, the current and the ionization in the gas will persist indefinitely. This irreversible process is referred to as breakdown of the gas. The current which flows then depends on the outer circuit. If it is transient, at atmospheric pressure it produces a short-lived plasma channel known as a spark. If the power supply allows a steady state current to flow, its magnitude governs the amount of ionization in the gas, which is said to be in the plasma state; under near atmospheric conditions the discharge is known as an arc.

The condition for the current to be self-sustained is therefore obtained by equating the denominator of Eq. 1.2.22 to zero. Thus

$$\alpha-\beta\exp(\alpha-\beta)d = 0 \qquad 1.2.23$$

If β exists as a major process, it must be very small because ions cannot ionize as readily as electrons since they have to acquire at least double the kinetic energy with which an electron is able to ionize. Therefore, at the same field, electrons ionize by collisions per unit length in the field direction much more frequently than ions do, that is, $\alpha>>\beta$.

In both Eq. 1.2.21 and Eq. 1.2.22 the difference $\alpha-\beta$ can be replaced by α with no significant error. Thus

$$n/N = i/I = \exp(\alpha d)/\{1-(\beta/\alpha)\exp(\alpha d)\} \qquad 1.2.24$$

and the condition for breakdown becomes

$$\alpha-\beta\exp(\alpha d) = 0$$

or

$$\alpha/\beta = \exp(\alpha d) \qquad 1.2.25$$

which is Townsend breakdown criterion. As was pointed out in the Introduction, objections to the β mechanism of Townsend arose and these lead to the search for the mechanism responsible for the successor electrons and the transition to the self-sustaining currents. The objections to the β mechanism can be summarised as follows:

1. Positive ions cannot effectively ionize the gas atoms at the fields at which breakdown occurs as easily as was believed by Townsend. They not only require the theoretical amount of twice the ionization energy, but their chance of giving the major portion of this energy in one single inelastic collision is quite small. For these reasons, it was observed that ions must have at least three times the ionization energy to ionize atomic gases in a detectable manner. Much higher energies are required to

ionize molecular gases because of their large cross-section.

2. If the β mechanism were alone responsible for breakdown, the material of the cathode surface should not alter the breakdown threshold. Experimental data show that this is not at all true and that cathode material work function is significant.

3. The β mechanism of breakdown requires ion transition times much higher than those measured for the total breakdown of the gap. In other words, the current becomes self-sustained in very short time intervals, in the order of 10^{-7} or 10^{-8} seconds, during which the ions can hardly move under the dominant fields. They can be regarded as stationary during such short intervals.

All the above objections have aided in lending some weight to a quite simple alternative mechanism that would secure secondary electrons and that can account for the over-exponential carrier multiplication on the one hand, and on the other can supply sufficient electrons to make the current independent of the outer ionizer and thus self-maintained.

The alternative mechanism is based on electron liberation from the cathode by various means, such as by positive ion bombardment (Thomson 1933). This mechanism, while satisfying the first two objections to their β-process, does not satisfy the third objection, which concerns the time required for transition to a self-sustained current.

However, it was found by experiment that in a few cases the formative time of breakdown is as long as 10^{-5}seconds, thus allowing for the ion transition and electron emission (Raether 1964, Thomson 1933).

Besides emission resulting from ion bombardment, radiation is incident on the cathode from the excited states that accompany gas ionization and this radiation of some electron-volts photon energy, is capable of causing photoemission. Therefore, the number of electrons emitted is augmented over the original value produced by external ionization alone.

The third possible mechanism for the supply of secondary electrons may be found in the action of metastables and/or molecularly-excited molecules on the cathode.

All these various processes are referred to as the γ-processes and a subscript is used to specify the particular type (e.g. γ_i, γ_p and γ_m).

They all lead to a type of breakdown in which the cathode is a very active agent. The discharges that become self-sustaining by means of one or more γ-processes are described as Townsend discharges.

These discharges are associated with relatively long formative time lags due to the transit time of the ionizing agent, whether ion, photon or metastable, from the anode region where they have the highest concentrations.

It is possible to derive an expression for electron multiplication in the gas and compare it with Eq. 1.2.24. Considering firstly that positive ion impact on the cathode is the γ-process occuring (γ_i) one obtains

$$n/N = i/I = \exp(\alpha d)/\{1-\gamma_i\{\exp(\alpha d)-1\}\} \qquad 1.2.26$$

which is similar to Eq. 1.2.24.

Here, the criterion under which the current becomes infinite is readily recognised when the denominator becomes zero; that is, when

$$\gamma_i\{\exp(\alpha d)-1\}= 1 \qquad 1.2.27$$

which is again similar to the condition in Eq. 1.2.25 for self-sustained current using the β-mechanism.

For the γ_p and γ_m mechanisms one obtains in a similar fashion the equations

$$n/N = i/I = \exp(\alpha d)/\{1-\gamma_p\{\exp(\alpha d)-1\}\} \qquad 1.2.28$$

and

$$n/N = i/I = \exp(\alpha d)/\{1-\gamma_m\{\exp(\alpha d)-1\}\} \qquad 1.2.29$$

with corresponding breakdown criteria

$$\gamma_p\{\exp(\alpha d)-1\} = 1 \qquad 1.2.30$$

and

$$\gamma_m\{\exp(\alpha d)-1\} = 1 \qquad 1.2.31$$

The metastable action is extremely delayed in comparison to the action of incident photons. It is even delayed compared with the emission by positive ion impact on the cathode. The reason for this lies in the fact that whereas photons travel with the speed of light and ions with a velocity proportional to the electric field, the metastables diffuse to the cathode.

The criterion for the transition from a discharge dependent on an external ionizer to a self-maintained discharge does not have to be associated with any of the γ(cathode processes) so far considered. A second generation of electrons can be

produced in the gas without the assistance of the cathode. This is accomplished by the action of photons on the gas atoms and molecules. Impurities, metastables, molecular processes and the Penning effect play a role in producing electrons by photoionization.

An expression for the number of electrons reaching the anode can be found as follows:
If θ is the number of excited states or photons per unit length in the field direction per electron, then the ratio

$$f = \theta/\alpha \qquad 1.2.32$$

gives the proportion of excited to ionized states. If n electrons arrive at the anode, they will be composed of two constituents:

1. The electrons due to multiplication of the initially externally produced N electrons whose number at the anode becomes $N\exp(\alpha d)$.
2. p electrons due to photoionization in the gas from excited states of the same or different species.

Therefore, one obtains

$$n = N\exp(\alpha d)+p \qquad 1.2.33$$

Under the above assumption, a great proportion of all electrons and excited states are created in the anode vicinity. The number of photons to be emitted from the excited states after a lapse of their very short life time of 10^{-8} to 10^{-13} seconds, is given by $n\theta/\alpha$. Since not all the photons emitted by a slab of thickness dy and at a distance y from the anode are directed towards the cathode but at best half of them are, one must use a geometrical factor g which specifies the fraction of the photons heading for the cathode. g is obviously a function of y and of the cathode size. If the plane of the cathode is round and has a radius r, g can be estimated from the equation

$$g = 0.5\{1-y/\sqrt{(r^2+y^2)}\} \qquad 1.2.34$$

If the electrodes are in finite planes and so is the slab, then g will approach 0.5. Otherwise, g is given by the above equation.

The attenuation of the photon beam by absorption with the slab can be determined using the equation $I=I_o\exp(-\mu x)$ so that I, the number of photons at any distance y, is given by

$$I = I_o\exp(-\mu x) \qquad 1.2.35$$

where I_o is the initial beam density and μ is the absorption coefficient. I_o may be estimated from the above assumption and most electrons are produced near the anode. Hence, the number of excited states is fn and the number of photons heading towards the slab is

$$I_o = gfn \qquad 1.2.36$$

The number of photons lost by gas absorption in the slab is therefore

$$dI = \mu I_o \exp(-\mu y)\, dy \qquad 1.2.37$$

They will cause excitation and/or ionization of the absorbing molecules or atoms. They might also lead to dissociation of molecules with or without excitation of the products. In any event, only a portion of these dI photons will be able to produce photoelectrons. If the ration of ionizing photons to the total number of absorbed photons is designated by ξ the number of photoelectrons produced in the slab will be given by

$$\xi dI = \xi \mu I_o \exp(-\mu y)\, dy \qquad 1.2.38$$

$$= \xi \mu gfn \exp(-\mu y)\, dy$$

by substituting gfn for I_o. These photoelectrons will be accelerated by the electric field and will form electron avalanches exactly as the initial N electrons did.

This contribution of the total electron number p due to secondary effects in the gas is dp, and hence,

$$dp = \xi\mu gfn.\exp\{y(\alpha-\mu)\}dy \qquad 1.2.39$$

p can then be determined by integrating the above expression from y = 0 to y = d. Thus

$$p = \xi\mu gfn \int_0^d \exp\{y(\alpha-\mu)\}dy \qquad 1.2.40$$

$$= \xi gfn\{\mu/(\alpha-\mu)\}\{\exp(\alpha-\mu)d-1\}$$

By substituting Eq. 1.2.40 into Eq. 1.2.33 one obtains, for the total number of electrons reaching the anode

$$n/N = \exp(\alpha d)/\{1-\xi gf\{\mu/(\alpha-\mu)\}\{\exp(\alpha-\mu)d-1\}\} \qquad 1.2.41$$

This equation also represents the ratio i/I. It has the same form as the equations derived previously, although the secondary mechanism is entirely different.

Metastables, when available, are also active in increasing the ionizing numbers. Their effect can be thought of as a MULTIPLICATION PROCESS On the other hand, attachment may take place, diminishing the number of ionizations. This can also be considered as a factor diminishing α. Hence in all the above α is regarded as a resultant value in which these effects have been lumped together.

It is impossible to add up all the contributions of secondary electrons. The reason for lumping together all these different processes lies in the fact that in the steady state current measurements it is very difficult, if not impossible, to distinguish between the different agents. Theoretically, since the equations are almost identical in form, it is logical to sum up all the individually produced electrons into one single number. In other words, all the processes mentioned act together to produce successor electrons that keep the discharge current flowing. They can be summed up in one single coefficient γ, where

$$\gamma = \beta/\alpha+\gamma_i+\gamma_p+\gamma_m+\gamma_g+... \qquad 1.2.42$$

is frequently referred to as the <u>second Townsend coefficient of ionization</u>.

The current equation in terms of γ, becomes

$$i/I = n/N = \exp(\alpha d)/\{1-\gamma\{\exp(\alpha-\mu)d-1\}\} \qquad 1.2.43$$

and the breakdown criterion is

$$\gamma\{\exp(\alpha-\mu)d-1\} = 1 \qquad 1.2.44$$

which physically means that each one of the initial N electrons must produce a successor by one means or another. This will make the current independent of N and maintain itself.

R E S U M E

1. SINGLE AVALANCHE — EXPONENTIAL INCREASE

$$n = N\exp(\alpha d)$$

2. SECONDARY PROCESSES — OVEREXPONENTIAL INCREASE

a) Townsend's β-process

$$n = N\{(\alpha-\beta)\exp(\alpha-\beta)d\}/\{\alpha-\beta\exp(\alpha-\beta)d\}$$

b) Ion impact on cathode γ_i

$$n = N\exp(\alpha d)/\{1-\gamma_i\{\exp(\alpha d)-1\}\}$$

c) Photon impact on cathode γ_p

$$n = N\exp(\alpha d)/\{1-\gamma_p\{\exp(\alpha d)-1\}\}$$

d) Metastables' action γ_m

$$n = N\exp(\alpha d)/\{1-\gamma_m\{\exp(\alpha d)-1\}\}$$

e) Gas ionizing photons γ_g

$$n = N\exp(\alpha d)/\{1-\gamma_g\{\exp(\alpha d)-1\}\}$$

$$\alpha/p = A\exp(-Bp/E)$$

$$\eta = \alpha/E = (Ap/E)\exp(-Bp/E)$$

1.3 Streamer Formation

1.3.1 The Limitations of the Townsend Mechanism

Because of invalidity of some of the assumptions made in deriving the theoretical expressions, and in view of modern advances in atomic physics in general and observations of the breakdown process in particular, the Townsend mechanism is unable to explain many results.

The most conflicting result is the time required for the formation of a channel of a self-maintaining discharge. The period of time required for this irreversible transition is usually referred to as the formative time lag of breakdown. The order of magnitude of time observed depends on the time of secondary emission active in supplying the successor electrons. It also depends on the number of generations of avalanches necessary to produce breakdown.

The longest formative times are obtained when emission by positive ion impact on the cathode, γ_i, is the most active secondary mechanism. Conversely, ionization by positive ion collision with the gas molecules should be much slower than by any action involving radiation. Hence, short formative times are expected when such secondary mechanisms as photoionization and photoemission are the most predominant processes.

Experimental measurements of the formative times were only possible when the cathode ray oscilloscope became available in the 1920's. Using voltage pulses, it was observed that the formative times are much shorter than the Townsend mechanism with any secondary action can predict. By applying voltages well above the breakdown threshold, extremely short formative time lags in the order of 10^{-8}sec were recorded. Even the electrons are not capable of moving a long distance, and, if the distance between electrodes is of the order of 1cm, they may not be even capable of travelling all that distance at atmospheric pressure.

Another weakness of the Townsend mechanism lies in its failure to consider the effect of the space charge left over behind earlier electron avalanche generations. In many instances, the concentration of positive ions can reach very appreciable values that distort the initial field to a great extent. This might lead to local augmentation of electron energies and ionization, with a resultant α above that resulting from the static field alone.

The same consideration applies to the case of the propagating avalanche in which its own space charge was totally neglected.

One more difficulty in justifying the correctness of the Townsend mechanism lies in the interpretation of the mechanism of spark formation at high values of pd. Here

in many instances the spark channel was found to be both branched and zig-zagged. The Townsend mechanism with all its versions cannot supply an explanation for such behaviour.

The same difficulty exists in the case of the nonuniform field, especially at high values of pd. In addition to the fact that the spark channel is by no means straight, the cathode material seems to have little or no influence on the breakdown values. This again throws doubt on any mechanism involving cathode participation. The same observations hold for the case of extremely large values of pd, such as in the natural breakdown between clouds and ground, known as lightning.

All this makes it very difficult to reconcile much of the experimental observations with the theory of breakdown based on the Townsend mechanism, although this mechanism supplied excellent interpretation of various observed phenomena. Thus, other proposed breakdown mechanisms do not in any way seek to replace the Townsend mechanism completely; they rather supplement it in the various instances where it does not apply.

All the above factors combined present a major conflict in the understanding of the phenomena involved. However, the Townsend mechanism does occur but not under all conditions. Limits are thus imposed upon its validity but these are not clearly defined at present.

Other mechanisms occur in the breakdown process when the Townsend breakdown mechanism cannot materialise. A great deal of work has been devoted to detect and explain the complicated and various phenomena involved, but they are still far from being fully understood.

1.3.2. The Space Charge Field of an Avalanche

The early investigations of spark formation in the uniform field, primarily using the cloud chamber as a detecting tool, have revealed that besides the occurrence of avalanches, another distinct form of ionization also develops.

In non-uniform fields, in which breakdown can be locally contained and therefore more conveniently observed, the formation of channels of ionization distinctly different from the electron avalanches predicted by the Townsend mechanism has indicated that another process must be taking place.

All these manifestations have similar attributes. The ionization channels are filamentary and branched, sometimes heavily. They can be started at relatively low voltages at asymmetrical anodes and are capable of reaching long distances. This phenomenon is known as a 'streamer', because of its filamentary nature. If breakdown occurs by transition from a streamer to a spark, the mechanism involved is some-

times referred to as the streamer-breakdown mechanism. Streamer processes develop in very short time intervals of the order of 10^{-8} seconds. While this supplies an explanation for the short time lags of breakdown, it makes the experimental study of these occurrences highly difficult.

The avalanche constitutes the "embryo" of most ionizing processes, including the streamer phenomena. The Townsend mechanism disregards the effect of the space charge on building up locally high fields that can distort the applied static field. To calculate an expression for the distorted field in terms of known quantities, various simplifying assumptions must be made.

Meek (1953) assumed that the electrons of an avalanche are contained in a spherical volume of radius r at the head of the avalanche. The number of electrons is $\exp(\alpha x)$ where x is the avalanche length in the uniform field E. At the surface of the sphere containing the electrons, the space charge field is

$$E_r = e.\exp(\alpha x)/4\pi\varepsilon_0 r^2 \qquad 1.3.2.1$$

where e is the electron charge. The radius r is given by the diffusion expression $r = \sqrt{4Dt}$, modified to give the average

displacement from the centre (Nasser 1971, p.254)

$$r \doteq \sqrt{(3Dt)} \qquad 1.3.2.2$$

where D is the diffusion coefficient for electrons and t the transit time of the electrons from x = 0 to x. Thus t can be evaluated from

$$t = x/v_d = x/k_e E \qquad 1.3.2.3$$

x being the avalanche length, v_d and k_e the drift velocity and mobility of electrons respectively. Inserting Eq. 1.3.2.3 into 1.3.2.2 one obtains

$$r = (3Dx/v_d)^{\frac{1}{2}} = (3Dx/k_e E)^{\frac{1}{2}} \qquad 1.3.2.4$$

Inserting Eq. 1.3.2.4 into Eq. 1.3.2.1

$$E_r = \{e.\exp(\alpha x)/4\pi\varepsilon_0(3Dx/k_e E)\} \qquad 1.3.2.5$$

The ratio D/k_e of the diffusion coefficient to mobility depends solely on the temperature and is given by the Einstein relation

$$D/k_e = \kappa T/e \qquad 1.3.2.6$$

K = BOLTZMANN'S CONSTANT

Since

$$eV = 3/2(\kappa Te) \qquad 1.3.2.7$$

one has

$$D = 2/3(Vk_e) \qquad 1.3.2.8$$

Inserting this value of D and that of t from Eq. 1.3.2.3 in Eq. 1.3.2.2, one obtains

$$r = (2Vx/E)^{\frac{1}{2}} \qquad 1.3.2.9$$

which when substituted in Eq. 1.3.2.1 yields

$$E_r = \{e.\exp(\alpha x)/4\pi\varepsilon_0(2Vx)\}E \qquad 1.3.2.10$$

The coefficient of E on the right hand side of the above equation denotes the ratio between the space charge field of the electrons and the applied field. When it approaches 0.1 field distortion starts to become appreciable and when it is near unity field distortion is very significant.

Let x_c designate the distance x at which E_r becomes comparable with E. To find x_c Eq. 1.3.2.8 can be rearranged to give

$$\exp(\alpha x_c) = (E_r/E).(4\pi\varepsilon_0/e).(2Vx_c) \qquad 1.3.2.11$$

In this expression, the only unknown quantity is V, the electron energy involved. V can be evaluated from experimental results of electron drift velocity. This uses the relation (Langevin equation)

$$k_e = 0.815(e\bar{\lambda}/m\bar{v})\{(m + M)/m\}^{\frac{1}{2}} \qquad 1.3.2.12$$

where m and M are the masses of the electron and gas molecules respectively. Since $m << M$ this becomes

$$k_e = 0.815(e\bar{\lambda}/m\bar{v}) = 0.89(e\bar{\lambda}/mv_d) \qquad 1.3.2.13$$

Also, since

$$eV = \tfrac{1}{2}mv_d$$

$$V = \tfrac{1}{2}\{0.89(E\bar{\lambda}/v_d)\}^2.(e/m) \qquad 1.3.2.14$$

E and $\bar{\lambda}$ are known from the experimental conditions and v_d is obtained as an experimental result. Evaluation of V from Eq. 1.3.2.14 yielded values between 1 and 6 volts for many gases. Hydrogen had relatively high electron energies of about 22 volts (Meek 1953, Raether 1964).

It is also possible to evaluate V from the cloud chamber tracks of the avalanches. Rearranging Eq. 1.3.2.9 and giving V the subscript r to differentiate it from V obtained by Eq. 1.3.2.14

$$V_r = \tfrac{1}{2}r^2E/x \qquad 1.3.2.15$$

Eq. 1.3.2.14 gives values of V that are much higher than those from Eq. 1.3.2.15. The divergence between V and V_r

may be attributed to the inexactness of Eq. 1.3.2.2 for the tip radius of the avalanche. In addition, one should question the applicability of Einstein's equation for electrons undergoing inelastic collisions since this equation was derived for ions under E/p values below the excitation threshold. Both equations were combined to determine r and assigned values to V.

Another approach to the calculation of the space charge field of the avalanche lies in determining the electron density, n', in the avalanche tip which will also be assumed to be spherical. Hence, the field at the surface of the sphere containing the electrons and having a radius r is

$$R_r = (en'/4\pi\varepsilon_0 r^2).(4/3.\pi r^3) = en'r/3\varepsilon_0 \qquad 1.3.2.16$$

n' is the number of electrons produced in a slab of thickness dx and cross-sectional area πr^2. Using $i = I\exp(\alpha x)$

$$n' = 1/\pi r^2.dn/dx = N\alpha\exp(\alpha x)/\pi r^2 \qquad 1.3.2.17$$

where N = 1 because only one electron creates the avalanche being considered. Hence

$$n' = \alpha\exp(\alpha x)/\pi r^2 \qquad 1.3.2.18$$

which, substituted in Eq. 1.3.2.16 gives

$$E_r = e.\alpha\exp(\alpha x)/3\pi\varepsilon_0 r \qquad 1.3.2.19$$

Comparing Eq. 1.3.2.19 and Eq. 1.3.2.1 it can be seen that both equations are similar but not identical.

To find another more satisfactory expression in which not all the electrons of the avalanche are considered to be in the tip but only those that have just been created, Eq. 1.3.2.18 can be followed. Let the ratio between $\bar{v}$, the average random velocity of electrons and v_d, their drift velocity in the field direction, be designated as s. Hence

$$s = \bar{v}/v_d = \bar{\lambda}/\lambda_E \qquad 1.3.2.20$$

where $\bar{\lambda}$ and λ_E are the mean free path and its component along the field direction respectively.

Since there is a state of energy equilibrium as the electrons move with a constant drift velocity, one may then say that under such conditions the energy gained by the electron from the field per unit length must be equal to the energy it loses by collisions with the gas molecules. The energy gained is $e\int Edx$ and for uniform fields it is eEx.

The energy loss per centimetre may be estimated from the average relative energy lost per collision, g, the electron mean energy and the number of collisions per centimetre advance in the field direction. Equating the energy gained and lost per centimetre

$$eE = (g/\lambda_E)(\tfrac{1}{2}mv^2) \qquad 1.3.2.21$$

and from Eq. 1.3.2.20

$$eE = (gs/\bar{\lambda})(\tfrac{1}{2}mv^2) \qquad 1.3.2.22$$

or

$$eE\bar{\lambda} = (g\bar{v}/v_d)(\tfrac{1}{2}mv^2) \qquad 1.3.2.23$$

From Eq. 1.3.2.12

$$\bar{\lambda} = (1/0.815)(m\bar{v}k_e/e) \qquad 1.3.2.24$$

and

$$eE\bar{\lambda} = (1/0.815)m\bar{v}k_eE = 1.225m\bar{v}v_d \qquad 1.3.2.25$$

From Eqs. 1.3.2.23 and 1.3.2.25

$$(v/v_d)^2 = 2.45/g \qquad 1.3.2.26$$

v is the effective or rms value of the random velocity. If one assumes a Maxwellian velocity distribution, the mean velocity $\bar{v}$ is related to v by $\bar{v} = (8/3\pi)^{\frac{1}{2}}v$ so that

$$\bar{v}/v_d = (1.44/g)^{\frac{1}{2}} = s \qquad 1.3.2.27$$

This equation relates the average relative energy loss per collision to the ratio of mean random velocity to the drift velocity.

From Eq. 1.3.2.23 one obtains using λ_o(at p = 1torr) = $\bar{\lambda}p$

$$(\tfrac{1}{2}mv^2)/eE = (\bar{\lambda}/g)(\sqrt{g}/1.44) = \lambda_0/(1.44p\sqrt{g}) \qquad 1.3.2.28$$

This can now be inserted in Eq. 1.3.2.9 giving

$$r = \{2x\lambda_0/(1.44p\sqrt{g})\}^{\frac{1}{2}} \qquad 1.3.2.29$$

And finally, E_r can be obtained by substituting the above for r in Eq. 1.3.2.19 to yield

$$E_r = \{e/\{3\pi\varepsilon_0(1.39\lambda_0/g)^{\frac{1}{2}}\}\}(p/x)^{\frac{1}{2}}.\alpha\exp(\alpha x) \qquad 1.3.2.30$$

This equation gives the space charge field as does Eq. 1.3.2.10. There are some differences between the two equations that are quite evident by comparison. Most significant is the fact that Eq. 1.3.2.30 does not include E explicitly but

its presence is reflected in α which is a function of E/p.

Using the empirical value of 0.03 for g in Eq. 1.3.2.30 and substituting the values of the physical constants, the expression becomes

$$E_r = 5.27X10^{-7}(p/x)^{\frac{1}{2}}\alpha\exp(\alpha x) \qquad 1.3.2.31$$

E_r becomes appreciable in distorting the original field E if its ratio to E, designated as K, becomes significant. Thus, with

$$E_r = KE \qquad 1.3.2.32$$

and since E is known for a particular case and K may be assumed to lie between 0.1 and 1.0, one can solve the equation

$$KE = 5.27X10^{-27}(p/x)^{\frac{1}{2}}\alpha\exp(\alpha x) \qquad 1.3.2.33$$

to find x_c, with the subscript c denoting that x is sufficient to cause E_r to be comparable with E.

1.3.3 Critical Avalanche Size

By taking logarithms of both sides of Eq. 1.3.2.11 it can be written in the form

$$\alpha x_c = \ln(8\pi\varepsilon_0 V/e) + \ln x_c + \ln(E_r/E) \qquad 1.3.3.1$$

V as defined in p.37.

Obtaining the numerical value of the first term for air with V = 1.5 volts (Raether 1964), and putting $K = E_r/E$ this expression can be simplified to give

$$\alpha x_c = 17.7 + \ln x_c + \ln K \qquad 1.3.3.2$$

The value of K required for an avalanche to streamer transition is not readily known. K should lie between 0.1 and 1. It is found, however, that the value of K does not influence x_c to a great extent and may be assumed equal to unity. This makes Eq. 1.3.3.2 even simpler, giving

$$\alpha x_c = 17.7 + \ln x_c \qquad 1.3.3.3$$

This is Raether's breakdown criterion. The numerical value on the right hand side will vary slightly with different gases.

Although x_c gives the distance at which an avalanche becomes 'critical', and thus has nothing to do with the breakdown of the gas, in the uniform field the occurrence of a critical avalanche leads to the formation of a streamer which usually, but not necessarily, develops into a spark. If one assumes

that this is always the case, we can substitute d for x_c to obtain

$$(\alpha/p)pd = 17.7 + \ln d \qquad 1.3.3.4$$

Since $\alpha/p = f(E/p) = f(V_b/pd)$ one can obtain the breakdown voltage from

$$f(V_b/pd).pd = 17.7 + \ln d \qquad 1.3.3.5$$

once the function f(E/p) is known.

Another criterion can also be formulated if one uses Eq. 1.3.2.31 derived under the assumption that not all the electrons of the avalanche are contained in the spherical tip of the avalanche. Rearranging Eq. 1.3.2.31 and taking logarithms of both sides with $E_r = KV_b/d$ one obtains

$$\alpha x + \ln(\alpha/p) = 14.46 + \ln(KV_b/pd) - 0.5\ln(px) + \ln x \qquad 1.3.3.6$$

This is Meek's breakdown criterion.

1.3.4 Streamer Growth

If in a parallel-plane geometry an electron starts at the cathode and builds up an electron avalanche whose space

charge becomes 'critical' at x = d, that is, close to the anode, an accumulation of positive ions will be left over after the electrons have been absorbed by the anodes.

During the build-up of this primary avalanche, excitation of gas atoms has been taking place at the same time ionizations have been occurring. Excited states have lifetimes that can be as short as 10^{-13} seconds. Thus before the primary avalanche has reached its full size, photons will be emitted from these excited states as they return to the ground state.

These photons will be heading in all directions and will be absorbed at various distances from their origin, depending on the absorption coefficient, μ, of the gas. Many processes can take place when a photon is absorbed and many processes combined may lead to photoionization. New photoelectrons are now available in the gas at various distances from the avalanche that is still advancing towards the anode. If it reaches a critical size there, this means space charge fields will be created that are of the same order of magnitude as the original field. Since α changes fast with small variations of E, such field enhancement can effectively increase the ionization yields of the second generation auxilliary avalanches that may now be started by some of the suitably located photoelectrons.

Similarly, all auxiliary avalanches will emit photons as they are being formed. These photons create new photo-electrons that are ready, together with the older photo-electrons, to give rise to a new third generation auxiliary avalanches. Since the space charge field distorts the original field appreciably, the electrons do not follow the original lines any longer. Besides, many avalanches may be created almost simultaneously. This is the cause of the observed branching, though the original field always acts as a guide line for the main trunk.

The existence of a uniform field enhances the probability of formation of a completed streamer channel. This is due to the fact that ionization by electron collision is a statistically varying quantity that is highly dependent on the electron energy and hence on the field. Since E is high enough everywhere, the probability that an electron forms an avalanche is quite high. This will ensure that adequate avalanches feed into the streamer tip and keep it advancing. The situation is different in the non-uniform field.

This phenomenon was called streamer because of its filamentary character. Since it propagates under the constant emission of photons surrounding the advancing streamer, this propa-gation develops in very short time intervals. In the uniform

field, when a continuous streamer exists between the two electrodes, a sudden increase in intensity of ionization in the channel develops and breakdown of the voltage between the electrodes is known to have taken place.

For this reason Raether's and Meek's breakdown criteria were based in the triggering capability of one avalanche as soon as it had reached a size that produces fields of the same order of magnitude as the applied field.

This description of a streamer is greatly simplified. The processes actually occurring are more complicated owing to the various activities that may take place either simultaneously or at overlapping periods of time.

1.3.5 Theoretical Formulation of Streamer Development

In the discussion of both Raether's and Meek's breakdown criteria, it is assumed that the breakdown occurs as soon as the field of the avalanche space charge attains the order of magnitude of the applied field. This assumption is not very satisfactory because it is not based on the actual physical processes that develop. A mathematical expression can be derived based on the actual physical picture outlined in the previous section. This must be general enough to establish that self-sustenance can be achieved if every

electron, on the average, simply produces a successor electron by some way or another. This expression should encompass the Raether-Meek criteria as a special case where the avalanche-streamer coincides with the breakdown threshold.

The derivation is long and tedious, but the main result can be quoted without any significant loss of its understanding. This is

$$1/3(pfr^3\mu/\sqrt{d})\int_r^d \alpha(y)y^{-3/2}\exp(-\mu y).\exp(\int_r^y \alpha dy)dy = 1 \qquad 1.3.5.1$$

p = fraction of photons producing photoionization.

f = θ/α = number of excitations per ionizing collision.

r = avalanche tip radius.

μ = coefficient of absorption.

d = electrode separation.

This equation has the proper form of the type

$$\gamma\exp(\int\alpha dx) = 1$$

but is definitely much more complicated. It contains all the important physical factors that are thought to govern streamer formation and propagation. The solution of the equation in a general form seems to be a formidable if not an impossible and hopeless task. This is complicated by

the fact that many of the factors and 'constants' are in effect dependent on the gaseous pressure and/or gas type.

No serious attempt has been undertaken until now to solve this equation and establish a breakdown criterion that would depend on the gas constants included in the equation.

1.3.6 Breakdown Mechanisms

At present only two different mechanisms of breakdown are known to occur in any gas, vapour or mixtures thereof. The Townsend mechanism and the streamer mechanism.

The streamer mechanism of breakdown develops much faster than the Townsend type of breakdown. Streamers can grow out of a single avalanche and proceed at very high velocities to the electrodes, making the formative time lag less than the electron crossing time.

In a Townsend type of breakdown, on the other hand, a few hundred generations must occur in order for adequate space charge to accumulate and cause the fast current rise. In the generation build-up, the cathode plays a crucial role by supplying the secondary electrons.

This is not the case when a streamer develops with the

action of purely gaseous processes, that is, without the participation of the cathode. This fact has great significance not only in analysing breakdown in uniform fields, but also in understanding the spatially confined breakdown in non-uniform fields where cathodes are either too remote or almost nonexistent.

1.3.7 The Lozanskii's Model

A calculation of streamer development was proposed by Lozanskii and Firsov (1969) based on the model of a streamer as an expanding conducting plasma.

Two growth mechanisms are postulated: the expansion towards the anode is due to the existence of a very high field with the leading electrons ionizing the gas; in the cathode direction photoionization liberates electrons in a high field and these multiply and develop into a plasma. The main conclusions are that the streamer propagating velocity is approximately proportional to its length and the streamer thickness is proportional to the square root of the length.

Assuming that the equipotential plasma takes the form of an ellipsoid of revolution that is elongated along the field E_0, then E_a the field intensity at the ends of this region is given by

$$E_a = E_0 a\{R\ln(2/e\sqrt{(a/R)})\}^{-1} \quad . \qquad 1.3.7.1$$

where a is half the streamer length and R is the radius of curvature of its ends (Fig. 1.3.7.1).

If the streamer were to have the form of two spheres with radius R connected by a thin filament of length 2a(a>>R) then

$$E_a = E_0 a/r \qquad 1.3.7.2$$

If the streamer is indeed elliptical then the field intensity on its surface and the velocity of the points of this surface are proportional to the cosine of the angle between the normal to the surface and the direction of the field E_0.

For a>>R, the rate of growth of the streamer is

$$|\dot{a}| = kE_0 a\{R\ln(2/e\sqrt{(a/R)})\}^{-1} \qquad 1.3.7.3$$

where k is the mobility; i.e. it is approximately proportional to its length.

The dependence of its length on the time is given by

$$a \simeq \exp(kE_0 t/R + C)^{\frac{1}{2}} \qquad 1.3.7.4$$

where C is a constant that depends on the initial conditions.

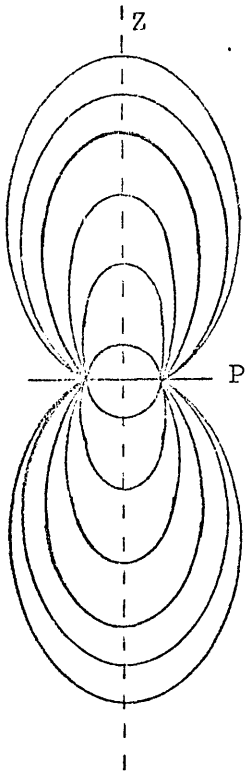

FIG. 1.3.7.1

Streamer geometry assumed in the Lozanski's model (1969).

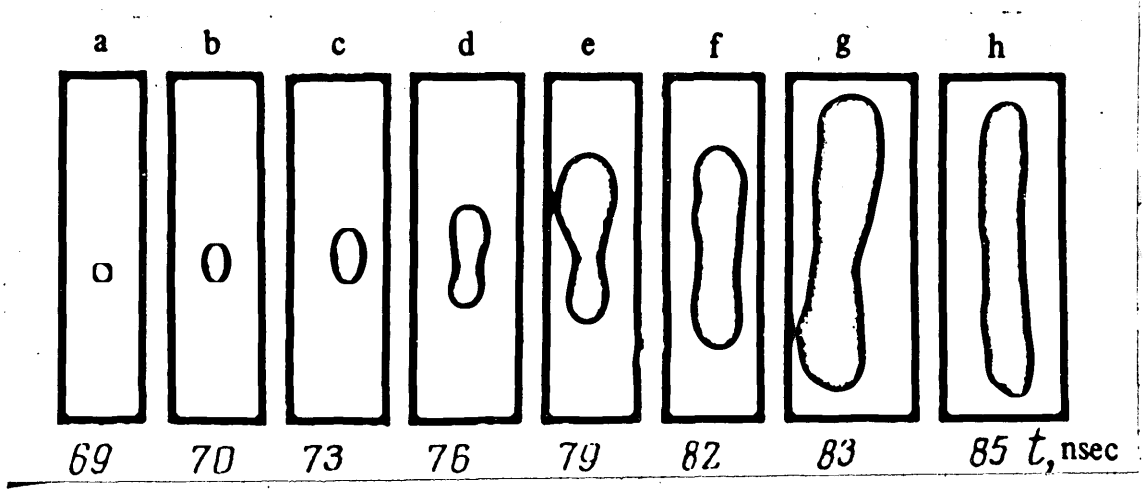

FIG. 1.3.7.2

Successive stages in the development of a streamer

E_o = 6.6KV/cm. Rudenko (1972)

The thickness of the streamer increases in proportion to the square root of its length and consequently it can reach large values. However, the eye of a photographic camera with a film of insufficient sensitivity will detect the total luminosity at the maximum with a thickness ~R, and the total thickness of the streamer ρ_{max} will be recorded only if the photographic film is sufficiently sensitive.

$$\rho_{max}\ 0.83\sqrt{(aR)} \qquad 1.3.7.5$$

Lozanskii and Firsov note that if the speed of the positive and negative tips of the streamers are not equal, then the neck of the streamer becomes smeared out and disappears completely.

Allowing for the finite conductivity of the streamer, if the field intensity within the streamer is E', then the field intensity on its end will be

$$Ea = (E_0 - \bar{E}')a/R.\ln\{2/e\sqrt{(a/R)}\} + E' \qquad 1.3.7.6$$

where it is assumed $E' \ll E_0$ and where $\bar{E}'$ is the average value of E'. The surface charge is given by

$$\sigma = (E - E')/4\pi \qquad 1.3.7.7.$$

Lozanskii and Firsov also calculated the fraction θ of the total energy released in a streamer $\theta E^2/8\pi$ and show that when the streamer propagates, the energy released in unit volume for ionization, excitation, etc., is $E^2/8\pi$.

Assume that the fraction due to ionization is $\theta E^2/8\pi$. The value of θ is known if the Townsend ionization coefficient α is known. In the absence of space charge, the fraction of energy going to ionization is $\alpha U_i/E$ where U_i is the ionization potential. In the presence of a streamer, the electrons move in a different field and θ is determined by

$$\theta = (8\pi U_i/E^3 k)\int_0^E \{\alpha(E)kE/4\pi\}dE = 2U_i\alpha(E)/(B + 2E) \qquad 1.3.7.8$$

B is found from $\alpha = A\exp(-B/E)$. For air at atmospheric pressure $B \simeq 200$KV/cm. Using this, $\theta \simeq 0.1$ and changes strongly with changing E.

Since $\theta E^2/8\pi = nU_i e$ (where n and e are the electron concentration and charge), the field within the streamer is given by

$$E' = 2U_i/\theta a \qquad 1.3.7.9$$

For air when a = 0.1 cm, E' = 3KV/cm which is about 10% of the breakdown field intensity. Thus the larger a, the better

the condition $E' << E_0$ is satisfied at the end of the streamer. However, the current density increases in proportion to a, but at each point on the streamer λ remains constant in the first approximation where λ = enk is the conductivity.

This leads to a field intensity comparable with the applied field and to development of ionization inside the streamer. At a larger streamer length when n reaches a value of the order 1% of the gas concentration, Spitzer conductivity, which does not depend on the further increase in n, sets in. If the streamer were to remain stable, then the Spitzer conductivity in air would set in at a = 10cm.

If the streamer became unstable at a<10cm, then such a conductivity would occur earlier. The presence of finite conductivity apparently is the main cause of the temporal instability of the streamer. The growth of a thinner streamer from the head of the main streamer is accompanied by a sharp increase of the current density, whereas the conductivity cannot follow the growth of the current. This causes a drop in field intensity at the head of the thin new streamer, and hinders its further development.

1.3.8 Experimental Work on Streamers

Experimental work by Davidenko et al (1969) has been held to support the Lozanskii model. They used an image converter

to study the development of an electrical discharge in pure neon and in neon with a molecular impurity. They measured the rate of development of direct and reverse streamers as a function of the electric field strength, and the streamer length, and they found that the linear dependence obtained by them for the velocity of the reverse streamer as a function of its length is in good agreement with the discharge mechanism proposed by Lozanskii. The very existence of streamers in pure neon supports the photoionization mechanism.

Rudenko and Smetanin (1972,1973) have also studied streamers in neon. An electron-optical method has been used to study breakdown in neon occurring in the centre of a discharge gap caused by cosmic ray tracks. They determined the time characteristics of the processes. In their studies, high voltage pulses (30-100KV) with a variable rise time of 2-10 nsec and 100 nsec duration were applied to a 38mm gap chamber. Photographs of the streamer as a function of time were obtained by means of a pulse electron-optical image converter. The photographs (Fig. 1.3.7.2) showed first the growth of the avalanche head towards the anode in a field of 6.6KV/cm. At 76nsec the sudden appearance of the cathode streamer can be seen. Thus in neon the electron avalanche transfers to an anode streamer before the appearance of the cathode streamer. At this instant, a large current flows in the external circuit and they register a sharp drop in the field.

At a later stage a moment arrives when the decline in field strength levels off, and this moment appears to coincide with an increase in acceleration of the streamer fronts.

The observed monotonic rise in streamer velocity with increasing length is in good agreement with the mathematical model proposed by Lozanskii.

Wagner (1966) also observed two stages in the growth of cathode directed streamers in hydrogen. This was interpreted as being due to photoionization at the cathode.

In Rudenko and Smetanin's case, processes at the cathode cannot affect the development of the streamer, since the dimensions of the discharge gap were considerably greater than the streamer length at which the acceleration sets in.

The existence of similar steps in oscilloscope traces of breakdown of medium gaps has been observed by Allen and Phillips (1964) and has been associated with transitions from the avalanche (Townsend) type of breakdown to streamer breakdown. However, in the Rudenko and Smetanin case these steps can be explained by processes in the developing streamer only without a change in the type of discharge.

R E S U M E

1. The Townsend mechanism fails to explain
   a) the very short formative time lags
   b) the heavy branching of corona discharges
   c) the effect of space charge field of avalanche

2. BREAKDOWN CRITERIA
   a) Raether's breakdown criterion

$$\alpha x_c = 17.7 + \ln x_c$$

   b) Meek's breakdown criterion

$$\alpha x + \ln(\alpha/p) = 14.46 + \ln(KV_b/pd) - 0.5 \ln(px) + \ln x$$

   c) Streamer breakdown criterion

$$1/3(pfr^3\mu/\sqrt{d}) \int_r^d \alpha(y) y^{-3/2} \exp(-\mu y) . \exp(\int_r^y \alpha dy) dy = 1$$

3. KNOWN BREAKDOWN MECHANISMS
   a) the Townsend mechanism
   b) the streamer mechanism

4. CONCLUSIONS OF THE LOZANSKII MODEL
   a) streamer velocity $\propto$ length
   b) streamer thickness $\propto \sqrt{(\text{length})}$

1.4 Corona Discharges

1.4.1 Characteristics of Corona Discharges

In principle corona discharges do not differ from the discharges with uniform electrical fields, since the same basic mechanisms, a first coefficient and a second coefficient such as are involved in the uniform field breakdown occur in the same generic relationships. They do, however, differ in that with non-uniform fields or asymmetrical electrodes, breakdown initiates at the high field now concentrated at one or both of the electrodes.

The weak field between the electrodes, or on one of them in asymmetrical gaps, however, precludes a complete breakdown of the whole gap to an arc at or near the threshold despite discharges at one or both of the electrodes. Thus breakdown will occur in a sequence of steps over a considerable range of potentials from the first manifestation to the complete spark breakdown.

The action of the low field region, aside from yielding fields too low for breakdown streamer propagation at the lower thresholds, is involved with the action of space charges which in some cases facilitate the breakdown procedure and in others impede it. It thus happens that the non-uniform field geometries lead to a stepwise break-

down spreading out in voltage and sometimes in time as a sequence of events which in the uniform field breakdown take place nearly in one act with a time scale in micro-seconds or less. In consequence, such discharges have been studied for the purpose of following the breakdown mechanism under various conditions as well as in their own right.

While any form of non-uniform gap might be studied, the phenomena of interest are more clearly delineated if the electrodes represent the extremes of divergence in shape such as a point-to-plane gap or coaxial cylinders with the inner cylinder of much smaller radius than the outer cylinder.

These have the properties of associating the breakdown sequences with the one electrode of small radius or high curvature. Hence the anode breakdown may successfully be studied more or less independently of the action of the other large electrode. Other geometrically asymmetrical systems, such as confocal paraboloids, or hyperboloids of revolution to plane, and concentric spherical or sphere-to-plane systems have been studied.

Probably, one of the most used because of its convenience has been the point-to-plane employing a hemispherically

capped cylinder for the point. The other frequently studied system is the coaxial cylindrical system. The coaxial cylinder, confocal paraboloids and the hyperboloid or sphere to infinite plane geometries have the advantage of permitting calculation of the axial electric fields preceding the first breakdown threshold.

After the first notable threshold is reached the fields, except for coaxial cylinders, are largely incalculable because of space charge distortion. If ion mobilities are known, the coaxial cylindrical geometry permits a fairly good first order approximation of the fields at steady state for most of the gap at lower currents and adequate pressures.

The field along the axis of symmetry for the hemispherically capped cylindrical point-to-plane gap before breakdown can be computed to about 1% for certain fixed ratios of gap length to point diameter as shown by Dodd (1950) who carried out the study for one ratio. The tedious computation can only be carried out for one ratio of point diameter to gap length at a time.

The point-to-plane and coaxial cylinder systems are easy to perfect and adjust which makes them particularly suited to study. The fields for confocal paraboloids, sphere-to-plane,

concentric spheres, and hyperboloid-to-plane are given by exact analytical expressions.

In the early days of the study of electrical breakdown in gases, it was generally recognised that, as potential was raised in such gaps, some sort of breakdown appeared at the highly stressed electrode with relatively low currents. These currents, lying in the order of microampere at relatively low potentials, frequently gave unsteady or fluctuating currents near threshold. At other times such difficulties were not encountered. For short potential ranges about thresholds, currents increase linearly with potential. With increase in potential the discharge also generally became more stable and steady. At this stage, depending on pressure and the nature of the gas, luminosity of some form or other appeared near the highly stressed electrode.

Thereafter, current increased somewhat faster than linearly approaching a parabolical increase with potential. Depending on the gap, the current and potential could be increased by considerable margins until a point was reached yielding a complete breakdown of the gap to a transient arc through the medium of a spark with a brilliantly luminous channel at the higher pressures.

The breakdown to a spark usually occurred at voltages from two to six times that for onset of the first glow and current.

As gaseous purity was adequately increased in later years, with the absence of negative ion-forming gases, it became clear that in very pure inert gases, as well as H_2 and N_2 with clean cathodes the highly stressed negative electrode corona did not occur in the absence of external current limiting resistors, but the gap broke down to a transient arc via a spark. Even in very pure inert gases the potential range between positive corona threshold and spark was much reduced.

Again, very confusingly, the breakdown thresholds in the same gas were at times observed to be lower for the highly stressed negative electrodes; under other conditions, such as different pressures, they were lower for the highly stressed positive electrode. This situation was somewhat puzzling as interpreted in terms of Townsend's basic breakdown theory especially with the confusion existing as to the significance of the thresholds.

The potential differences required to initiate the presparking currents and luminosities were always far below the breakdown for a uniform field gap of the same length. In most

cases, even the sparking potential for the non-uniform field gap was markedly lower than for the same length uniform field gap. The potential for the spark transition from non-uniform gaps, with the possible exception of extremely pure inert gases and H_2 and N_2 is universally lower for the highly stressed positive electrode than for the negative, unless the pressure is sufficiently low to exclude a filamentary spark.

Except at relatively low pressures the luminous manifestations at the highly stressed electrode near the threshold for the low currents take on various characteristic shapes such as glows, multiple spots, haloes, coronas, brushes, streamers etc. In consequence, these luminous manifestations gave the phenomena the general name coronas.

This expression, corona, is used to describe the general class of luminous phenomena appearing associated with the current jump from some microamperes at the highly stressed electrode preceding the ultimate spark in the gap.

Where observed the sudden current jump, usually just preceding the initial appearance of the corona and the associated value of the potential is designated as the corona threshold. The threshold for the appearance of a corona form may be further classified in terms of the character-

istic phenomenon or mechanism associated with it, such as the burst pulse threshold, the streamer threshold, the Trichel pulse threshold or the glow discharge threshold.

The current in many such thresholds is pulsating or intermittent in nature. Depending on the geometry and the spectroscopic nature of the gas, the intermittent or pulsed thresholds may not show luminosity in all cases. If the potential is raised on the order of some hundreds of volts above threshold, the frequency of the intermittent pulses becomes so great that they merge to a nearly steady state but slightly fluctuating current.

Transition from intermittent to steady state is sometimes sharp and is described as the onset of steady corona. Above the onset of steady corona there will be a limited region, in which current increases nearly proportionally to potential increase. This is called the Ohm's law regime. After this, the current increases more rapidly than potential, that is, parabolically, eventually leading to a complete spark breakdown.

1.4.2 Visual Appearance of Coronas

The number of forms of corona discharges is enormous because their characteristic shapes are highly dependent upon the electrode geometry used, the gas type, the applied voltage form and the working pressure.

With highly positively stressed electrodes, perhaps three rather characteristic forms are noted (Loeb 1965). In the intermittent regime just above threshold, the most highly stressed area of an electrode will be covered by a seemingly tightly adhering velvety glow as burst pulses appear. This is particularly notable and becomes intense and thin at higher pressures, especially above onset of steady corona. With coaxial cylinders it will appear as spots at the onset.

As current increases with potential increase, the glow will extend out into the gap a millimetre or two when the pre-onset streamers appear. From points, the glow may have a paint-brush-like appearance with a short, intensely bright stem and a flare below. These will appear at the point tip or in spots on a wire.

The forms which at high pressure project into the gap, including the paint-brush-like manifestations, are due to the appearance of pre-onset streamers, and the range is a rough indication of streamer advance in that gap. The tightly adhering glow of the quiescent steady corona, beyond the pre-onset streamer potential, is a form of a recently interpreted glow discharge (Hermstein 1960) with negative space charge, characteristic of electron attaching gases such as air, which suppresses the streamers.

Generally speaking, with or without negative ions the glow will adhere closely to the anode near threshold. As potential increases, it will project out into the gap, especially where the glows are restricted to patches. Reduction in pressure causes an increase in thickness or extension of all glows into the gap roughly in inverse proportion to the pressure.

At very high potentials approaching spark breakdown, especially in gaps in which point radius is small compared to gap length, a narrow bundle of luminosity composed of many superimposed filamentary streamers extends well into and across the gap along the axis. These streamers are a manifestation of insipient breakdown streamers. They do not always appear preceding breakdown with larger electrodes and short gaps. Reduction in pressure will broaden and diffuse all such luminosities in three dimensions because of augmented diffusion.

For the highly stressed negative electrodes at threshold and above breakdown the luminosity occurs in limited spots in air and in electron attaching gases. For a point of small to moderate radius, there will at onset be one spot. This discharge is an intermittent localised glow discharge of some 0.02cm diameter near the cathode surface and extends into the gap perhaps a millimetre or two. Decreasing

pressures reveal it to be complex, having a Crookes dark space, a constricted negative glow, a Faraday dark space, and a flaring positive column. This gives it a shaving-brush-like appearance. The shape is dictated by the relative potential gradients along the discharge axis and in the space outside the discharge.

In free electron gases at threshold, the discharges may appear first as a faint glow extending into the gap which contracts to a spot and then reverts to the initial form, oscillating between the two forms.

As potentials and current increase, these glows settle down at points and yield the same general configuration as for air but are more diffuse and extend further into the gap. In some gases the spots will be cusped with the base on the electrode. As potentials increase, the spot at first increases in intensity, but presently a second spot appears, then a third. On a wire, the spots multiply along the wire.

In some cases, they are in ceaseless motion; in others they are quiescent at one point. Both positive and negative glow patches or spots appear to and actually do, repel each other. On larger smooth surfaces, the quiescent spots,

owing to mutual repulsion and field gradients, form regular patterns (Thomas 1930). The reduction in pressure, as indicated, extends the discharges in three dimensions, roughly inversely proportional to pressure.

Near breakdown in air, and possibly in other gases, though not readily observed, the negative glow increases in extent, and at low pressures the Crookes dark space and a faint general glow extending to the negative electrode are all that is seen near the point where pulses cease. Near breakdown, a very sharp luminous spike will usually appear along the axis of the spot in the fan, and with increase in potential it will extend backwards towards the negative glow. At a point where this spike approaches the cathode, the spark occurs. In air in the region just referred to, the intermittent pulses characteristic of the threshold and above, have ceased.

When a spark suppressing gas like freon is mixed with air, the discharge takes on a fantastic number of curious and elaborate forms which are not understood.

The spectral behaviour of breakdowns in air is of some significance because it reveals important discharge characteristics (Fowler 1956). Possibly similar inferences

could be drawn from single lines or bands in other gases.

Low electrical fields yield ionization and excitation that favour the arc spectrum of N_2 and nitric oxide which yields a reddish purple glow. This is characteristic of the fan in the negative point discharge and the outer areas of the paint-brush in the positive streamer region.

High electrical fields produce highly excited N_2 molecules, the spectra of which are represented largely by the second positive group bands with just a few second negative bands shown. These lie largely in the green to violet end of the spectrum, and yield an intense electrical blue light. They have been photographed in colour film in air (Loeb 1965). This colour will be noted in the closely adhering glow of the steady positive corona, in the filamentary breakdown streamer channels, and in the axis of streamers. The negative glow of the Trichel pulse corona in air is also quite white or bluish, as fields there are high.

Thus the colour of the discharge manifestations in air is a guide to field conditions. In other gases, the colours follow spectral distribution but do not clearly designate high and low field regions except possibly as they affect single lines or bands.

In some cases, notably in O_2 and CO_2, spectra are of such low intensity in the visible as to delay the appearance of luminosity until thresholds have been exceeded by a considerable margin.

1.4.3 Impulse Coronas - Lichtenberg Figures

If a voltage pulse, rather than a steady (d.c.) voltage is used and if the pulse declines to about one half of its magnitude in a few microseconds, then ionic space charge drift and accumulation can be neglected.

Because of the transient development of the ionization processes under such pulse conditions, their detection has always been quite difficult. Inserting a photographic film in the passage of the discharge has been helpful in supplying information regarding the discharges which develop from their onset up to the transition to spark breakdown. This method of detection yields photographic patterns that resemble the 'glide' figures attributed to Lichtenberg (1777). Although these photographs exhibit a great deal of fine detail, their interpretation in accordance with modern atomic physics was attempted only in 1939 by Merril and von Hippel.

When a positive voltage pulse is applied to the point of a point-to-plane geometry the first detectable ionization is

of a filamentary branched nature (Fig. 1.4.3.1.). These branches are called streamers as in the uniform field where they are less branched. As the voltage magnitude is increased just above onset, the first streamers which develop are so weak that they can hardly be detected by the naked eye or with an ordinary photocell.

For this reason detection and recording of transient forms of ionization has always been very difficult. This difficulty can partly be overcome, however, by the use of the Lichtenberg figure technique for their study (Loeb 1965, Nasser 1959, 1963).

The basic idea in these studies is to place a sensitive photographic emulsion in the path of the ionizing events and because ionization is always accompanied by excitation, radiation so emitted will produce traces in the photographic emulsion.

These photographic traces have provided a great deal of information regarding impulse streamers and their dependence on various parameters. Most of this work has been carried out by Nasser (cf. Loeb 1965, Nasser 1971).

The original Lichtenberg figures were produced by a dielectric dust settling down on the surfaces where sparks had occurred. Later photographic emulsions were used to

obtain these patterns. Another method of observing these figures consists of interposing a dielectric surface in the path of the discharges. The electric charges produced ionize the gas close to the surface of the dielectric and spread out over it due to electrostatic attraction, giving rise to observable patterns similar to the "glide" figures of Lichtenberg.

The work of Nasser on impulse coronas using the Lichtenberg figure technique showed that there is a large statistical spread in the range of streamers and that these cease to propagate at external fields of the order of 500V/cm or less. It was also found that the radial range of streamers varied linearly with the applied voltage.

For the case of positive streamers (derived from applying a positive pulse to the stressed electrode) it was also found by Nasser that the speed of propagation of the streamers declines very quickly as they move into low field regions. At a voltage of 38.7KV and at a distance of 1cm from the point anode the speed of propagation is 4×10^6m/sec as given by Nasser (Nasser 1971).

The model of streamer propagation for the case of the non-uniform field does not differ greatly from that for the uniform field. The major difference lies in the fact that the magnitude of α is strongly dependent on local field

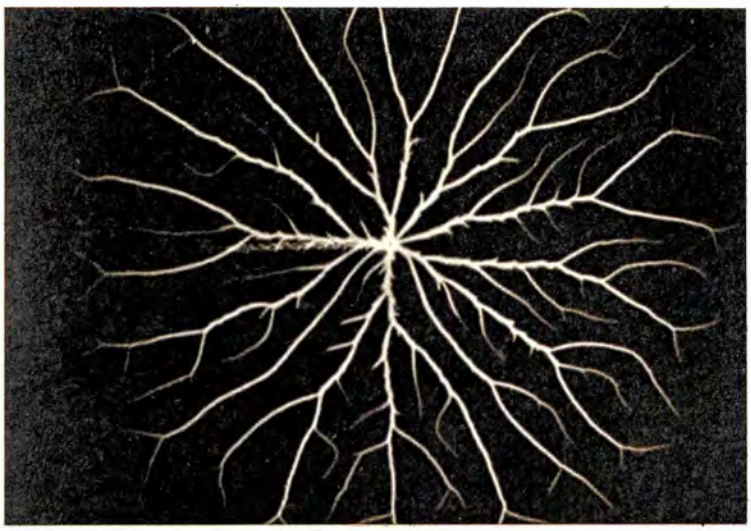

FIG. 1.4.3.1

Lichtenberg Figure of Positive Polarity.

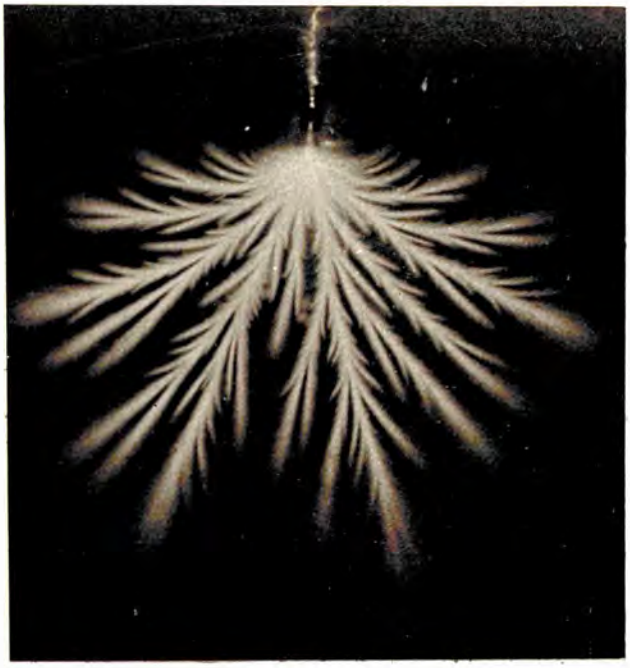

FIG. 1.4.3.2

Feather-like Discharge from a Negative Point Electrode.

conditions and so Eq. 1.2.15 must be used when computing electron concentration in the avalanche.

The breakdown criterion obtained when proper account is taken of the field dependence on x, the distance from the point electrode, and of the dependence of α on the local field is similar in form to the criterion obtained for the case of the uniform field, namely

$$\gamma\exp(\int\alpha dx) = 1 \qquad 1.4.3.1$$

However, the analytical form of γ in this equation is much more complicated, being a function of x,α,μ,f and r (cf. Section 1.2).

When a negative voltage pulse is applied to the point electrode, feather-like traces are observed on a photographic film or dielectric placed in the path of the discharge (Fig. 1.4.3.2). The intensity of these feathers is seen to decrease gradually and to show very vague boundaries. These are also found to start at a slightly higher voltage than their positive counterpart. Their radial spread is also less than the positive streamers and their channels are wider.

Using rectangular pulses of adjustable duration the speed of propagation of the negative streamers (feathers) has been measured. Typical values lie in the range of

2.2 to 14 X 10^6m/sec for fields of the order of a few tens kilovolts and distances from the cathode of a few centimetres (Nasser 1971, Loeb 1965).

1.5 The Glow Discharge

1.5.1 Luminous Appearance of the Discharge

When an electric discharge passes through a gas at low pressure, a non-uniform distribution of luminosity is observed along the direction of the discharge. The actual position of the various regions and in some cases the occurrence of a few of them depends on the kind and pressure of the gas, and on the current, or the voltage across the discharge. This form of discharge with its distinctive pattern of luminous and dark regions between the cathode and anode is known as the glow discharge.

Typically, starting from the cathode, a primary dark space or Aston dark space totally dark in nature first appears. This is bounded by the first cathode layer - a thin layer of faint luminosity. Sometimes this pattern may be repeated, each luminous layer in turn becoming fainter and fainter. For this reason rarely more than two such layers are usually seen.

Farther from the cathode is the cathode dark space or Crookes dark space. This is usually taken as the entire space between the cathode and the boundary of the next region, the

negative glow, and thus includes the cathode layers and dark spaces. This is (with the exception of the Aston dark space) not totally dark, but appears so to the eye in comparison with the luminous parts of the discharge.

Bounding the Crookes dark space on the anode side is the negative glow. This is the most luminous zone of the discharge. It has a sharp boundary with the Crookes dark space but is diffused on its anode side. The light increases to a maximum near the middle of the glow and diminishes towards the anode where it merges into the Faraday dark space. The length of the glow is comparable with that of the cathode dark space: its colour is characteristic of the gas.

The Faraday dark space again is only relatively dark and in pure neon does not exist at all, the space being filled with red light. A small trace of impurity produces a dark space, however, and it seems to exist in all other gases. Its length depends on the length of the discharge tube, being large in wide tubes and it is usually longer than the negative glow.

The positive column is a long luminous column filling the rest of the tube almost to the anode. Its colour is characteristic of the gas but is not the same as that of

the negative glow, nor is it as bright. It is often uniform (or apparently so) but sometimes striated, i.e. it consists of a regular pattern of lighter and darker regions distributed along its length. These striations may be stationary or moving; sometimes they may move so fast that the column appears uniform to the eye. The boundary with the Faraday dark space is diffused.

Often close to the anode a thin dark space can be seen at the end of the positive column, accompanied by a glow on the surface of the anode. These are called the anode dark space and glow.

1.5.2 The Striated Glow Discharge

Striations in a great variety of patterns have been noticed in limited ranges of current and pressure in many gases. They were first observed by Abria in 1843 and the literature contains a number of beautiful photographs of striated columns (Thomson 1933). Many measurements have been made with the object of finding how the distance and potential difference between striations, their radiation and associated space charge depends upon the nature and pressure of the gas, the current and the diameter of the tube. It has been found that the properties of striated columns depend strongly on the purity of the gas.

Individual striations are curved convex towards the cathode, due to the effect of negative wall charge. They are usually sharp and bright on the cathode side and more diffuse and dimmer on the anode side. J.J. Thomson (1909) measured the electric field distribution through a striation by the deflection of an electron beam, and found a small negative field just in front of the striation. However, more recent electron beam measurements by Warren (1955) have not shown this negative field. Measurements of the potential distribution with Langmuir probes show similar field distribution but with a smaller or zero negative field.

The potential difference δV between striations has been measured by moving the anode through them and noting the difference in potential required to maintain constant current in the discharge (e.g. Penning in rare gases). Earlier experiments of Wehner, Neubert and Holm show that as the current density increases, δV decreases to a constant value independent of the gas pressure and tube diameter.

In rare gases Penning found δV = 20volt for He, 18.5volt for Ne and 11.9volt for Ar. These values are close to the excitation potentials of the lower states of these gases.

The distance between striations ℓ varies in a complicated way with current density. It has been found that ℓ often approaches a constant value as current density increases for N_2, H_2 and CO_2. In H_2, ℓ decreases with increasing current density, but in CO_2 the opposite occurs.

Striations are spaced further apart at lower pressures in common with other regions of the discharge. A relation by Goldstein (1881) gives $\ell \propto 1/p^m$, later extended by Wehner to include the radius R of the tube in the form

$$\ell/R = C\{1/(pR)^m\} \qquad 1.5.2.1$$

where m is a constant approximately equal to 0.5 (e.g. for H_2, m = 0.53) and C depends on the current density.

The conditions for the formation of striations are complicated and different types of striations occur at different values of current and pressure. Although there have been many attempts to derive a theory to explain the behaviour of the striated column, no convincing solution exists. A theory of the striated column was given by Thomson (1933) and more recently a paper by Pekarek and Krejci (1961) indicates a better understanding of the phenomena of the striated column along with the discovery that all positive columns have striations.

Some evidence has also been reported on the presence of acoustic oscillations associated with moving striations and standing striations have also been produced by an acoustic standing wave (Subertova 1965, Crandall and Cooper 1967). Still many uncorrelated observations in the striated column are far from being even qualitatively understood.

1.6 Other Striated Discharges

1.6.1 The Holst-Oosterhuis Discharge

When the Townsend discharge passes over into an internally maintained discharge at small currents (10^{-7}amp) between plane parallel electrodes, and in noble gases, a beautiful laminar emission pattern is observed shown schematically in Fig. 1.6.1. This was first observed and studied by Holst and Oosterhuis (1921, 1923) and bears their name.

It is found that the number of lamina times the ionization potential of a gas is equal to the potential difference between the electrodes. In the case of the noble gases the theory of the lamina is that the electrons, all of which originate from the cathode, acquire energy in the uniform field between the plates which they successively lose and gain in flights of one excitation mean free path. The current is so small that space charge does not distort the field, and the layers are regularly spaced. If the current is increased space charge distortion sets in and the layers

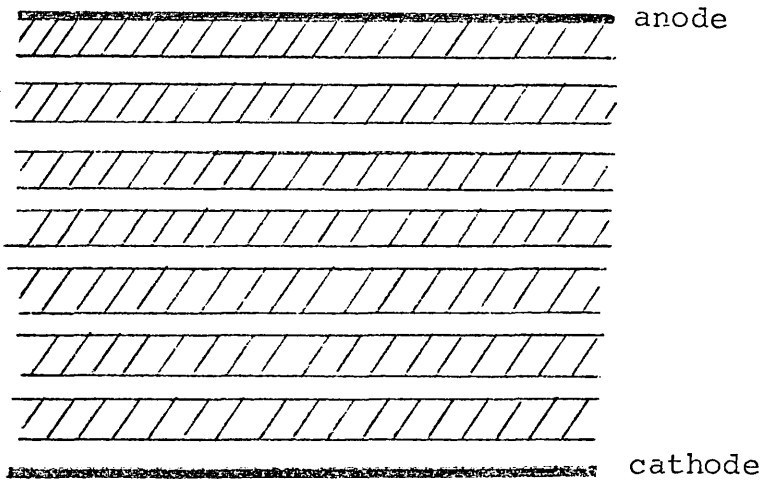

FIG. 1.6.1

Schematic Diagram of a Holst-Oosterhuis Discharge.

first become compressed in from the cathode and finally merge into the cathode glow of the ordinary glow discharge. As the anode is approached the electrons begin to straggle in velocity with an accompanying loss of definition of the layers.

The sharpness of the layers and their potential increments of one ionization potential at a time lead to the conclusion that if they are due to electron excitation for their radiation, then electron excitation must be a comparatively rare event when compared with ionization, since a 20% discrepancy in energy loss between processes of comparable importance would result in a complete disorganization of the electon beam in the course of four or five lamina, whereas as many as twenty have been observed.

While the electrical explanation of the discharge seems satisfactory, the experimental knowledge about the laminar discharge radiation is insufficient to justify such a simplified view of the radiation process which may be quite complex.

A second uncertainty is whether the cathode current is maintained by positive ion or photon impact. Recent evidence suggests the latter process in the glow discharge, but the difference between the layer potentials found by

Druyvesteyn (1931) together with the transition behaviour which he finds with increasing currents, suggests ionic cathode processes in the internally-maintained laminar discharge, with a possible shift in process to photon impacts at the higher currents.

1.6.2 A Striated Townsend Discharge

Some studies in free electron gases with a stressed point-to-plane geometry have shown striations of a kind so far not explained. These have been reported by Loeb (Rees 1972). Weissler and Miller (Loeb 1965) investigated the breakdown of spectroscopic grade He with Alpert vacuum techniques using a flashed hairpin filament tungsten point in a point-to-plane gap of 4cm length. Flashing the cathode was essential to prevent liberation of gases through the sputtering of the cathode by ion bombardment. Pressures ranged from 50 - 200 torr. Current-potential, current-photomultiplier and photomultiplier-potential observations of luminous events were recorded. Two photomultipliers were used, one at the cathode, the other at various points in the gap, which noted the progress of luminosity across the gap.

Still photographs enabled the shape and size of the arc channel at current peak to be observed. Impulse potentials of short rise time, 10nsec, from a storage condenser were used.

The discharge was found to initiate as a Townsend discharge with a photoelectric secondary γ_p. As for the case of the Trichel pulse it quickly builds up a space charge with high cathode field followed by the subsequent secondary liberation by energetic positive ion bombardment. Negative ions did not form. Thus the discharge was not interrupted as in air. However, the photomultiplier oscillograms indicated oscillations of 7×10^7 cycles/sec caused by ion plasma oscillations with a positive ion density of 4.5×10^{11} electron $/cm^3$. These were constant during the span of the luminosity and on occasion still photographs of the arc showed striations.

These oscillations were independent of instrument and circuit constants and were an inherent property of the arc. The explanation proposed by Loeb is that with the observed exponential increase in time, the electrons accumulated beyond the ionic space charge more rapidly than they were removed from the field. Thus the electron space charge was sufficient to reduce the current momentarily, allowing the discharge to spread laterally over the electrode surface and setting the ionic space charge into oscillations characteristic of the ion density.

CHAPTER 2

The Streamer Chamber

2.1 Introduction

The streamer chamber consists of a perspex chamber containing the active gas (sensitive volume) sandwiched between two parallel plate electrodes. The passage of a fast ionizing particle through the chamber is detected by two scintillation counters placed above and below the chamber. The electrons created in the chamber gas by this ionizing particle are within a short interval after their production accelerated along the line of the high short duration electric field between the electrodes.

The high voltage pulse necessary for this electric field is supplied by a Marx generator. After the passage of the ionizing particle, the signals from the two scintillation counters are fed into a coincidence unit, the output of which operates a trigger amplifier. The fast rising output pulse of the trigger amplifier, which is a few kilovolts in amplitude, triggers the voltage generator and the high voltage pulse is subsequently applied to the chamber. The electronic system should be fast enough to enable the overall delay between the detection of the event and the application of the high voltage pulse to the chamber to be

less than one microsecond, otherwise the ionized particles will be lost by recombination.

The accelerated electrons in the chamber cause further ionization and avalanches are formed which after sufficient amplification cause streamers to appear. These streamers are highly luminous and visually define the path of the ionizing particle in the chamber to within narrow limits.

2.2 Description of the Chamber

2.2.1 Mechanical Details

The box enclosing the sensitive volume of the chamber was 20 X 20 X 20 cms^3; it was constructed of half-inch thick perspex cemented with ICI tensol cement number 7; the box had a small hole on a side wall in which a perspex tube was held by clamps screwed to the side wall of the chamber. The clamp and screws were also made of perspex. Between the wall of the chamber and the tube a rubber 'O-ring' was used to make the connection vacuum tight. The inner surface opposite the sides through which the photographs were taken was painted black with Rustin black paint to minimize back-reflected light.

The electrodes were 60cms^2, 1/4'' thick Duraluminium plates with their edges rounded off. The perspex boxes and the

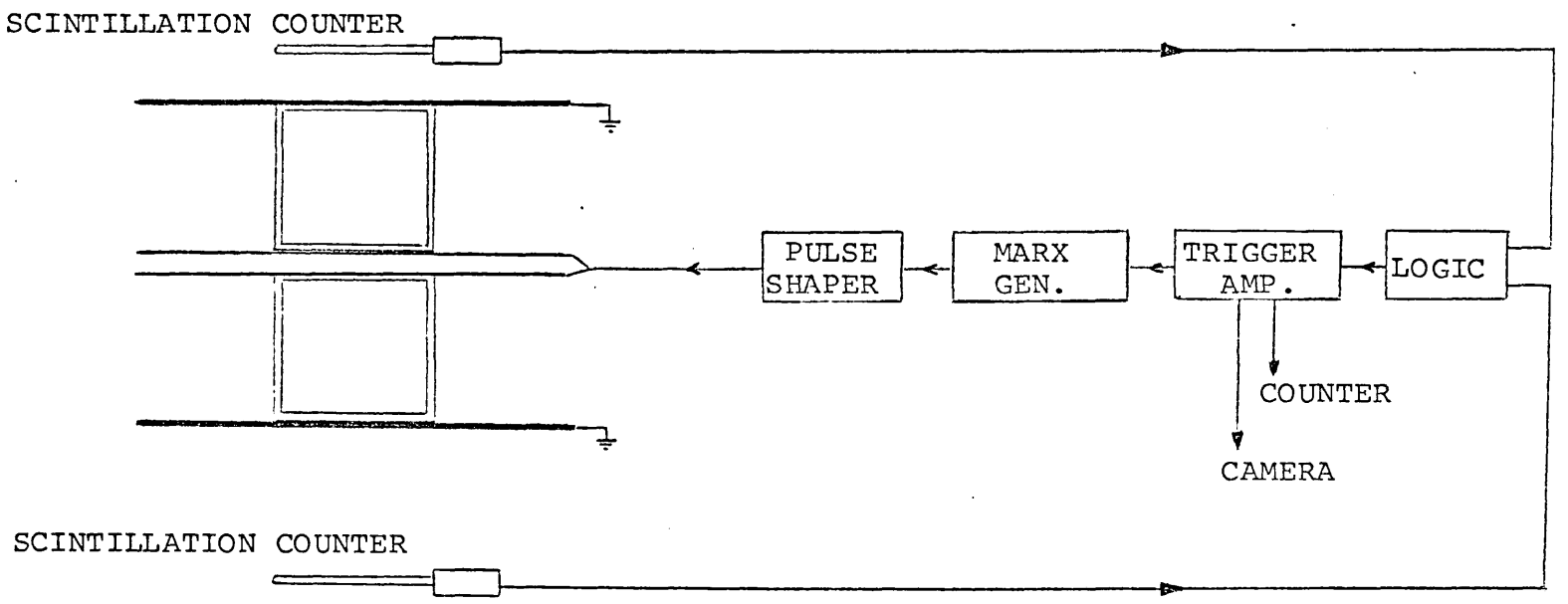

FIG. 2.2.1.1

The Streamer Chamber and Associated Electronics

electrodes could be clamped together by four 2 X 2 X 22 inches wooden joists with 0.5 inch diameter nylon rods threaded at both ends and the whole arrangement was clamped using Tufnol nuts.

When the apparatus is employed for scattering experiments two perspex chambers are used and these are sandwiched between four aluminium electrodes (Fig. 2.2.1.1). The scatterer is then placed between the two central electrodes between the two gas chambers.

An alternative chamber could also be used which was open at two opposite ends and could be made vacuum tight by two 'O-rings' bordering the two openings and closed by two slightly larger perspex lids. This chamber had the advantage of allowing access to the sensitive volume of the chamber and was extensively used in the low voltage work (cf. Chapters 4 and 5).

2.2.2 The Vacuum and Gas Filling System for the Chamber

The chamber could be evacuated to approximately 0.01 mm Hg before filling with the working gas. The system employed for evacuating and filling the chamber is shown in Fig. 2.2.2.1. Tap T1 which opened up when the gas pressure inside the chamber became higher than atmospheric pressure was used as

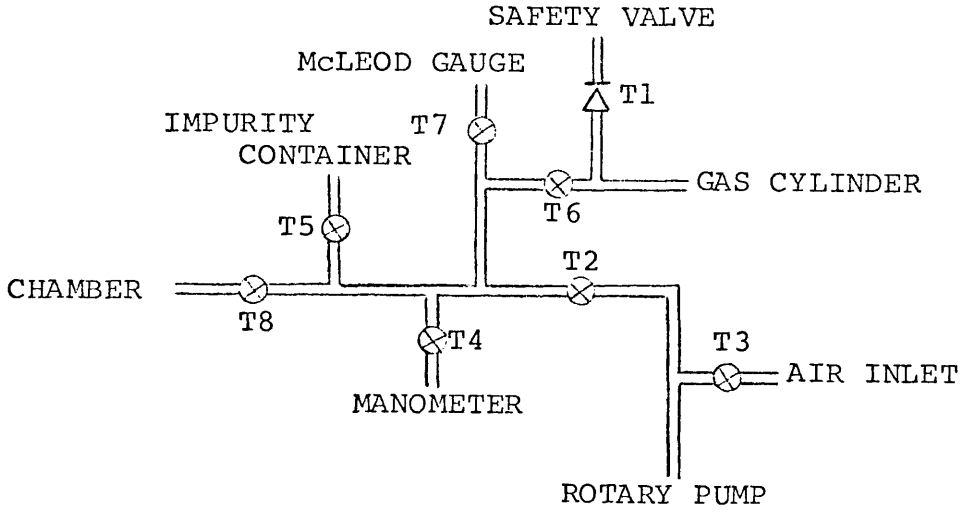

FIG. 2.2.2.1

The arrangement for evacuating and filling the chamber.

a precaution to prevent explosion of the chamber. A facility to introduce gas admixture to the filling gas was available through tap T5.

With a rotary pump the pressure inside the chamber could be reduced to 0.005 mm Hg. A McLeod gauge was used to measure this pressure. In addition a U-tube manometer measured the pressure of the filling gas which consisted of a mixture of 30% helium and 70% neon.

2.3 The Scintillation Counters

In the high voltage work described in Chapter 3 cosmic ray particles were employed to initiate gas discharges in the chamber. These particles were detected with a scintillation counter arrangement; two counters, each consisting of 9 inch square, 1/2 inch thick plastic scintillator NE 102 A coupled with a triangular light guide to a 13 stage photomultiplier tube EM19594B. Each assembly was covered by a white sheet of polystyrene foam to reflect the photons created in the plastic scintillator and then covered by black polythene sealed with PVC tape to make it light tight. The light guide was half an inch thick perpsex plate, the length of the edge in contact with the scintillator being nine inches, and that in contact with the photomultiplier one and a half inches.

The light guides for the two units were cemented to the scintillators and the photomultipliers by optical cement NE580 which has a refractive index close to that of the NE102A plastic scintillator.

2.4 Logic Control and Coincidence Circuit

2.4.1 General Description

This unit was built with integrated circuits and semiconductor devices. One of the major difficulties of using semiconductor devices arises from the production of a heavy radiation background by the high voltage pulse generator. Even though the electronic control unit was in the same room as the generator, the difficulty was overcome by using sufficient screening around the logic unit as well as building it with carefully selected components. The whole logic control unit fitted into a Harwell 2000 standard double width module.

2.4.2 The Limiter/Pulse Shaper

The circuit diagram for this limiter/shaper is shown in Fig. 2.4.2.1. The limiter section of the circuit was employed to protect the integrated circuit used as a pulse shaper. This unit was sensitive to 50mV negative input pulses; the output pulse was a standard TTL.

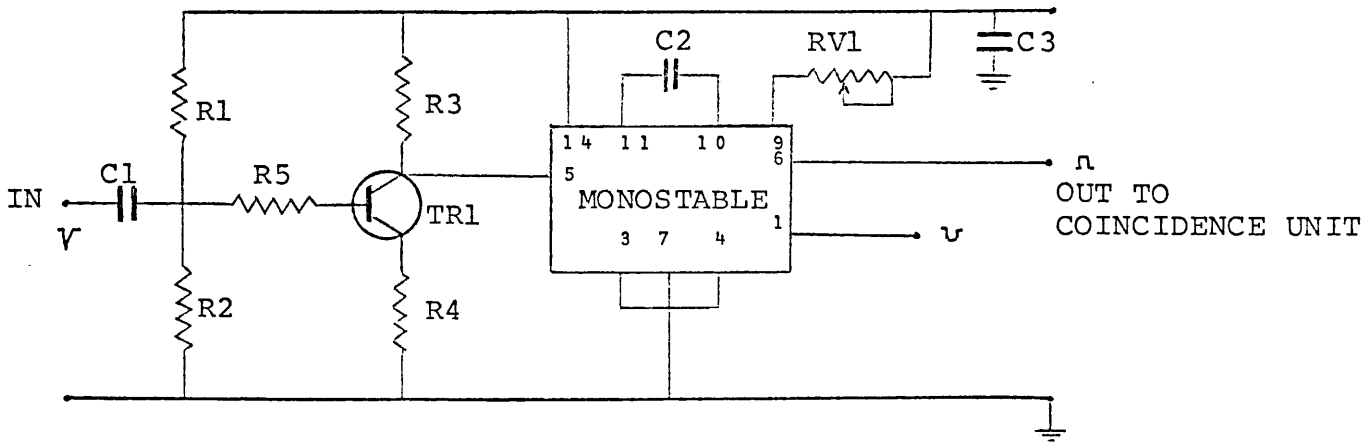

FIG. 2.4.2.1

The Limiter Pulse Shaper.

A choice of positive or negative output pulse was available. A negative anode pulse from a photomultiplier applied to the base of a n.p.n. transistor which was normally conducting turned it off, giving rise to a fast positive pulse whose amplitude was limited to 5 volts. The output from the limiter was shaped by a monostable SN74121N which gave a standard output. The width of the output pulse could be changed by varying the value of the resistance RV1.

2.4.3 The Coincidence/Anti-Coincidence Circuit

The circuit description that follows includes an anti-coincidence part which is used for event selection in cosmic ray studies. In the present work only the coincidence section of the circuit was used as a means of triggering the streamer chamber.

A block diagram of this unit is shown in Fig. 2.4.3.1. Pulses from the limiter pulse shapers fed to the three inputs of the first gate (NAND IC_1); the third input could be used as an inhibitor or as another input for triple coincidence work. For the present work one input was coupled to a d.c. level. When two pulses arrived simultaneously at inputs 1 and 2, an output was obtained from the first gate. This output was inverted and a delay could be

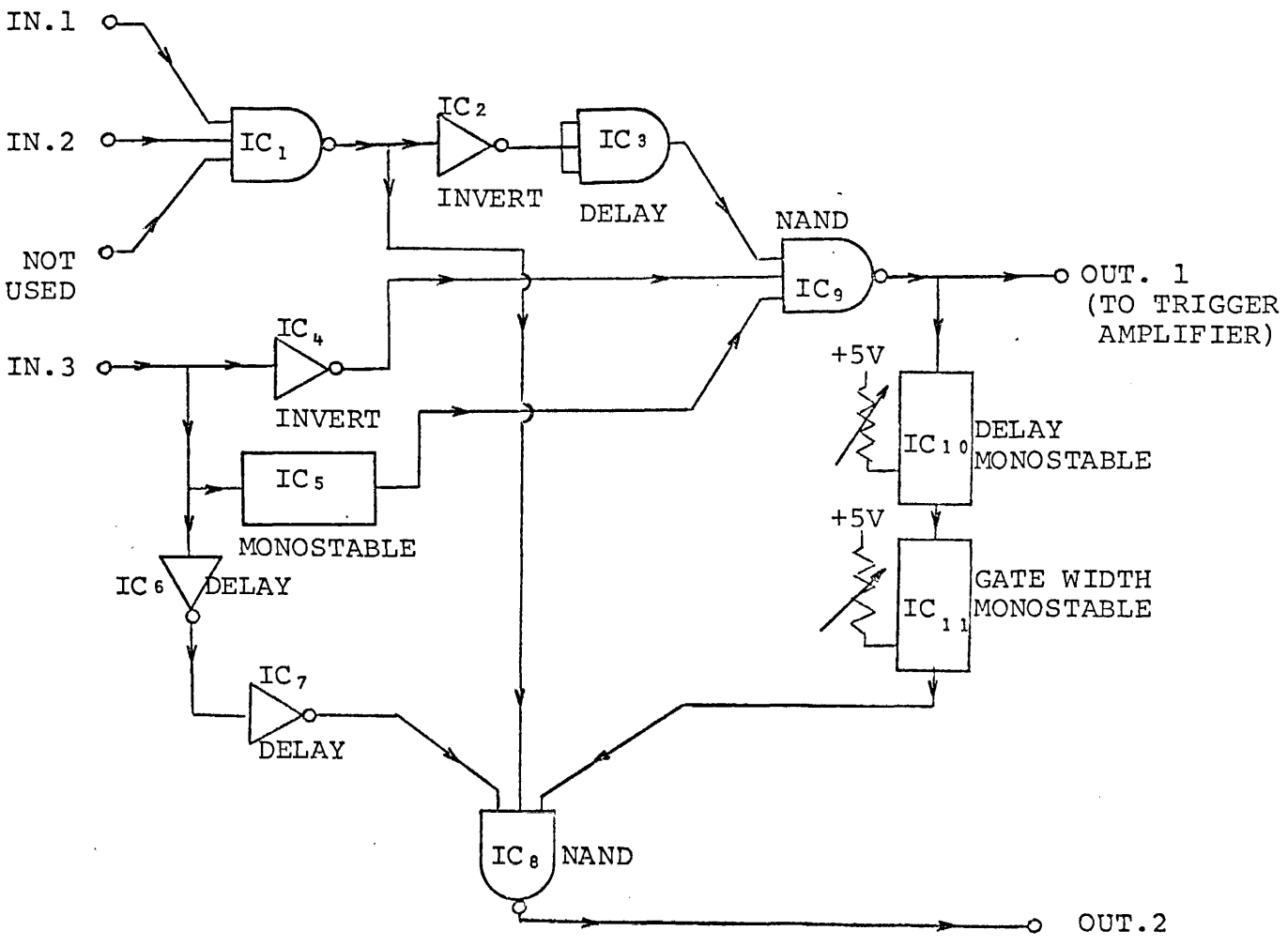

FIG. 2.4.3.1

Block Diagram of the Control Electronics.

used if necessary and applied to the input of the second gate (NAND IC_9). If no pulse was observed simultaneously at the anti-coincidence input (IN.3) no voltage was applied at the other input of the second gate, and a coincidence output pulse was obtained (OUT.1). If, however, a pulse was applied to the anti-coincidence input, it would be inverted after passing through the limiter/shaper and fed to the second gate to inhibit its output. Thus output pulses from the second gate were obtained only if two simultaneous pulses were applied to inputs 1 and 2, and no pulse at input 3. A detailed diagram of the circuit used has been published by Rice-Evans, Hassairi and Betts (1975).

For some of the work of Chapter 3 a dead-time unit was used which consisted simply of a monostable oscillator giving out a long pulse of 30 seconds duration. This prevented coincidences to occur for the period the pulse was applied to one of the inputs of the coincidence circuit.

2.4.4 High Speed Trigger Amplifier Unit

The circuit used consisted of four stages (cf. Rice-Evans et al 1975). The first was a buffer to protect the logic unit from the high voltage section. A fast pnp transistor 2N3906 was used; under normal conditions the transistor was conducting, a negative logic output pulse applied to the base of the

transistor giving a negative output which was of the same amplitude as the input pulse. A pulse transformer (L2) was used to invert the output of the buffer, the ratio of the transformer being 1:1. The positive pulse from the transformer switched on the high speed avalanche transistor Tr2 (RT3333A) of the second stage giving a fast rising negative pulse of 50 volts amplitude. Another pulse transformer of 1:5 ratio was used to invert this pulse. The third stage was used as a pulse shaper because the inverter output was too short to turn on the valve V2(EL360) of the fourth stage. A diode-triode EAC91 was used, the diode part as a pulse shaper to lengthen the pulse and the triode part as an amplifier/buffer to drive the automatic camera and provide a suitable pulse for a scaler.

The fourth stage consisted of an EL360 valve. This valve was normally cut off but a positive 180 volt pulse from the output of the diode pulse shaper applied to the control grid would switch it on, giving a fast negative pulse of about 4KV and a rise time of 10nsec. This pulse was used to trigger the intermediate spark gap. Since the pulse needed to trigger this spark gap was 5KV, a 2KV negative d.c. bias was applied continuously to it. This improved the delay for switching the spark gap. The total delay over the trigger amplifier was about 25nsec and the overall delay of the whole logic unit from limiter to the trigger amplifier was less than 75nsec.

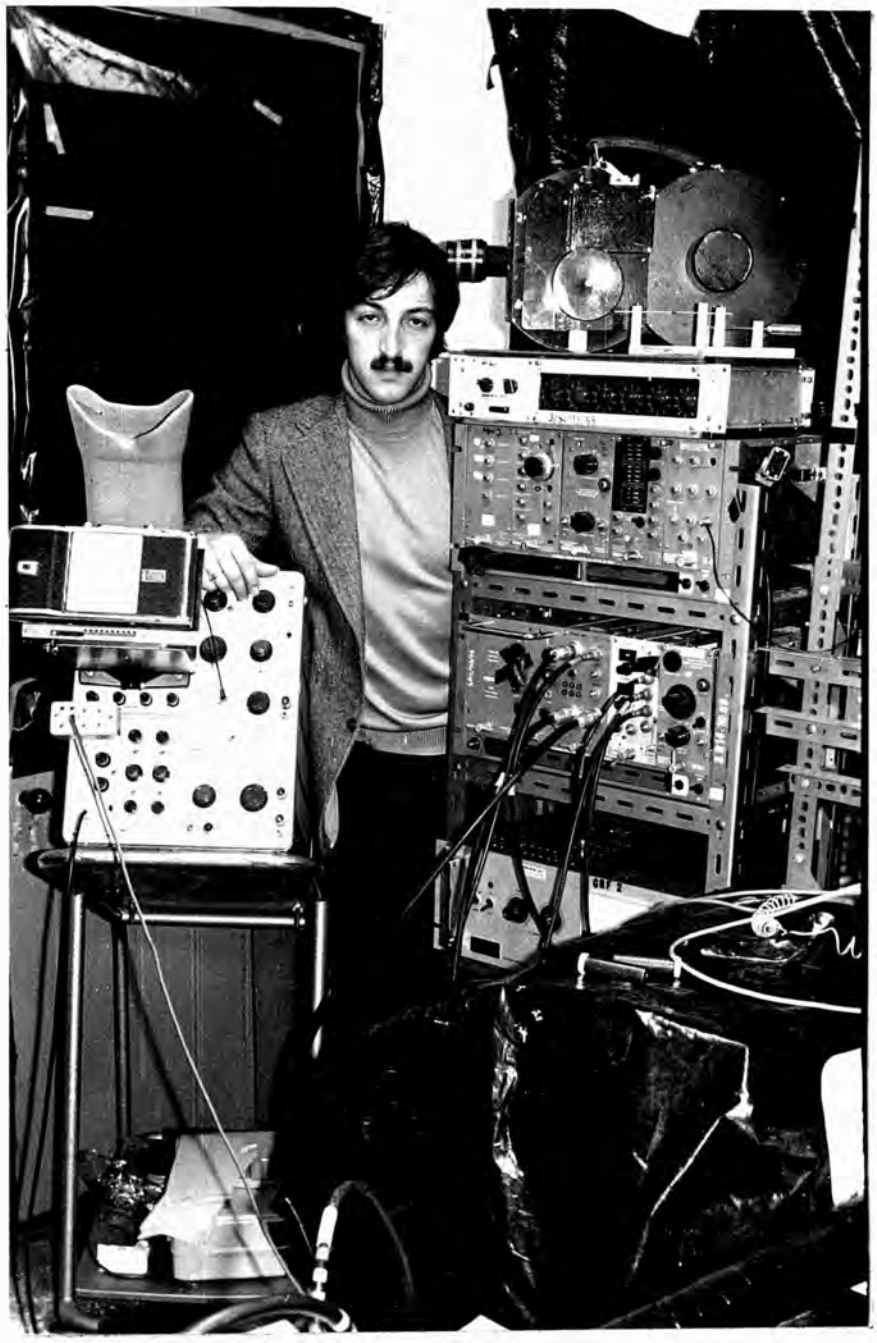

FIG. 2.4.4.1

A Photograph of the Control Electronics

2.5 Recording of the Discharges

An automatic 35mm camera was initially used to record the discharges. It had a 50mm focal length and a stop number from 1.8 to 22. The clear perspex of the chamber walls transmitted about 90% of the visible light. Before photography began the chamber was surrounded by a blck cloth to cut down the background light from the spark gaps, and the indicator lamps of the instrument were removed or covered by pvc black tape. The camera was focused at the middle of the chamber from a distance of about four feet, so the depth of the field would cover the whole of the chamber. The camera had no shutter so photography had to be done in complete darkness.

When an event had been selected and the Marx fired, a pulse from the trigger amplifier would advance the film to the next frame and the camera would be ready to record the next event. The film used was Ilford HP4 which has a speed of 650 ASA when developed in Ilford Microphen for 5.5 minutes at 20^0 C., giving a contrast gradient of 0.55. The speed of the film could be further increased by increasing the developing time. For a developing time of 15 minutes at 20^0C. the speed of the film becomes 1250 ASA with a contrast gradient of 0.9.

Later, it was found convenient to use a smaller non-automatic camera with a shutter and a 35mm lens. This could be more easily manoeuvred and placed at different positions for photographing the discharge from different angles. The film used was, however, the same throughout.

2.6 The Intermediate Spark Gap

Since the 6KV pulse from the trigger amplifier was not sufficient to trigger the Marx generator, an intermediate gap was used. This switch consisted of a storage capacitor and a spark gap. Two rapid discharge condensers 1000pF each and 15KV working voltage of a very low inductance were connected in series between the high voltage and earth through a 1K resistance. The spark gap was made of two stainless steel hemispherical electrodes each of 2.5cm diameter. The earthed electrode was a hollow with a 3mm hole;this hollow space was filled with Tufnol having a central hole through which passed a 1mm diameter tungsten electrode which was connected to the trigger amplifier output. A barium titanate annulus with an inner diameter of about 1mm and an outer diameter of about 3mm was placed in the space between the earthed electrode and the tungsten wire.

The barium titanate was used to intensify the field, advantage

being taken of the fact that the reduction of electrical field in an insulator due to its dielectric constant can cause over volting of an adjacent air gap (Lavoie 1964). The high voltage applied across the gap was in the region of 25KV. Thus when this spark gap was triggered a 25KV pulse was transferred to the first stage of the Marx generator.

2.7 The Marx Generator

The Marx generator is a high voltage pulse generator which can be triggered. It consisted of condensers which were charged in parallel and discharged in series. Such a generator consisted of an array of n condensers C_0 and n switches between them, the condensers being charged in parallel through a number of high resistances up to a voltage V_0. The total voltage between ground and the output of the generator was zero. On closing all switches, the voltage over them adds and a resultant output voltage V is obtained across the output terminal which is equal to nV_0. V will decay within a time interval determined by RC. Fast switching is best realised by using spark gaps. Switching times and inductances are minimized by the use of small gap widths. The dielectric strength of a gap is determined by the electrode material, the kind of gas and its pressure.

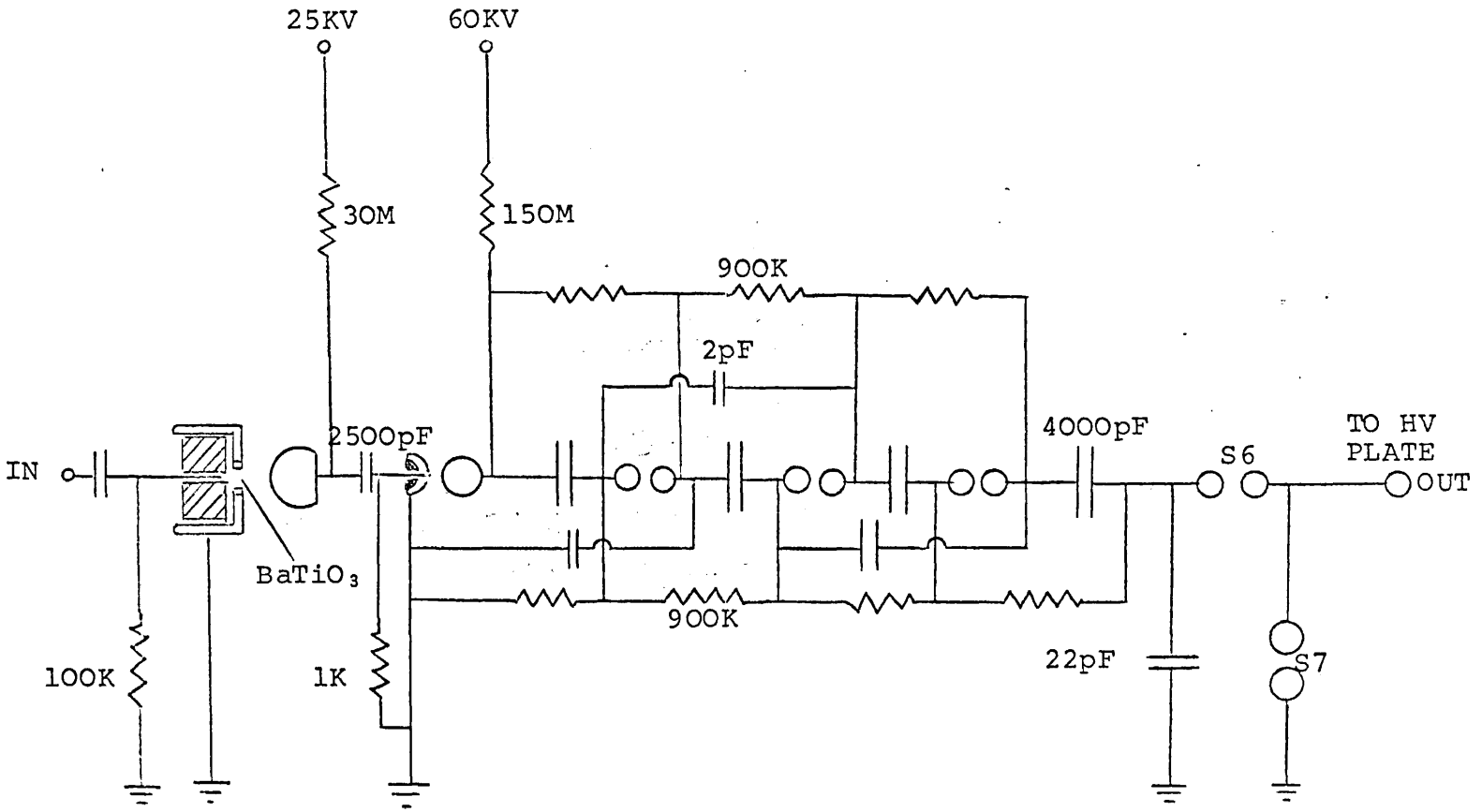

FIG. 2.7.1

The Marx Generator and Intermediate Spark Gap

When the first switch was closed (Fig. 2.7.1) by a trigger pulse, a step pulse of amplitude V was applied to the remaining gaps. To reduce the time lag between the first breakdowns the gaps had to be over volted by larger pulses. The use of a small value coupling condenser to couple adjacent stages allowed the second gap to be over volted by 100%, i.e. by V_0 independently of the number of stages.

The generator used in this work was described by Rice-Evans and Mishra (1969). It was capable of producing 240KV and it consisted of four stages using large paper condensers 4000pF each. The total inductance of the four capacitors was 0.8μHenrys; the working voltage of the charging resistors was 25KV and they were 20 watt resistors.

CHAPTER 3

Studies at High Voltages

3.1 Introduction

In 1972 while carrying out investigations into cosmic rays by means of a streamer chamber, I. Hassairi noticed some curious figures centred around the cosmic ray tracks in the chamber. These figures had the appearance of successively dark and bright rings on the inner surfaces of the perspex chamber as seen in Fig. 3.1.1a) and b). They always appeared spread radially from the track extremities. Sometimes they showed a spoked appearance reminiscent of the wellknown Lichtenberg figures. The discovery of these 'ringed Lichtenberg figures' was reported by P. Rice-Evans and I. Hassairi (1972) but no consistent investigation of their origin was attempted at the time.

In the present work, a study of these figures was conducted which, besides bringing to light the nature of their ringed structure, in some cases also posed some questions as to the validity of the generally accepted mechanism for the formation of positive Lichtenberg figures as described by many authors (Merril and von Hippel 1939, Loeb 1965, Nasser 1959, 1963, 1971).

A preliminary search through the extensive literature on gas discharges led to a comparison of the figures with the glow

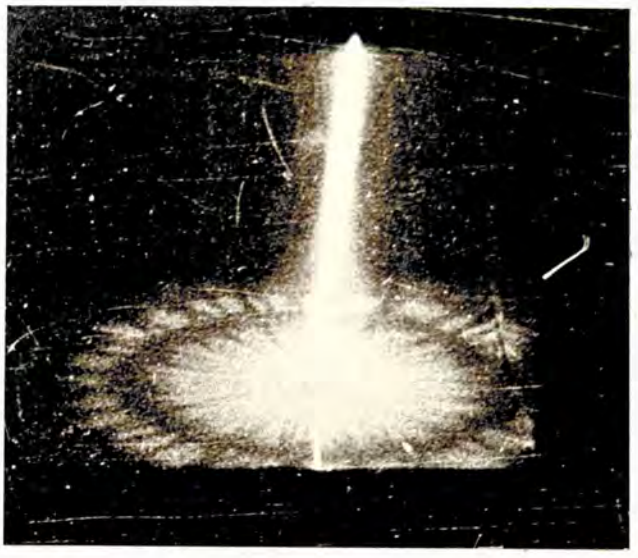

a)

b)

FIG. 3.1.1

Ringed Lichtenberg Figures arising from a Cosmic Ray Track

a) showing streamer channels b) unspoked figure

discharge where in the first instance similar dark and bright regions are present (Aston, Crookes and Faraday dark spaces, and the luminous cathode and negative glows and the positive column). Indeed, going somewhat further, the striations often found in the positive column of the glow discharge might also have provided an explanation for the rings observed.

However, the accepted description of the above two phenomena proved to be unsatisfactory to explain these rings for two reasons. In the first place, the glow discharge is produced by application of a d.c. voltage to the plates of a discharge tube containing a gas at low pressure and the subsequent appearance of the discharge is explained by the effects of space charge accumulation in the volume of the gas and at the electrodes. In the present case, a voltage pulse of duration in the region of 10μsec was applied to the chamber which would preclude space charge effects from setting in (Nasser 1971).

Secondly, if the phenomena had had any close relation to the mechanism of the glow discharge, then, by rearranging the external circuit variables and/or the gas pressure, the rings should be seen to be mobile over at least some ranges of these variables. This is observed to be the most common case for the positive column striations of the glow

discharge. This did not occur. The rings were always observed to be static relative to each other and to the chamber walls and very stable unlike the glow striations.

Another relevant fact is that the positive column striations of the glow discharge do not appear to have their origin in the fluctuations of the externally applied electric field, although there is still a great deal of controversy as to their actual origin (cf. Chapter 1, Section 1.5). They are more generally believed to be an intrinsic phenomenon associated with the dynamic properties of the gas.

While carrying out the latter part of the present work, it was found that the external circuit produced electric field oscillations which led to the formation of the rings and that these were therefore not entirely of the same nature as striations.

These initial considerations led to the work presented in the following sections where the effect of some obviously important variables such as the gas pressure, pulse length and voltage magnitude on the ringed figures was investigated.

During these preliminary studies it was concluded that a proper interpretation of the figure formation mechanism

required a knowledge of the exact shape of the voltage pulse applied to the chamber. This was found to be impracticable at the high voltages used because the radiated and mains borne interference made it impossible to observe the pulses on the oscilloscope and an alternative way of pulsing the chamber was attempted, which led to the results constituting the main body of this work.

3.2 The Effect of Pressure on the Rings

The first attempts at obtaining quantitative results on the phenomenon were directed at investigating the effect of the gas pressure on the radii of the figures. The discharge voltage could be set at a given value by fixing the Marx generator d.c. supply voltage at a specific setting. Sufficient time was allowed for complete charging of the generator for every discharge photographed. Consistency in the charging period was obtained by the use of the dead-time unit described in Chapter 2.

The failure to obtain the pulse shape on the oscilloscope due to radiation noise from the spark gaps of the Marx generator compelled the use of the d.c. voltage reading as a measure of the voltage applied to the discharge chamber. This value was quadrupled to obtain the average peak voltage output for the four-stage Marx generator.

This procedure could not lead to absolute values of the voltage applied as the actual output peak voltage would be higher due to overshooting. It did, however, yield a relative indication of the voltages applied. The analysis of the correct pulse shape and its relation to the d.c. supply voltage for the Marx generator used has been given by Mishra (1969).

Before each experiment the chamber was evacuated for periods of over twelve hours to ensure a high vacuum. The working gas (70% neon/30% helium) was then allowed to fill the system to the required pressure. A voltage was selected on the d.c. supply generator and this remained fixed throughout the experiment. The pulse shaping Lecher wire was also maintained at a fixed length throughout the experiment. This procedure ensured that only the pressure variation was responsible for the change in the radii of the figures. These showed the red-orange colour characteristic of neon and were photographed by the automatic camera described in Chapter 2. The black and white Ilford HP4 film used was developed in microphen.

At each pressure setting the number of exposures taken was of the order of seventy. This was necessary because the variation in the radius of the figure was quite large from discharge to discharge. This was not due to the statistical

variations of the underlying mechanism of the discharge under study (as was concluded from later work) but was possibly due to non-uniform ionization along the track of successive cosmic rays which would in turn strongly affect the size of the streamers merging to form the visible track. It is also conceivable that the output voltage of the Marx generator was rather irregular. This would be due to its construction based on four spark gaps. These can introduce quite a large statistical difference between successive output voltage levels. Whichever the cause, its origin was not pursued further.

After film development the rings' radii were obtained by placing the film through a photographic enlarger and measuring them by ruler. Scaling to actual size was easily done by comparing the photographic chamber of known size to its size as observed in the projected image from the enlarger.

The results obtained are shown in the graph of Fig. 3.2.1. A 1/p curve fit was computed which agreed closely with the experimental points. This choice of fit was taken because theoretical predictions indicate that this should be so at least approximately (Loeb 1955, Merril and von Hippel 1939). This is often the case in many types of gas discharges as the mean free path of electrons is related to the pressure

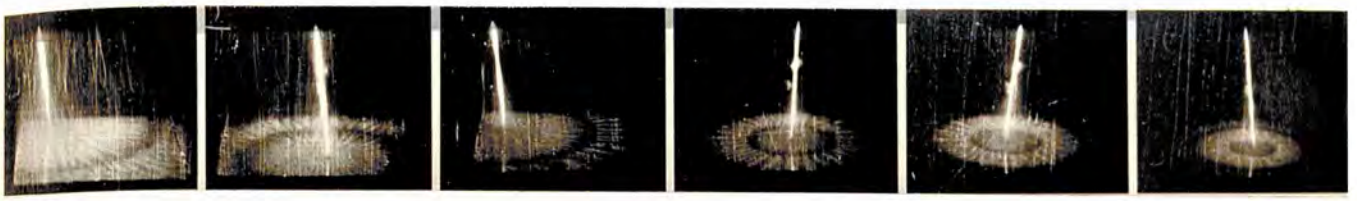

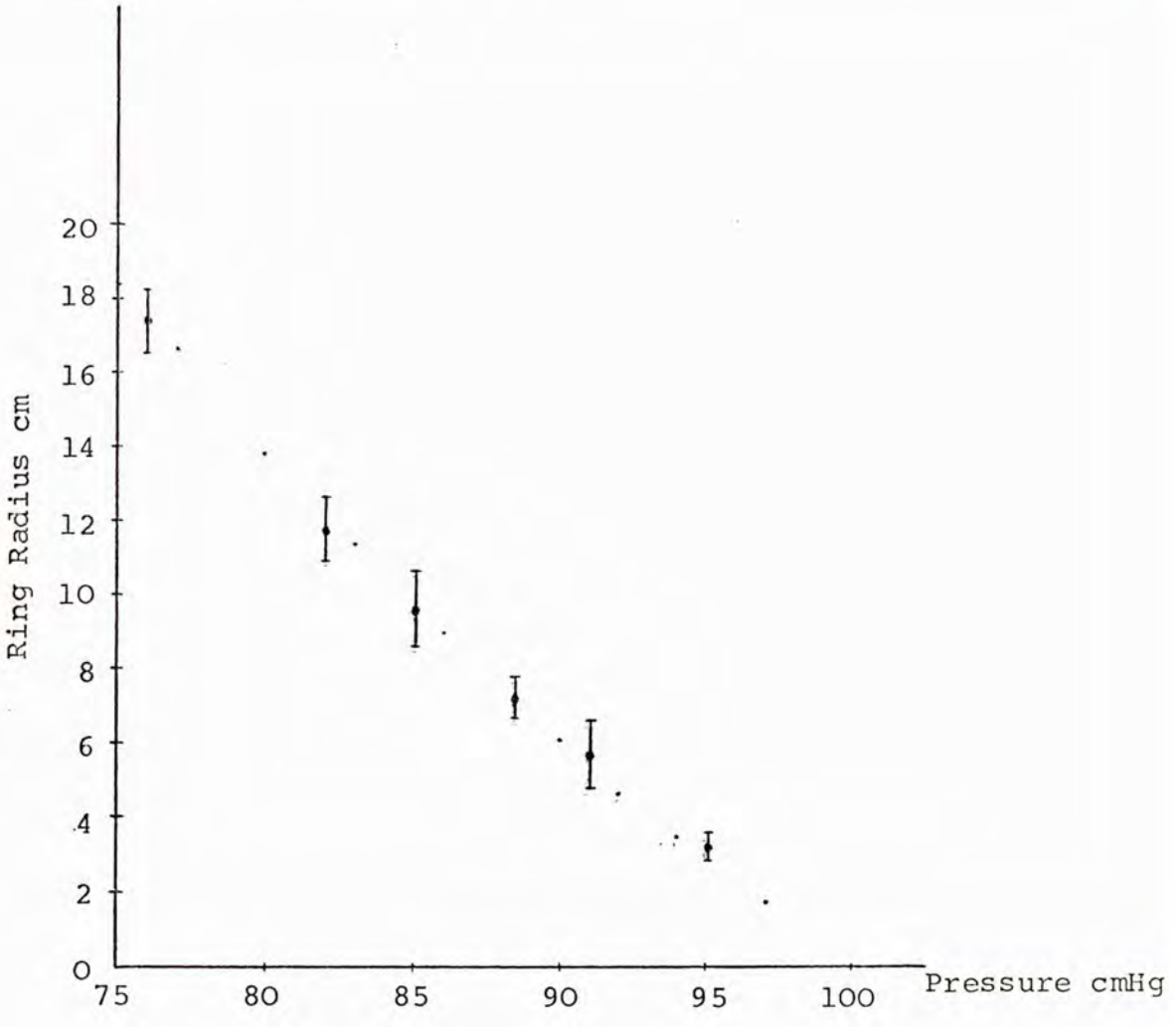

FIG. 3.2.1

The variation of ring radius with pressure. The isolated dots represent points of the theoretically fitted 1/p curve.

by an inverse relation obtained from kinetic theory. In some cases, however, this is not so, an example of this being the striated glow discharge where Wehner's law applies (Eq. 1.5.2.1). This predicts, as has been experimentally verified by many workers (cf. Francis 1956) that

$$\ell \propto 1/p^m$$

where m is a constant approximately equal to 0.5 and ℓ is the distance between neighbouring striations. This discrepancy in behaviour with pressure again presents a strong argument against the identification of the observed rings with the striations of a glow discharge.

3.3 Ring Radius Variation with Pulse Length

The pulse shaping system of the streamer chamber consisted of two parallel wires shorted at the far end. Fig. 3.3.1 shows the wire arrangement. The wires used were 2mm diameter copper wire. The inverted pulse reflected from the end cancelled the field in the chamber after a time controlled by the length of the transmission line.

For a parallel transmission line with an arbitrary impedence Z connected across the far end of the line the transmission coefficient is given by

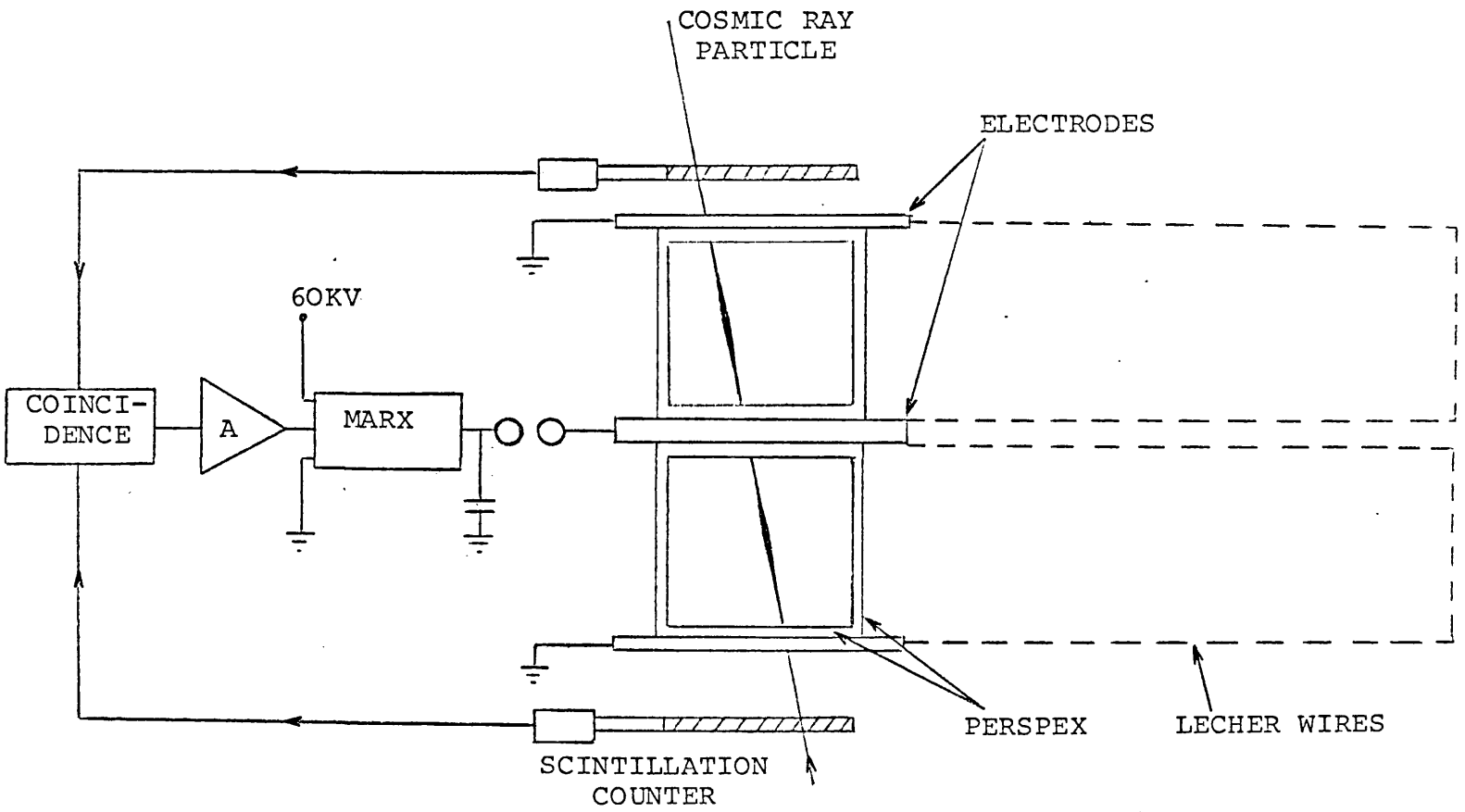

FIG. 3.3.1

High Voltage Pulse Shaping Arrangement using Lecher Wires

$$\rho = (Z - Z_0)/(Z + Z_0) \qquad 3.3.1$$

where Z_0 is the characteristic impedence of the line. In the present case the far end of the line was shorted, i.e. $Z = 0$, and so $\rho = -1$. Therefore the reflected wave was of the same amplitude as the input but opposite in sign.

The characteristic impedence of a parallel transmission line is given by

$$Z_0 = 276 \ln(d/a) \quad \text{ohms} \qquad 3.3.2$$

where a<<d (Lewis and Wells 1956). Here a is the wire radius and d is the separation. The conductors are assumed to be lossless and if embedded in a medium of relative permeability K_m and relative permittivity K_e the expression for Z_0 (which is given in ohms) must be multiplied by K_m/K_e. For a rectilinear line the inductance and the capacitance are given by

$$L = K_m Z_0/300 \quad \mu H/m \qquad 3.3.3$$

$$C = 10^4 \times (K_e/3Z_0) \quad pF/m \qquad 3.3.4$$

The transmission line used is referred to as a rectilinear uniform line because it consists of two parallel conductors of constant cross-section along the line. The velocity of

propagation is independent of frequency, in particular there does not exist any low frequency cut-off as in a wave guide. The speed of propagation is equal to that of a plane wave in an infinite volume of the dielectric (air) which filled the space between the conductors.

If T is the time delay per unit length then

$$T = (\varepsilon\mu)^{\frac{1}{2}} = 10/3 \times (K_e K_m)^{\frac{1}{2}} \quad \text{nsec/m} \qquad 3.3.5$$

From Eqs. 3.3.3 and 3.3.4

$$T = (LC)^{\frac{1}{2}} \quad \text{sec/m} \qquad 3.3.6$$

In the present case it was found that T = 3.3 nsec/m and that the line impedence Z_0 = 635 ohms.

Thus the pulse length on the chamber could be altered by changing the transmission line length and the study of the radius of the figures against pulse length was carried out for a given pressure and voltage. The results are shown in Fig. 3.3.2. Each line obtained corresponds to one of the rings of the discharge figure. From this, the speed of propagation could be estimated as the slope of the straight line graph obtained. Again each point obtained represents the average of about fifty different exposures. The Marx

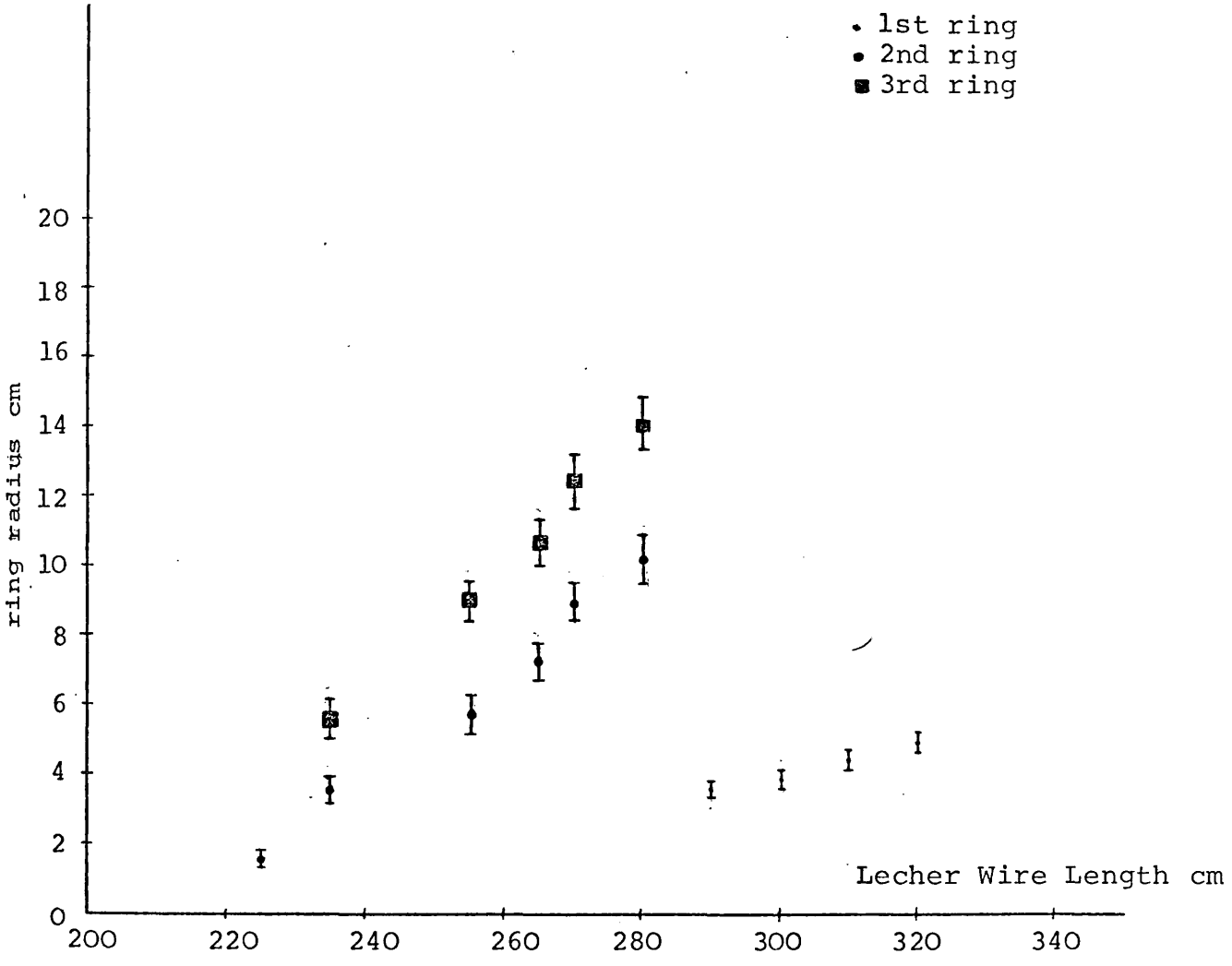

FIG. 3.3.2

The variation of ring radius with pulse length τ

τ = Lecher wire length/c (c = 3 X 10^8cm/sec)

generator was allowed to trigger at one minute intervals only by the use of the dead-time unit to ensure its charging to the same level.

It is seen that the diameter of the rings increases with increasing length of the Lecher wires in a linear fashion for the range of pulse lengths studied.

The speed obtained for the larger ring was from the slope of the graph of the order of 5×10^7 cm/sec.

3.4 Variation of Ring Radius with Voltage

It has been known for a long time that the radii of the Lichtenberg figures are proportional to the applied voltage (Anstey 1947). This fact has been used in engineering applications to measure very high voltages by using the Lichtenberg figure technique.

To verify whether this linear relationship was still effective in the case at hand an experiment was conducted at a fixed pressure and Lecher wire length (i.e. pulse length) while the d.c. supply voltage for the Marx was varied. This, as has already been mentioned, could not supply an absolute indication of ring size with voltage as the actual pulse applied to the chamber would overshoot this d.c. level

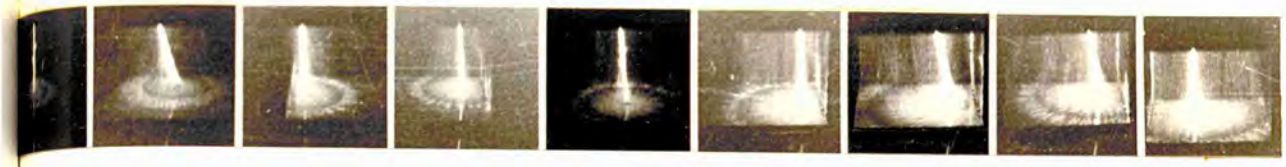

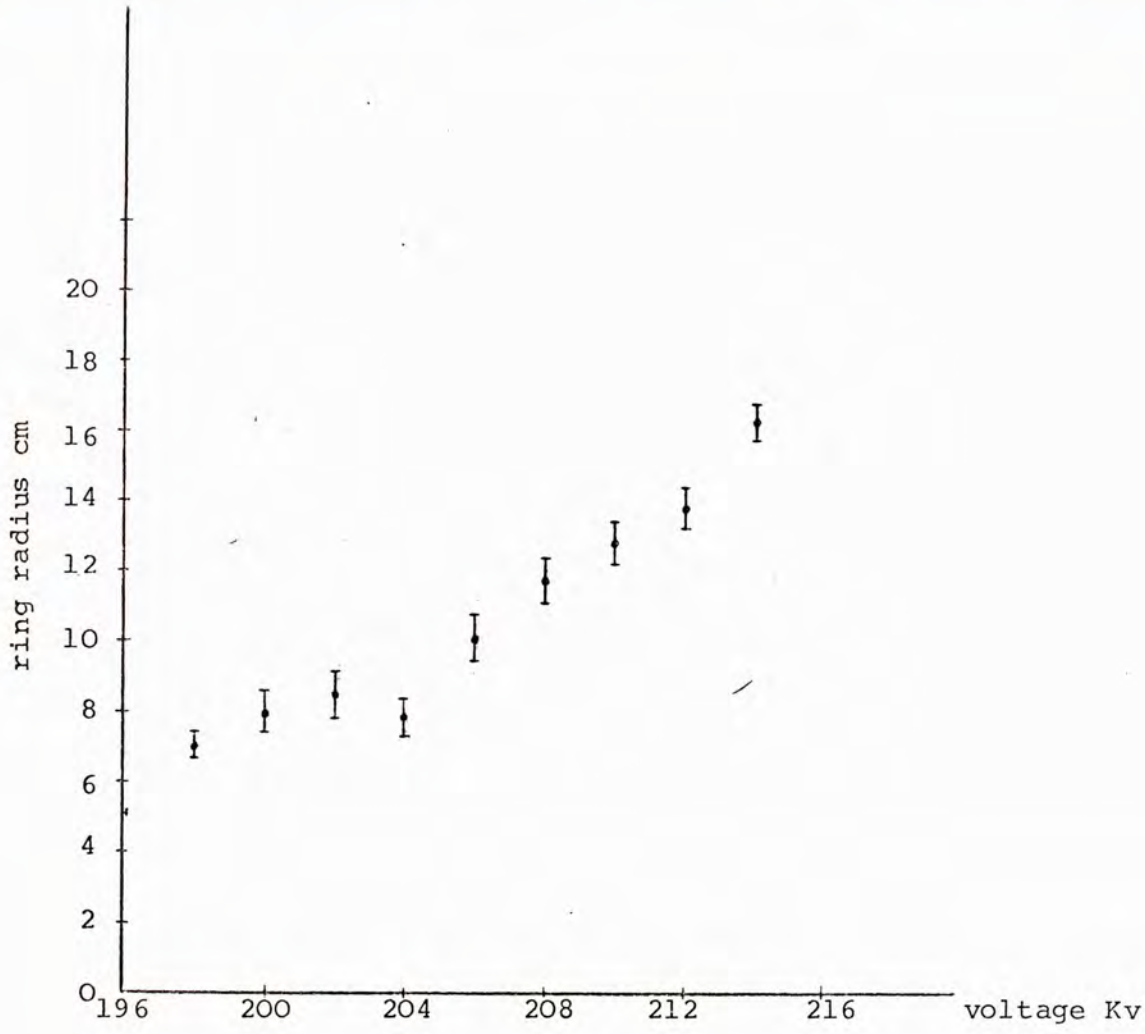

FIG. 3.4.1

The variation of ring radius with voltage.

by some undetermined amount. It did, however, show the correct relation between radius and voltage.

The range of voltages used was of necessity restricted, because the Marx generator could only be triggered in this small range without a lengthy readjustment of the four spark gaps used in its construction. The results obtained are shown in Fig. 3.4.1.

The graph shows a nearly linear increase of radius with voltage but a small fall and rise above this linear behaviour can be detected. It may be significant that in the results published by Merril and von Hippel (1939) the same sort of behaviour can be seen although no comment is made to the fact. No inference as to its cause can be made in this work.

3.5 Speed of Formation of the Lichtenberg Figure

It had been observed by P. Rice-Evans and I. Hassairi (1972) that when two ringed figures were simultaneously created on the dielectric surface of the chamber floor, they 'interfered' in the manner shown in Fig. 3.5.1. This is presumably caused by the cancellation of the electric field in a region of two approaching streamer tips of the same polarity.

FIG. 3.5.1

Two incoming cosmic ray particles produce simultaneous tracks in the streamer chamber and the corresponding ringed Lichtenberg figures are seen to 'interfere' with each other.

As has been mentioned, radiation noise from the Marx generator spark gaps precluded the observation of the exact shape of the voltage pulse applied to the chamber. If speeds of formation of the discharge were to be obtained, one needed to know the time development of the pulse and be able to compare it with the spatial development of the discharge. A method based on the observed interference of two simultaneously formed figures was devised, whereby their speed of formation could easily be obtained without the need to know the exact voltage pulse shape.

In the process of attempting to explain the ring formation mechanism one was led to investigate whether the cosmic ray track in the chamber could be modelled by a conductor which shorted the chamber capacitance and therefore allowed complete breakdown to occur even at the low voltage (earthed) electrode (the figures were observed at both ends of the tracks).

For this purpose a wire was placed centrally in the chamber and the voltage pulse applied to it. The result was the ringed figure shown in Fig. 3.5.2a) and b) where the cosmic ray track is absent. This immediately suggested that the figures could be obtained at will by automatically triggering the voltage generator without the necessity of waiting for cosmic ray particles to start it off.

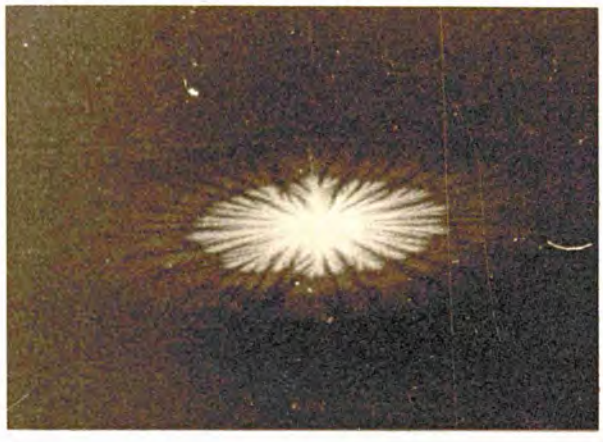

a)

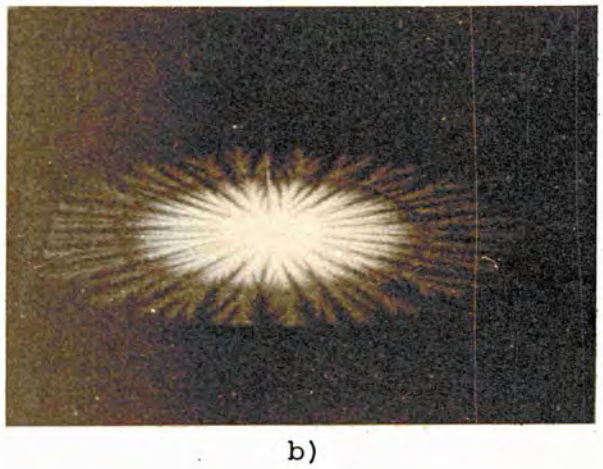

b)

FIG. 3.5.2

The ringed Lichtenberg figure caused by a wire placed centrally in the chamber to simulate the cosmic ray track.

a) negative polarity b) positive polarity

a)

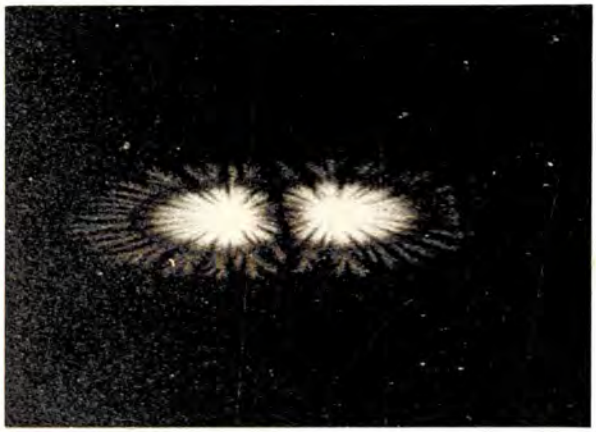

b)

FIG. 3.5.3

'Interfering' ringed Lichtenberg figures

a) negative polarity b) positive polarity

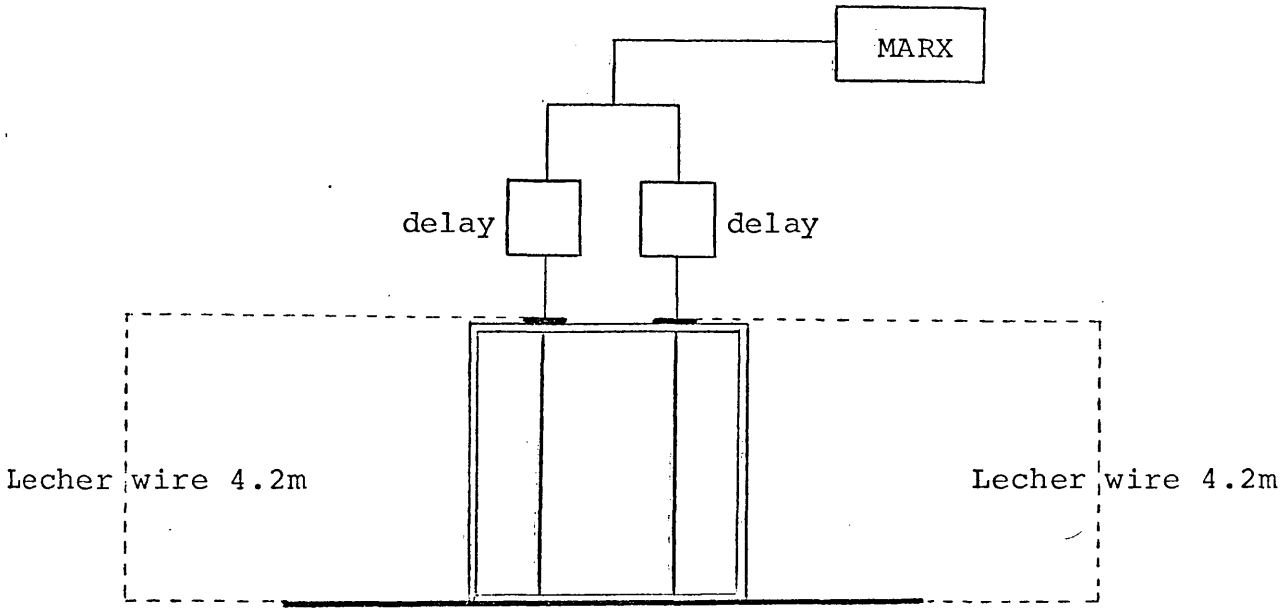

FIG. 3.5.4

The arrangement for the determination of the speed of formation of the figures by 'interference'.

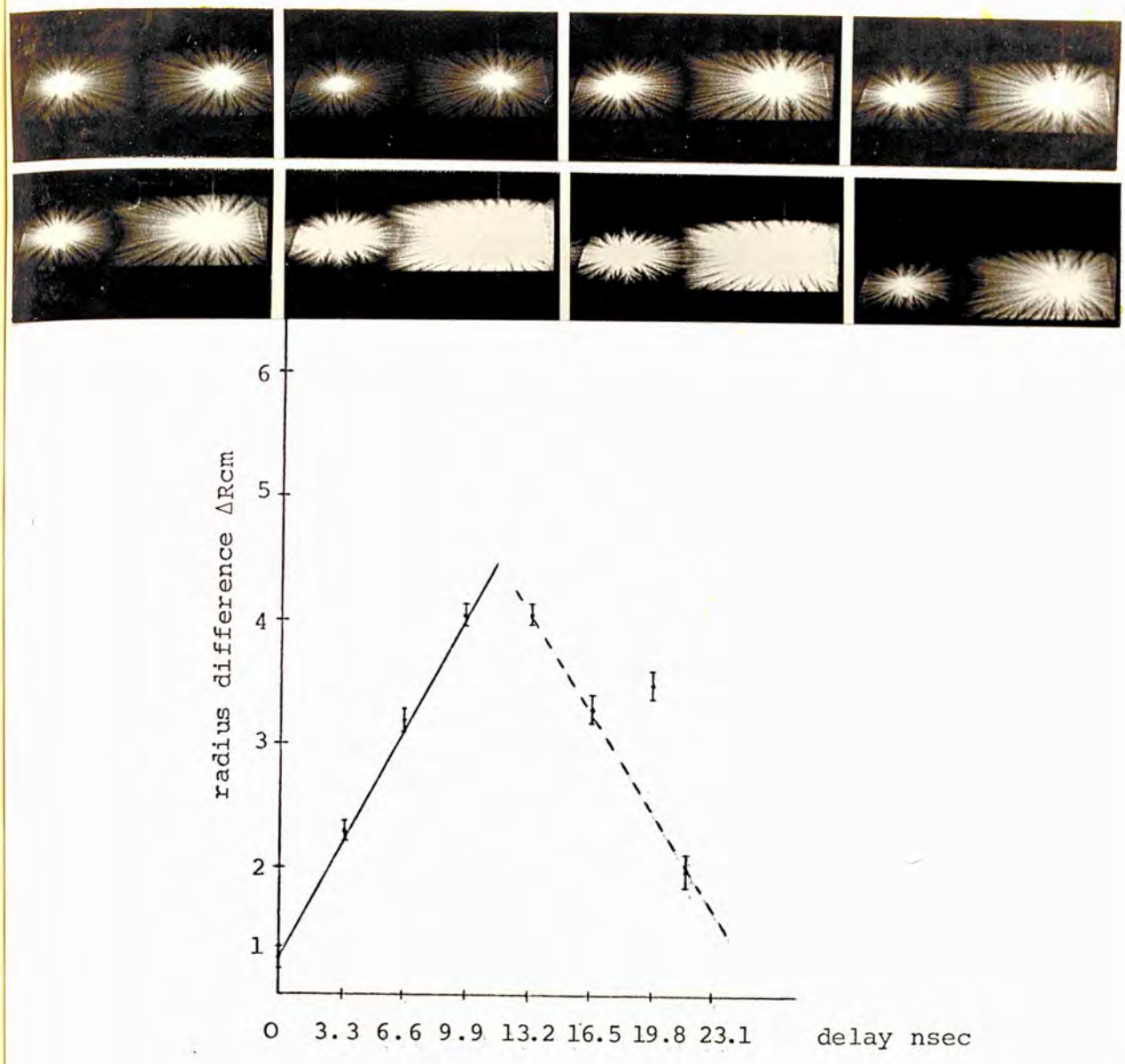

FIG. 3.5.5

Graph of the relative change of radii of 'interfering' figures with applied voltage pulse delay.

the Lecher wire and back. In the present case the Lecher wire length was 4.20m, which corresponds well with the observed peak of the curve of Fig. 3.5.5.

The speed obtained for the formation of the positive figure by this method was 2.7 X 10^8cms/sec. This is in good agreement with observations by other investigators (Nasser 1971, Raether 1964).

It can be observed from the photographs of Fig. 3.5.5 that after the peak is reached the figures start to overlap instead of showing the dark 'interference space'. This happens only when the delay between the approaching streamer tips is exceeded by a few tens nanoseconds and is an indication of the lifetime of the excited states producing the radiated light (red-orange colour) characteristic of the gas mixture used (helium 30%/neon 70%).

3.6 Other Observations at High Voltage

During attempts to attain some quantitative results regarding the size of the field between the plates, a straight wire probe was placed between them, its other end being connected to the CRO through a HV probe. This did not yield any significant results but instead caused distortion of the field between the plates and when the Marx was discharged

many complicated discharges appeared in the chamber. Some of these are shown in Fig. 3.6.1. A few of them have the appearance of 'Christmas trees' and the interference dark spaces abound as well as heavy branching even from the distorted cosmic ray track. These discharges occurred both on the side walls of the chamber and on its bottom and top surfaces.

At the start of this work, some thought was also given to deciding whether the rings could have been the result of a magnetic field produced by the current of the discharge cosmic ray track. This was not strongly believed because it was known that the currents are small as the volume of the gas is insulated by the dielectric perspex making up the chamber. However, it was decided to place a wire in the chamber spanning its height and terminating in a loop at the chamber bottom. The figure obtained is shown in Fig. 3.6.2. These qualitative observations did not lead to any significant understanding of the mechanism of ring formation, but they are curious enough in themselves to be mentioned.

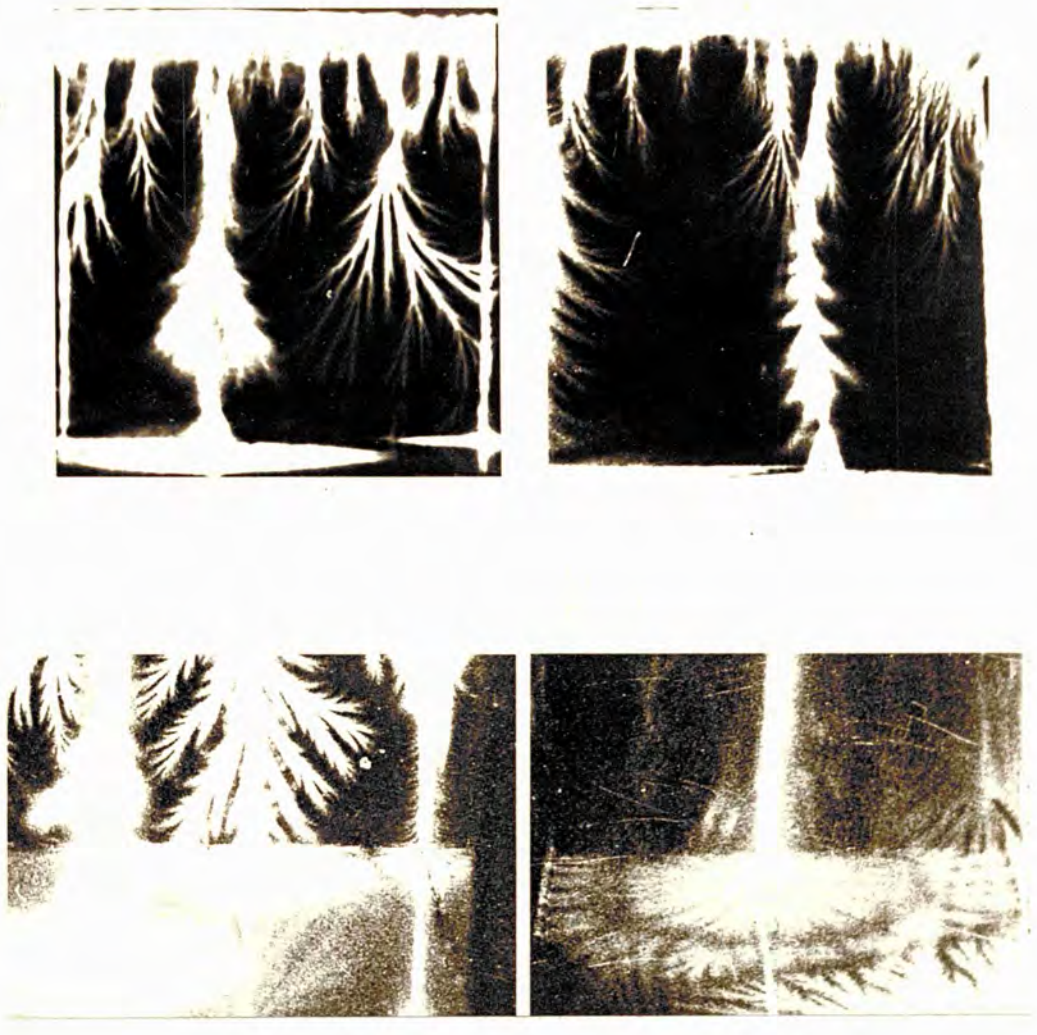

FIG. 3.6.1

Discharges observed with a highly distorted electric field between the electrodes.

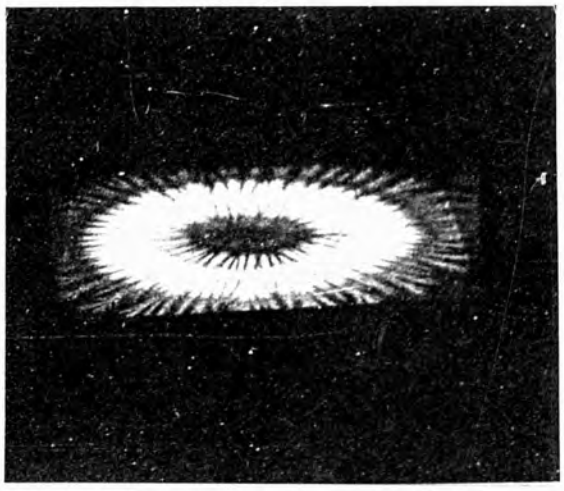

FIG. 3.6.2

The appearance of the discharge from the track simulating wire terminated by a loop.

CHAPTER 4

Studies at Low Voltage

4.1 Introduction

The use of the Marx generator to produce the required voltage pulse for the ringed Lichtenberg figure formation had the great disadvantage of making it impossible to observe the pulse on the CRO because of radiation noise from the Marx four spark gaps.

Many quite fruitless attempts were carried out to somehow diminish this interference and enable, in this way, the observation of the expected voltage pulse on the scope. Screening by means of a well constructed Faraday cage was considered impractical and costly due to the large area occupied by the experimental apparatus. ()

One of these attempts consisted of taking the CRO to a room distant from the experimental laboratory and using a doubly shielded coaxial cable to bring the pulse applied to the chamber into the input of the oscilloscope. Both shields on the cable were earthed for these experiments. It was found, however, that although this caused some decrease in the spurious spikes and oscillations present on the scope screen it did not clarify the pulse shape and had to be abandoned.

Resistive and capacitive probes were also used in the attempts to monitor the high voltage pulse. With the series/parallel spark gap arrangement (cf. Chapter 2) a resistance chain was used. The output pulse was fed to a Tektronix 581A oscilloscope after attenuation, first by a resistance dividing (1/10) chain, and then by a 1/1000 H.V. probe (P6015). Noise and both mains borne and radiated interference still prevented the pulse from being seen; instead, a ringing noise was observed every time the Marx fired. With the Lecher wires used as a pulse shaping network (i.e. the chamber was part of a transmission line) a capacitive divider was used (Fig. 4.1.1). Such a probe could be mounted just inside the ground plate of the transmission line, in this case the earth chamber electrode.

The probe was made of thin aluminium foil mounted between two perspex rings, the output lead being taken through a hole in the earth electrode. The capacitive division was equal to the distance between the earth electrode and the aluminium foil divided by the distance between the chamber electrodes. This was 2mm/200cm = 1/100. The pulse was therefore attenuated by 1/100 by this probe, which was followed by an additional resistive divider of 25 ohms/ 1000 ohms = 1/40. Thus the total attenuation was 1/4000. A 1000 ohm resistor was connected in series with the output so that the pulse was not severely differentiated by the

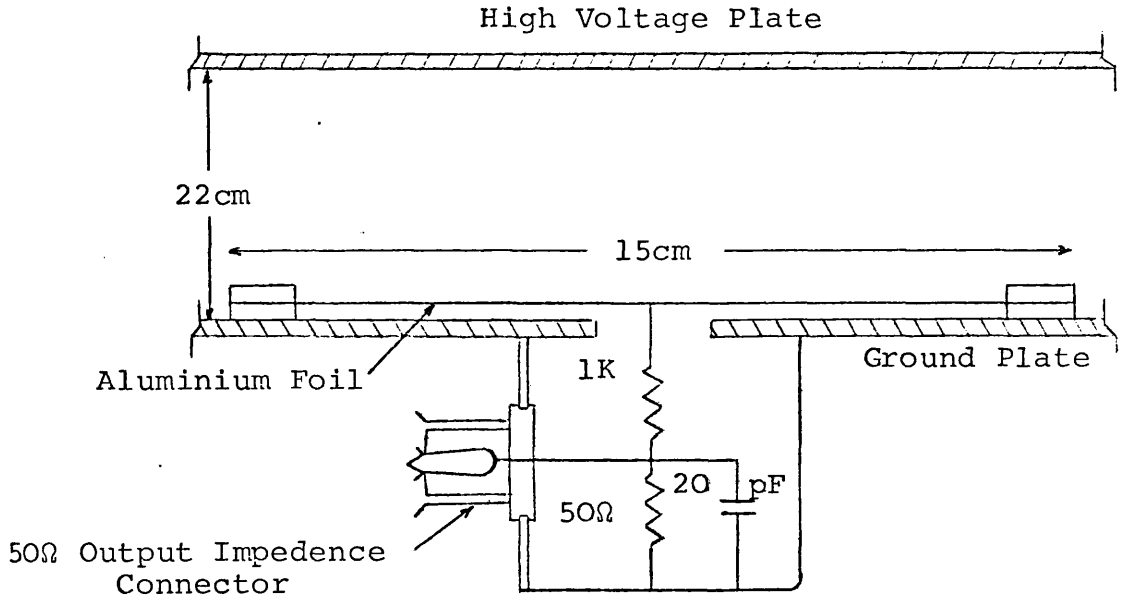

FIG. 4.1.1

The Capacitive Probe

probe capacitor across the 50 ohms cable terminated by 50 ohm resistors at both ends.

Capacitive probes tend to ring. An important source of the ringing of a capacitive probe mounted on a transmission line is the difference in wave velocity in the dielectric of the probe and that of the transmission line. There are two ways of solving this problem: either by using the same dielectric in both the probe and the transmission line (Bulos et al 1967) or by making the thickness of the metallic conductor of the probe less than the skin depth as suggested by Gygi and Schneider (1964). In this work the first method was adopted and the same dielectric (air) was used in both the probe and the transmission line. Using this pulse attenuation arrangement radiated interference prevented the pulse from being observed.

At this stage there was still a great deal of uncertainty as to whether the noise was coming in through the mains or actually consisted of radiated noise from the discharged gaps. The behaviour of the observed complex signal on the scope was quite capricious and this did not help in deciding which of the above two effects was most responsible for producing the observed interference. The CRO used a separate screened mains line and filter to eliminate possible mains borne interference, but this did not always

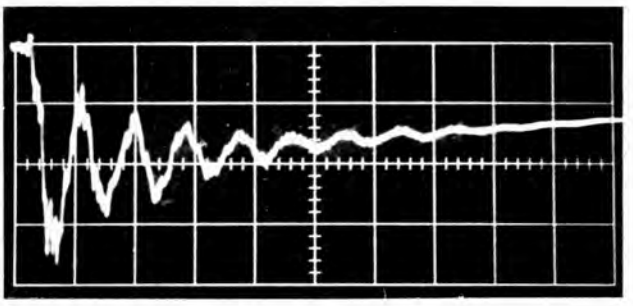

a)

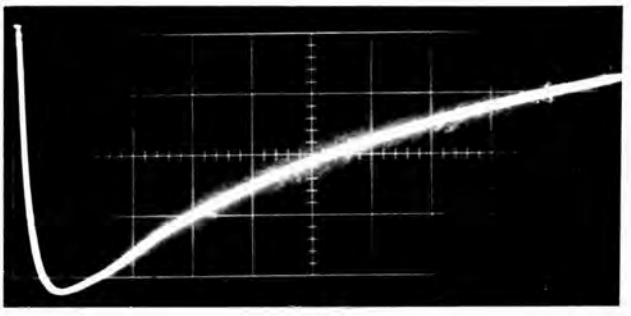

b)

FIG. 4.1.2

Two negative voltage pulses obtained with the low voltage circuit. (200 ns/division, 5KV/division).

seem to be carrying out its function. On other occasions its function seemed quite proper.

The Marx generator was started by an 'intermediate' triggered spark gap as explained in Chapter 2. While trying to identify which section of the generator was causing the greatest noise, one was led to apply the pulse from this 'intermediate' gap directly to the chamber, excluding the Marx generator altogether.

It was found that with this single gap the pulse could be observed on the scope and also that similar ringed figures appeared on the chamber base and lid when the shorting track simulating wire was in position inside the chamber. The pulse observed from this arrangement was similar to the one shown in Fig. 4.1.2a).

The work presented hereafter was possible on the basis of such single spark gap circuit being able to yield the same kind of figures as were under study. It made it possible to relate the ringed figures to the voltage pulse and the success of many other related observations.

4.2 The Low Voltage Circuit

The circuit used for all the following observations is shown in Fig. 4.2.1.

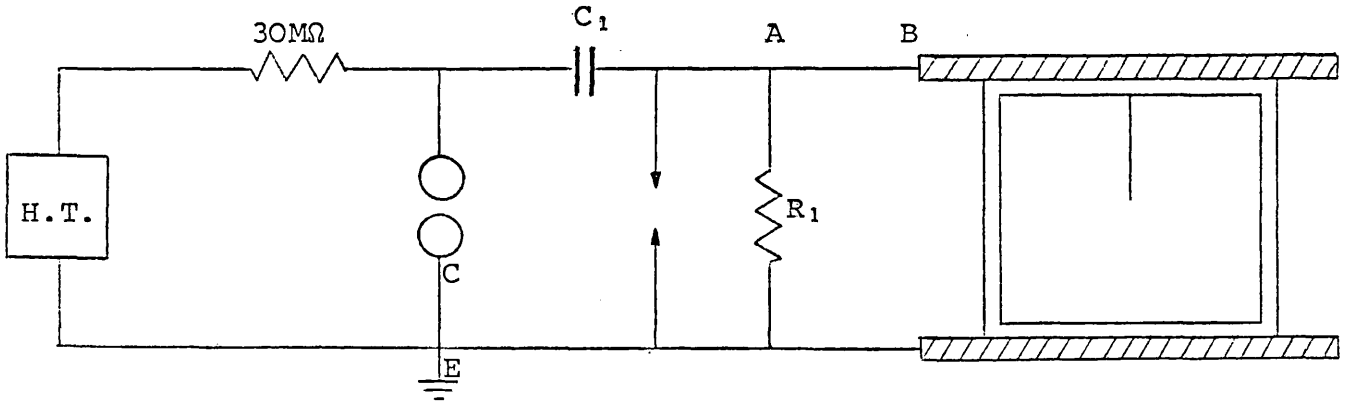

FIG. 4.2.1

The Low Voltage Circuit

A spark gap consisting of two spherical electrodes of 2.5cm diameter was used to produce the pulse and both the capacitor C_1 (typical value 0.001μF) and resistor R_1 (typical value 5KΩ) controlled the rise and decay time of the pulse. A typical pulse from such a circuit is shown in Fig. 4.1.2a).

No theoretical analysis of such a circuit was attempted as a great number of variables which were important in the mathematical derivation of the resultant pulse could not be accounted for. These included stray capacitances and inductances as well as the inductance and capacitance of the firing spark gap. The pulse shape and frequency of oscillation could be altered by changing the value of R and/or by introducing variable inductances in the connecting link (AB) from the capacitor to the chamber. Similar circuits giving rise to rippled pulses of somewhat longer duration than the one produced by this circuit have been described by Kuffel and Abdullah (1970).

By experimentation it was found that a small resistor of the order of 100 to 200 ohms placed between the usually earthed sphere and earth of the spark gap (CE) could wipe out the superimposed oscillation on the pulse which then had the form shown in Fig. 4.1.2b). When this was done and the pulse applied to the chamber, the alternatively

light and dark rings on the Lichtenberg figure were seen to disappear. This observation proved conclusively that the rings were associated with some sort of pulse oscillation, a fact which had so far not been verified, although it had been suspected.

The noise background produced by such a circuit on the CRO was very low and pulse monitoring could be carried out quite simply by the use of a high voltage probe from the chamber high voltage plate to the scope.

4.3 Observations on the Rings

Using the circuit described in Section 4.2, many observations of the way the rings behaved with the change of pulse shape were made.

By closing the spark gap the figure was seen to diminish in diameter and the number of rings was increased. At the same time, the pulses showed a decrease in height and an increase in the number of oscillations (this being clearly due to the change in the gap capacitance and inductance). Thus, a small pulse height, not surprisingly, decreased the size of the figure and more oscillations caused a greater number of rings to appear.

Although this was quite a significant observation, one still did not know at this stage which ring was associated with which peak of the pulse. The first ring was always a bright one and from this it was expected that the peaks of the pulse were responsible for the luminous rings while the troughs corresponded to the dark rings.

To be able to correlate each ring with the part of the pulse producing it, another gap was included in the circuit as is shown in Fig. 4.1.1. This spark gap consisted of two moveable needle electrodes and its function in the circuit was to short out the applied pulse at any required time after its application to the chamber. This shunting spark gap thus chopped the pulse at different points by having its width varied accordingly (Fig. 4.3.1a) and b)).

Chopping in this way was quite erratic, but it nevertheless allowed observations to be made to decide on the above question (whether the luminous rings corresponded to voltage peaks or not). It was concluded that the peaks of the pulse were indeed responsible for the bright rings, whereas the lower voltage dips gave rise to the dark spaces.

To improve the shunting gap operation attempts were made at producing some preionization in the vicinity of the gap by means of a suitable radioactive source, and also by

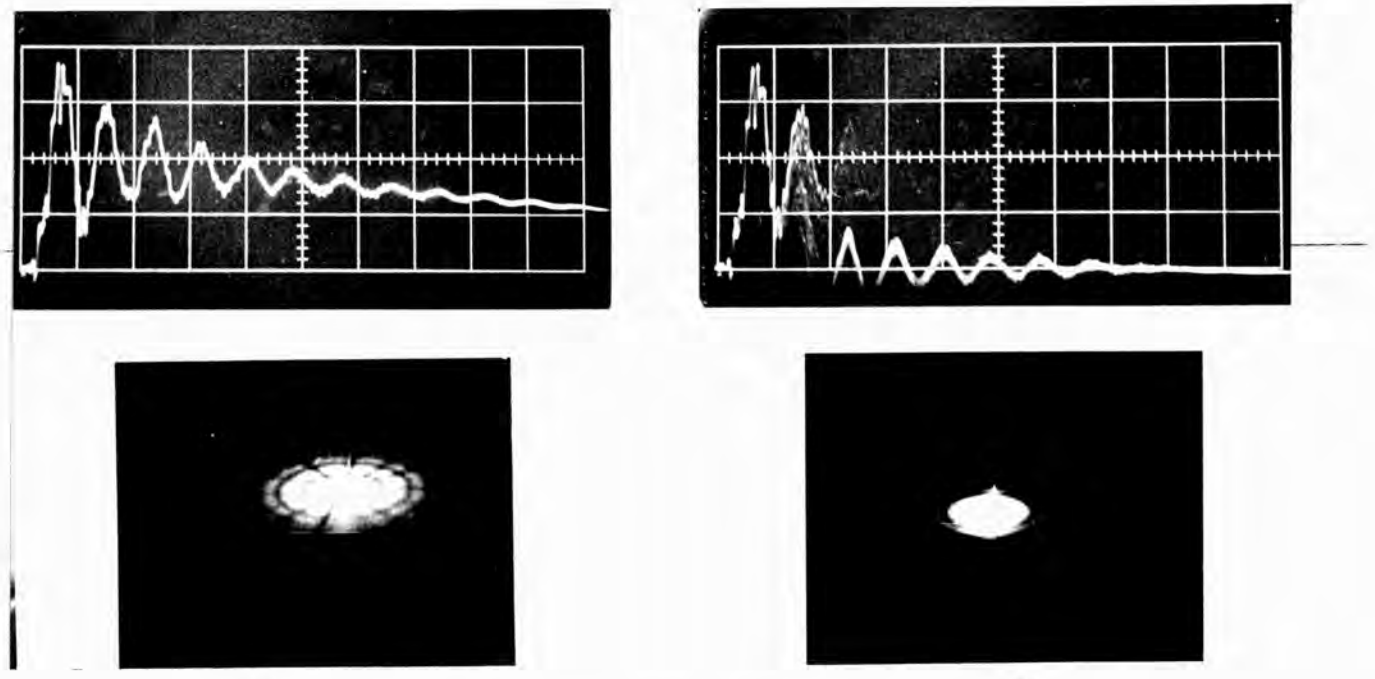

a) b)

FIG. 4.3.1

A voltage pulse of positive polarity and corresponding ringed figure in He/Ne.
a) unchopped b) chopped
(200nsec/division, 5KV/division, pressure = 34cmHg)

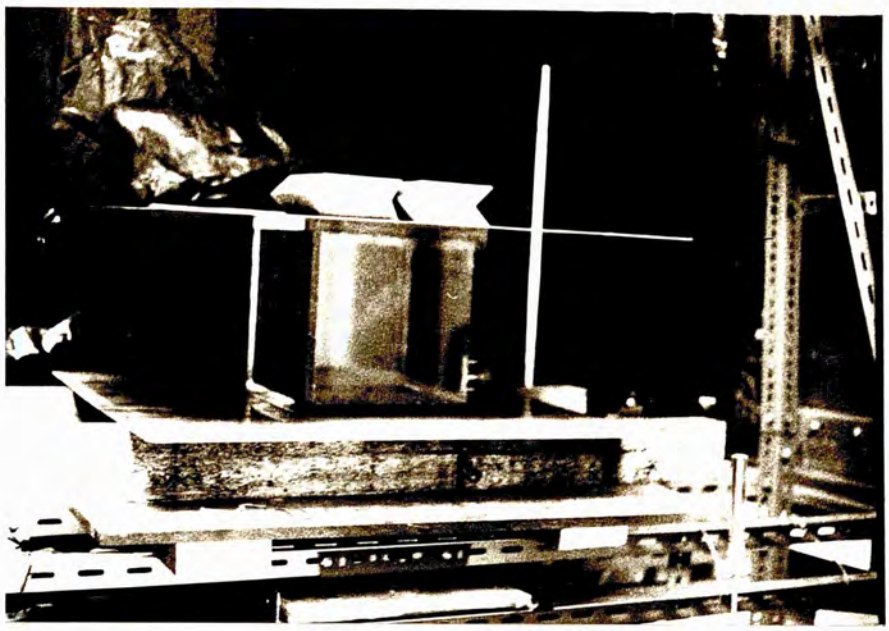

a)

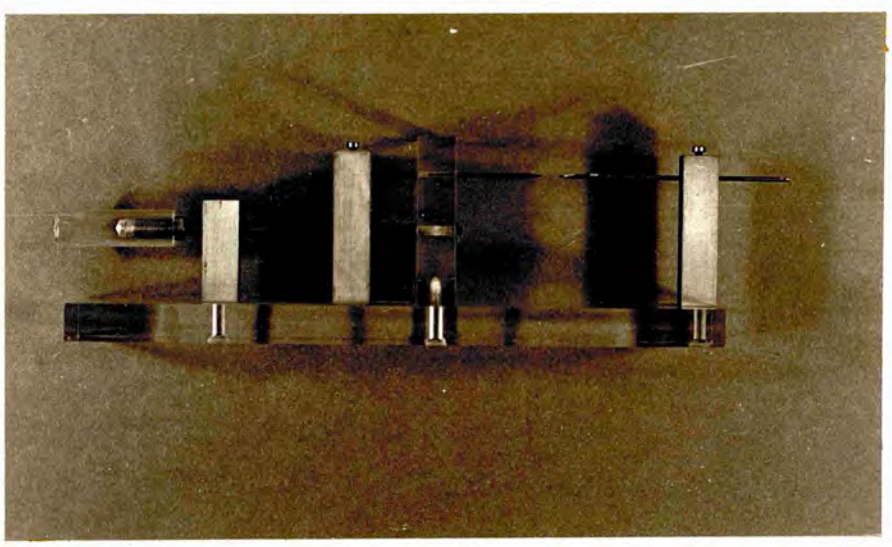

b)

FIG. 4.3.2

The perspex chamber a) and shunting spark gap b).

having a sharp needle point nearby connected to a d.c. voltage supple, thus producing a continuous corona discharge. This improved the chopping to some extent, but finally it was decided to build a spark gap with accurately designed electrodes which were finely sharpened and aligned. This is shown in Fig. 4.3.2b). With this shunting gap, an accuracy within 50 to 100 nsec in the chopping time was achieved which was quite sufficient for one's purpose.

Another observation which was not pursued further was connected with the pulse rise time. With the pulse shown in Fig. 4.1.2a) the observed figures showed quite distinctly straight branches which were in turn ramified themselves. When the rise time of the applied pulse was lengthened, the branches lost their straightness and snaked rapidly over each other. These moving branches were broader than the usual ones, and could not be successfully photographed owing to their incessant motion. Also, they were much less branched than the ones obtained with fast rising times. No explanation of these was attempted in this work.

4.4 Pressure and Low Voltage Variation of Ring Diameter

The low voltage circuit allowed a greater control of pulse shape to be achieved because of its simple form. Setting the spark gap at a given length permitted the d.c. supply

voltage to be raised causing an increase in the frequency of successive discharges applied to the chamber. This frequency could be made quite high (20-30 per second) and made visual observation and photographing of the discharges a much easier task. The higher the frequency (or d.c. supply voltage) the brighter and more permanent did the discharge appear. Increasing the d.c. voltage in this way did not affect the pulse shape or its height as this was solely determined by the breakdown potential of the circuit sphere gap and the other circuit parameters. This breakdown voltage is fixed by quantities independent of the d.c. level applied (e.g. gap width, pressure, gas type).

The difficulties in measuring the ring diameters at the high voltages were not present with the low voltage circuit. The high voltages allowed only a single discharge per exposure and under low voltages and higher pressures the developed film showed rather faint negatives which made difficult the measurement of the ring diameter. This was due to the lower light emission from the discharges under these conditions.

The low voltage circuit, however, produced successive discharges which could be repeated with great accuracy. Many exposures could be superimposed on a single frame of the film, thereby increasing the developed image definition.

The reproducibility of the figures was remarkable. The boundaries of the rings were just as sharp for multiple exposure photographs as for a single exposure, showing an almost complete absence of statistical spread. This is not in agreement with observations on streamers as it is known that they show a large spread in range (Raether 1964, Loeb 1965).

It was decided to take advantage of this reproducibility to obtain more concrete results on the variation of ring radius with pressure and voltage. Experiments were therefore carried out at several pressures and voltages and at each stage pulse monitoring was also carried out. This allowed velocities to be accurately measured by extracting the time information from the oscillograms.

The procedure for each experiment was similar to that already described for the high voltage work. Evacuating of the chamber was carried out over a period of several hours, and before evacuating was completed the circuit would be switched on at high discharge frequency, first at one polarity and then at the opposite, to ensure complete de-absorption of gas molecules from the chamber walls. The vacuum was always observed to decrease once the discharges were started and to revert to its previous higher value after half an hour or so.

The spark gap was polished before each experiment as pitting occurred in the course of many discharges and made triggering more difficult and irregular. A smaller hand camera was also used instead of the automatic camera to photograph the discharges because its flexibility made it easier to position and photograph at different angles.

The results obtained are shown in Fig. 4.4.1 and Fig. 4.4.2 where radius variation with pressure and voltage are plotted respectively. No standard deviation bars are plotted because each point already corresponds to a statistically averaged radius of about 30 or so discharges. The reproducibility of the discharges was so great that statistics were irrelevant. The appearance of the discharges corresponding to one curve of each of the graphs of Figs. 4.4.1 and 4.4.2 are shown in Fig. 4.4.3 and Fig. 4.4.4 respectively. The spoked appearance of the figures became more apparent at the higher voltages and pressures while at low values of these quantities the figures have a smeared out appearance.

By combining the results on Fig. 4.4.2 and the times measured from the oscilloscope traces the speeds of formation at various voltages were obtained. These are shown in Fig. 4.4.5.

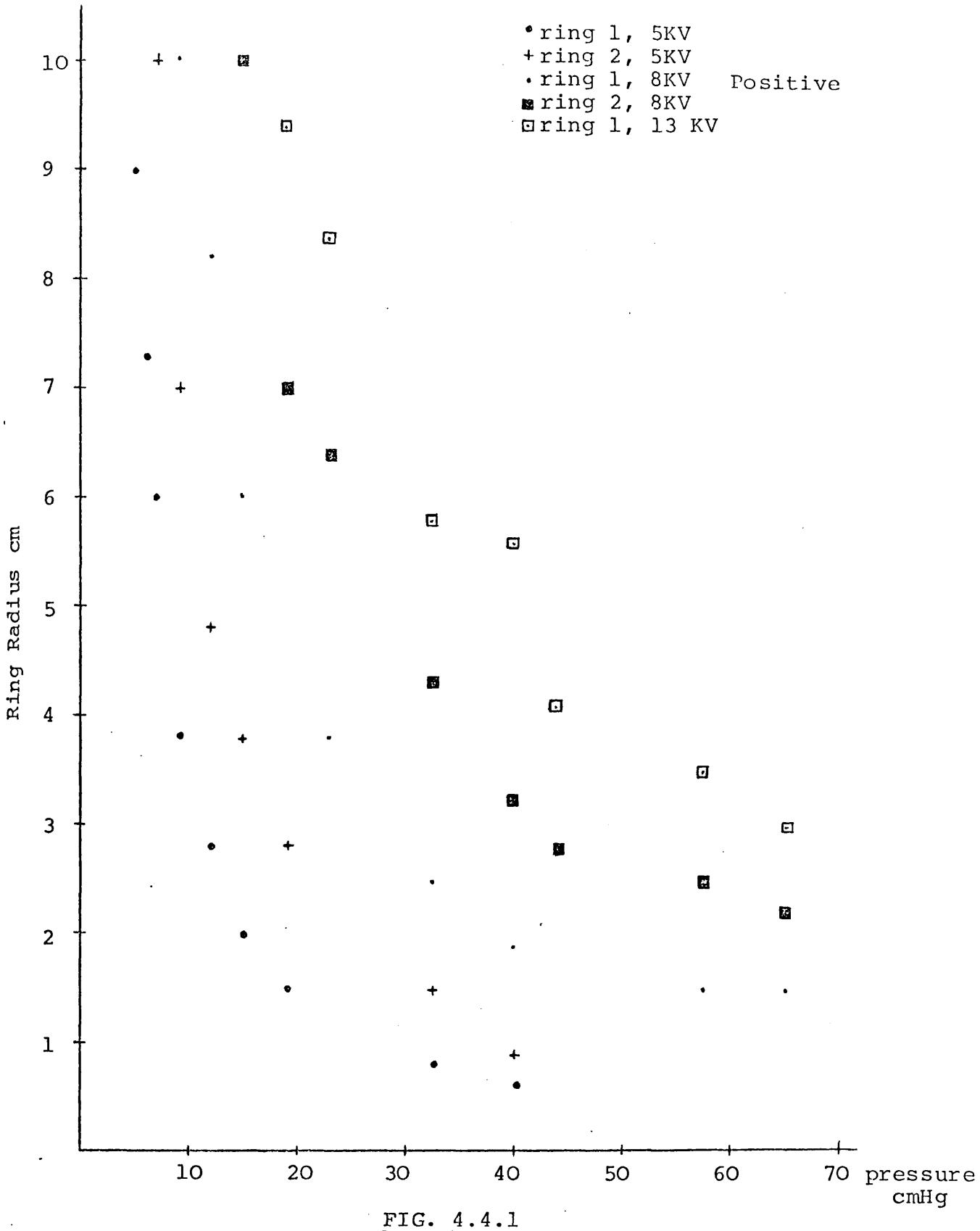

FIG. 4.4.1

The variation of figure radius with pressure.

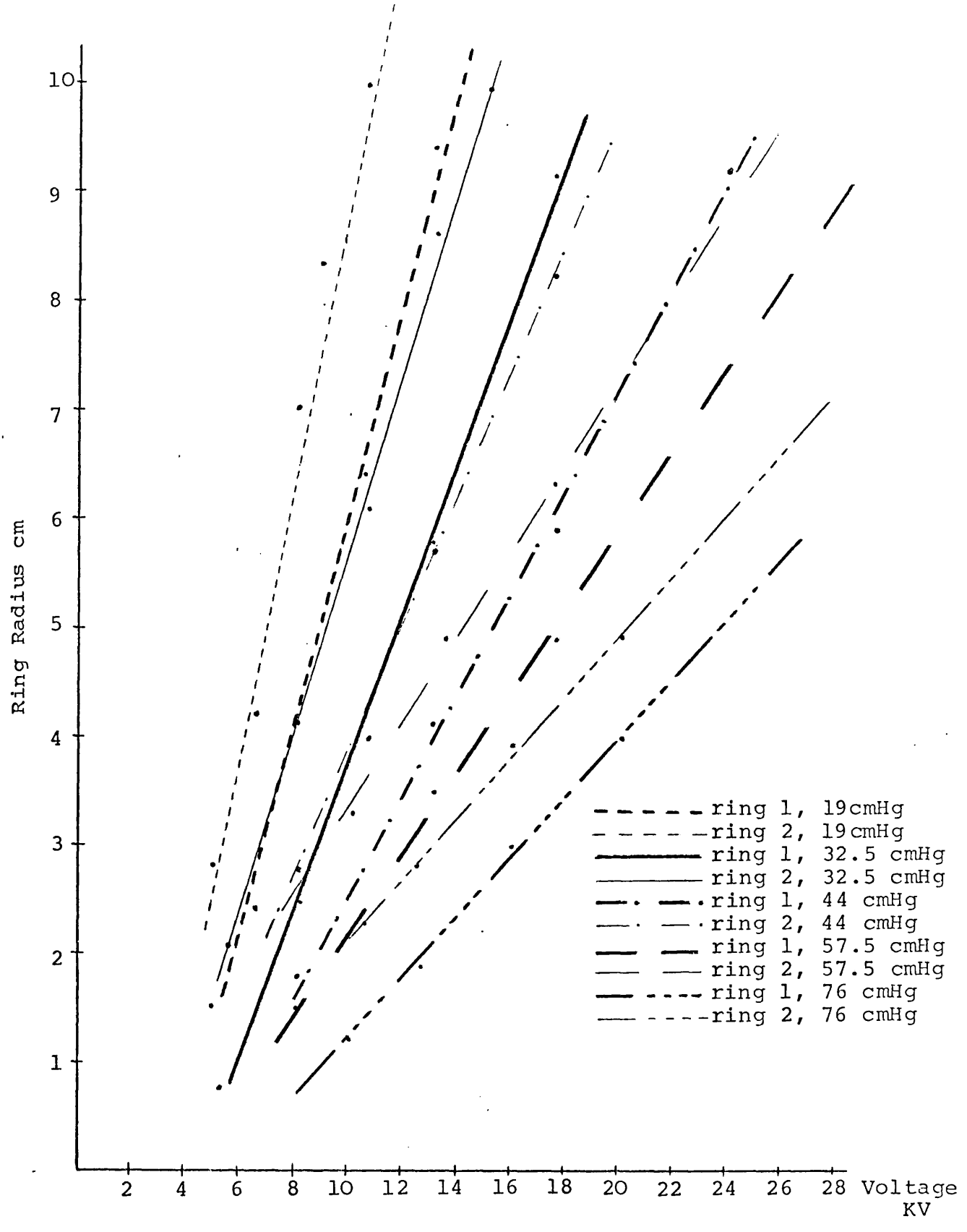

FIG. 4.4.2

The variation of ring radius with voltage.

FIG. 4.4.3

The'ringed Lichtenberg figures' used to obtain the plots of Fig. 4.4.1.

FIG. 4.4.4

The 'ringed Lichtenberg figures' used to obtain the plots of Fig. 4.4.2.

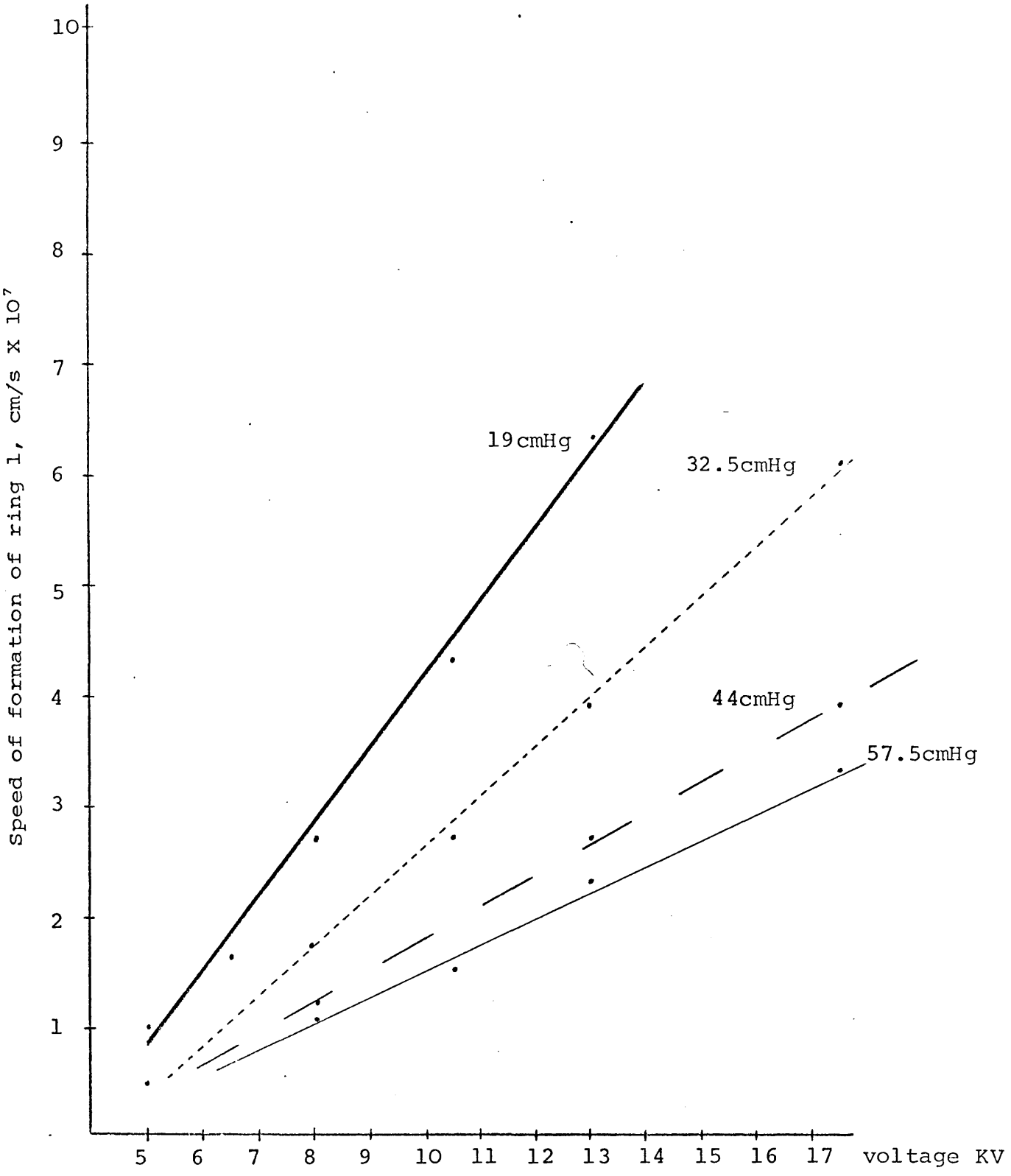

FIG. 4.4.5

The variation of speed of formation of ring 1 with voltage at various pressures.

4.5 The Effect of the Oscillating Pulse in Air

Much of the work done on the study of corona discharges using the Lichtenberg figure technique has been done for air. This is because in the first instance it is freely available, and secondly because in engineering problems involving electrical discharges air is almost exclusively the gas concerned.

Atmospheric air consists of approximately 21% oxygen and 78% nitrogen, the former being strongly electronegative. Electronegative gases have atoms one or two electrons defficient in their outer shell and tend to easily capture one electron, thereby filling the outer shell of the atom and forming a singly charged negative ion. Helium, neon and other rare gases do not have this tendency and are known as free electron gases.

The behaviour of an electronegative gas, even when present as a small impurity in another gas, differs appreciably from that of the free electron gases where electrons can move freely without being captured by atoms or molecules.

The above reason compelled the use of air in the chamber to verify whether the rings could be a specific form of discharge in He/Ne and would possibly be absent in a gas which generally presents a different sort of behaviour under breakdown conditions.

The usual evacuating procedure was carried out and air allowed to enter the chamber at a pressure of about 50cmHg. A pulse of 20KV peak voltage was then applied to the chamber. No visible discharge could be detected. Increasing the pulse height to about 30KV still did not cause any visible manifestation.

The pressure was then slowly decreased while the voltage pulses were applied to the chamber at a moderate frequency. Some dim light started to appear at about 5cmHg and when the pressure of 0.6cmHg was reached the appearance of the figure was as shown in Fig. 4.5.1a). The pulse applied was of negative polarity and of a form similar to that shown in Fig. 4.1.2a).

The discharge in air still showed the rings which were accompanied by strong thick branches which apparently initiated from the outermost bright ring. Two of these branches can just be observed to the left of the figure (Fig. 4.5.1a)).

When a pulse of the same form as the above but positive polarity was applied the discharge had the appearance shown in Fig. 4.5.1b). These were smaller in diameter and did not show the strong branches of the negative figure.

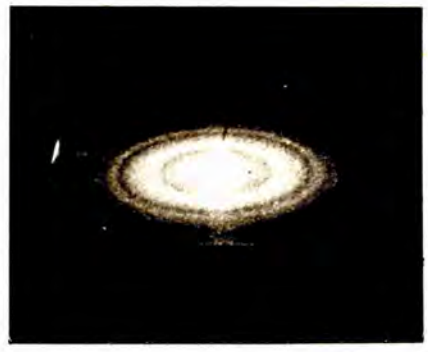

a)

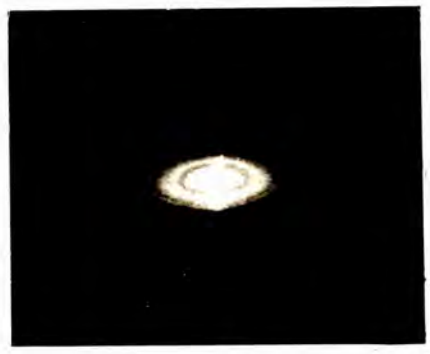

b)

FIG. 4.5.1

The 'ringed Lichtenberg figures' in air.

a) negative b) positive

The presence of the rings both in air (electronegative) and in helium/neon (free electron gas) must indicate that whatever the mechanism responsible for the formation of the rings, it cannot be due to any extent to negative ion formation.

CHAPTER 5

The Columnar Discharge

5.1 The Point-to-Plane Geometry

The use of the shunting (chopping) gap in the work described in the foregoing chapter enabled one to associate each bright ring with the corresponding peak of the voltage pulse, and it was concluded that this higher voltage was responsible for the increased ionization and accompanying excitation, giving rise to the observed higher light output of the bright rings.

It has been known for a long time that the Lichtenberg figures have their origin in the light emitted from discharges occurring in the gas close to the surface of a dielectric or photographic plate. Because the streamers associated with these branched discharges form a 2-dimensional pattern on a plane surface the Lichtenberg figures are also often called 'glide figures'.

The work of Merril and von Hippel (1939) on the interpretation of the Lichtenberg figures showed conclusively that the patterns produced on photographic plates were due to the faint light emitted by the discharge branches as they passed over the film.

This interpretation was later also put forward by Nasser and Loeb (Loeb 1963). To explore the nature of the figures they placed a microscope slide of a soda glass 1.2mm thick in contact with the photographic plate of a point-to-plane geometry. It was found that those branches which headed towards the glass passed over it. The light from the streamers was still faintly visible, but diffused and attenuated by the glass and its distance above the film. The streamers having passed over the glass again came down to the film surface and continued in the air near it.

This kind of behaviour was also observed during the course of this work. When a slab of perspex was placed in the chamber with the shorting wire in contact with its upper surface, the branches of the figures were seen to propagate over this surface, turn over the edges of the slab and go down vertically to the bottom of the chamber where again they spread horizontally.

It had also been observed at the time of Merril and von Hippel's experiments that it was possible to see discharge figures on plane glass plates by application of high voltage pulses to the point of a point-to-plane geometry and that these could be made visible even after several days by breathing on the surface of the glass. These are known as breath-figures.

They were also observed during the course of this work. After application of the Marx voltage pulse to the perspex plate in air, at atmospheric pressure, figures similar to the Lichtenberg figures were observed once a condensation film on the surface of the perspex was created.

The observation of these breath-figures, which are clearly caused by some permanent arrangement of dielectric charges on the surface of the dielectric, led one to speculate whether the observed rings had their origin in space charges so accumulated on the dielectric and whether these had any influence on successive discharges.

As a result it was decided to shorten the wire inside the chamber (Fig. 4.2.1). If the rings observed were indeed associated with any effect caused by the dielectric, this new geometry could strongly affect the observed pattern. Fig. 5.1.1a) and b) shows two views of the discharge obtained with an 8cm gap between the wire point and the dielectric surface. Quite remarkably the dark rings became dark spaces in the column. Lengthening the gap to 16cm allowed many dark spaces to be photographed in the column (Fig. 5.1.2a).

These had a similar regular appearance to striations and yet, in contrast to that d.c. equilibrium condition they result from single field pulses. These discharges were

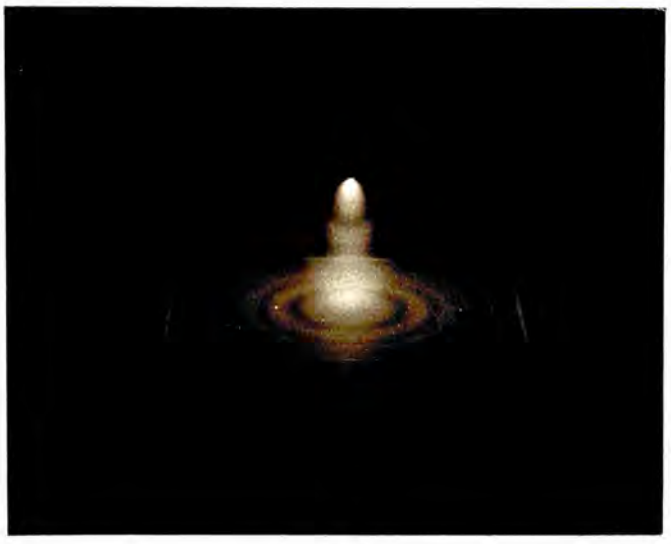

a)

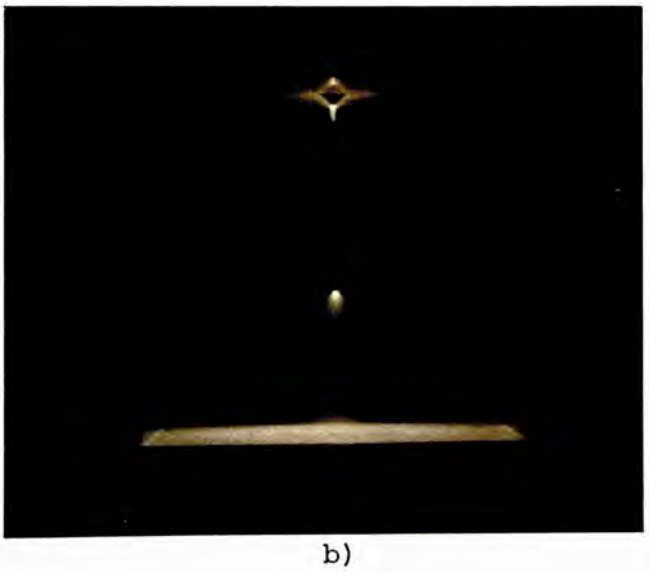

b)

FIG. 5.1.1

Two views of the same discharge with a point-to-plane geometry and an 8cm gap (50cmHg, 9KV).

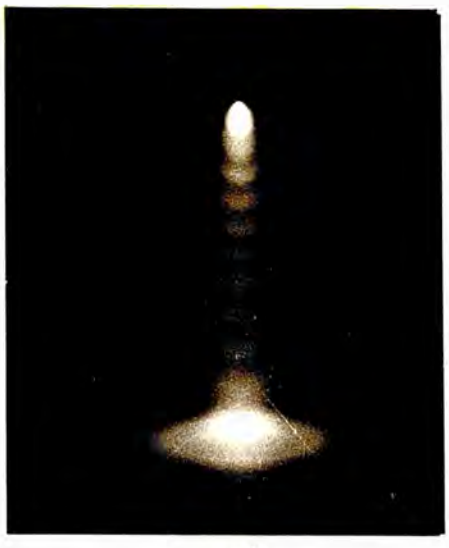

a)

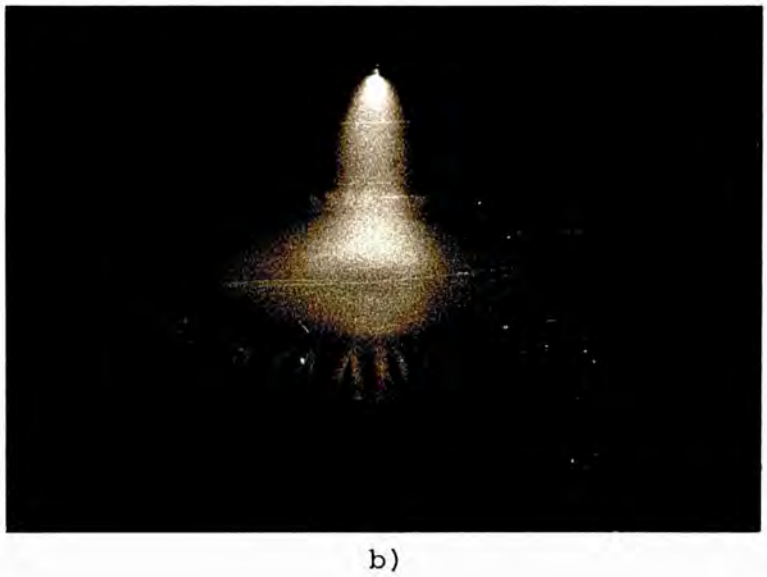

b)

FIG. 5.1.2

a) View of the discharge with a 16cm gap.

b) Branches originating from a sharp ring boundary.

clearly visible to the naked eye but because of the lack of film sensitivity they were photographed by allowing multiple exposures (about fifteen) to superimpose on each film frame.

The pattern observed could be repeated with extraordinary lack of statistical variation as can be seen from the photographs; the sharpness of the layers was maintained even after many discharges had been photographed in a single exposure.

It is known that streamers exhibit large random fluctuations in length (Rice-Evans 1974, Nasser 1972, Raether 1964). Nevertheless, these are not observed in the present discharges. This is shown even more clearly by the photograph shown in Fig. 5.1.2b). Here the unmistakable branches due to streamers propagating from the clearly defined sharp ring can be observed. This photograph was obtained at a higher pressure than the previous photographs, thus reducing diffusion and causing individual radial branches to be seen. It was also observed that heavier branching occurred at higher pressures.

The sharpness in the rings and layers of these discharges is not unique. It is also observed in the striations of the glow discharge positive column; however, the mechanism whereby

the velocities of all the electrons are reduced to approximately zero at the same point has never been wholly explained (Penning 1957, Francis 1956). It is probable that in some gases the formation of negative ions plays some part in it, but this cannot be extended to all gases, especially to the rare gases, where electron attachment does not occur.

5.2 The Striated Column

After the observation of how the dark rings became dark spaces in the column by shortening the wire in the chamber, application of a voltage pulse without the high frequency oscillations superimposed was tried again to see whether the striations were indeed caused by these oscillations or by a mechanism similar to the usual striations of the positive column of a glow discharge.

The discharge appearance obtained is shown in Fig. 5.2.1a). ig. 5.2.1b) shows the corresponding applied voltage pulse.

The striations were not present as had already been ascertained for the case of the rings and this observation again precluded a mechanism of the kind proposed for the glow discharge striations. Effects due to space charge accumulation could also be ruled out on the basis of the

a)

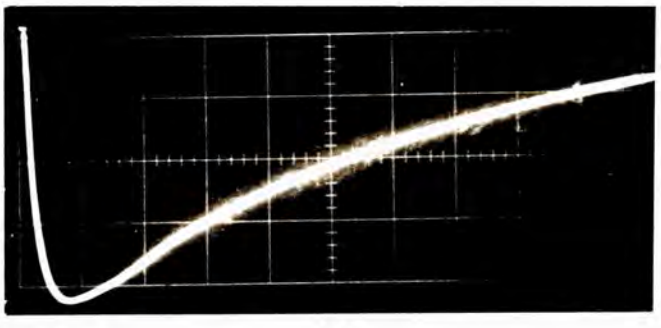

b)

FIG. 5.2.1

A non-striated columnar discharge (a) produced by application of a voltage pulse without the high frequency oscillations superimposed (b).

short duration of the pulse which was less than 10 μsec. This, however, did not exclude space charge effects due to accumulated charges in the gap from previous discharges.

To this effect, a d.c. clearing field of 90 V/20cm was applied to the chamber. By rapidly discharging the circuit to maintain the discharge in the chamber and switching the d.c. clearing field on and off, any effect due to the drift of charges could be observed. The results were negative. No effect could be detected even when the polarity of the d.c. field was changed.

To ensure that enough time was allowed for even massive charged particles (ions) to be completely cleared, each of the fifteen or so discharges which made up a visible photograph were separated by a time interval of 60 seconds.

The same permanent pattern was obtained, and it was concluded that if indeed space charges existed permanently in the gap, they were not responsible for the pattern.

Triggering of the discharge with a short wire had always been quite temperamental. It was always easier for a negative pulse on the wire than for the opposite positive polarity, but still not flexible enough for one's purposes. To be able to initiate the discharge at will, a short 20μm

diameter gold-plated tungsten wire was attached to the point electrode. This greatly improved triggering, presumably by electron field emission from the wire tip in the case of the negative point.

5.3 Chopping the Discharge

With this easily-triggered arrangement, the shunting gap was then used to short-circuit the chamber and thus arrest the high voltage pulse after chosen periods. Fig. 5.3.1a) and b) shows the discharges from a negative and positive point corresponding to the arrested wave forms shown in Fig. 5.3.2.

In Fig. 5.3.1a) with a negative polarity on the wire, it is clear that one peak of the oscillation gives rise to one bright patch; two peaks to one dark space; three peaks to two dark spaces, etc. Similar, but not identical arrested discharge patterns are seen in the case of a positive point (Fig. 5.3.1b)).

At the voltages used, because luminosity was low, about 15 independent exposures were needed with HP4 film in the open-shuttered camera. In the case of the negative point the discharge could be initiated at will, presumably by electron field emission from the wire tip. In the negative wire case

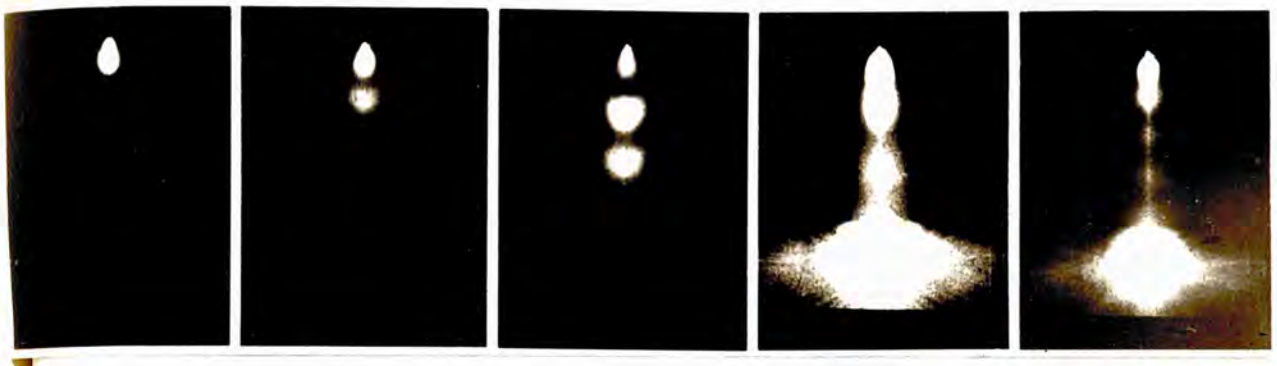

a)

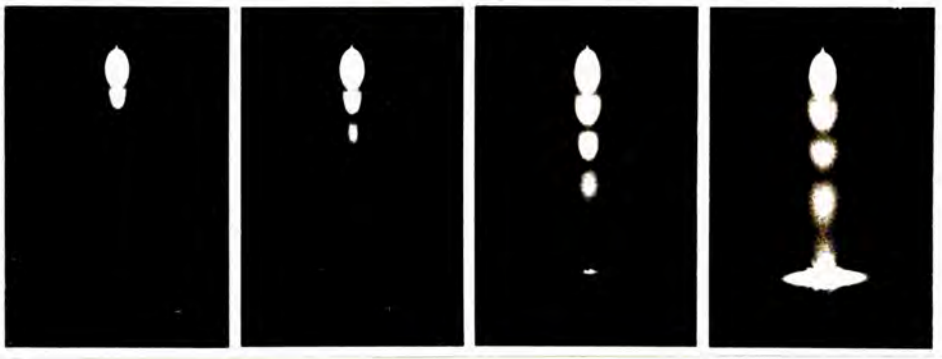

b)

FIG. 5.3.1

Discharges arrested after chosen periods with a negative point (57cmHg, 17KV) a), and with a positive point (71cmHg, 20KV) b).

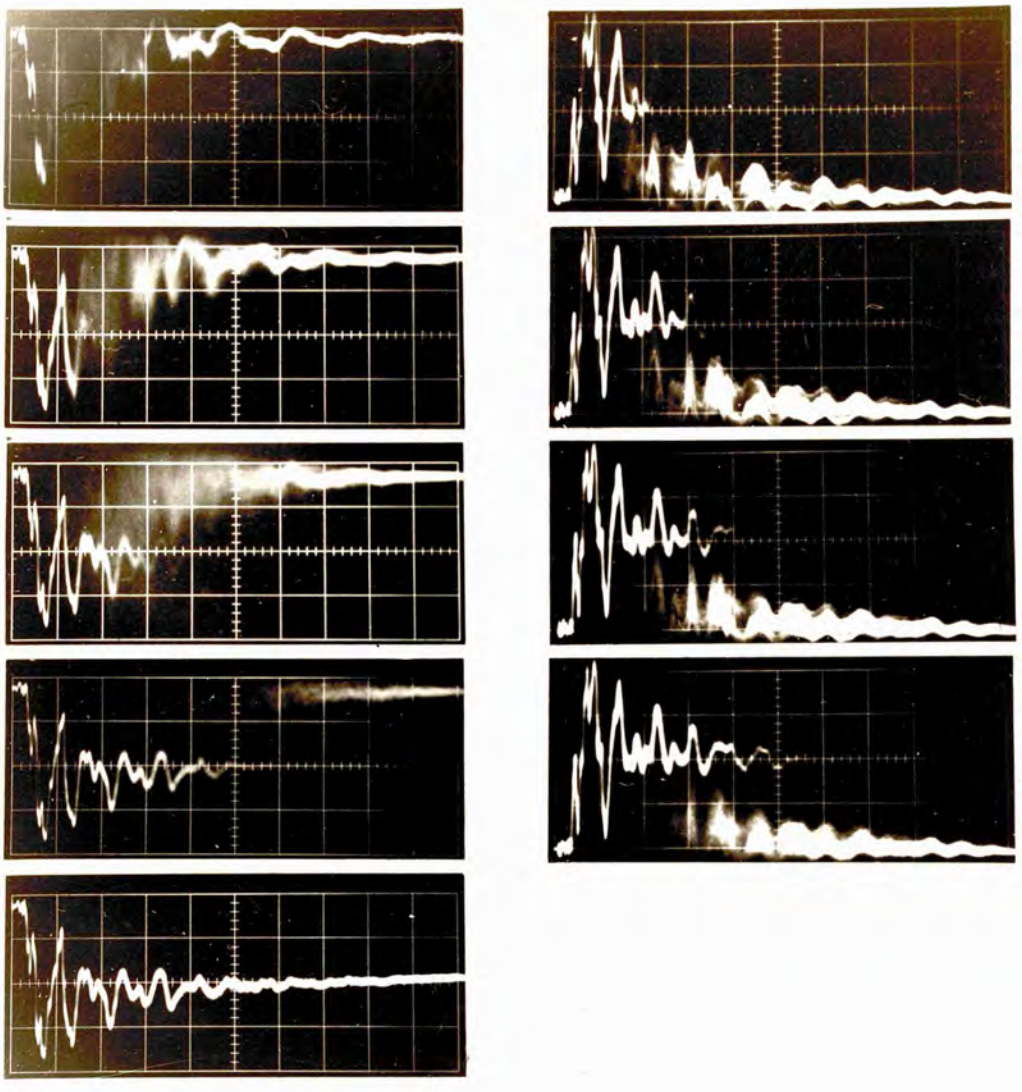

a) b)

FIG. 5.3.2

Arrested pulse shapes corresponding to the discharges of Fig. 5.3.1 a) and b) respectively (200ns/div, 5KV/div).

(Fig. 5.3.1a) a clearing field 90V/20cm existed, and successive discharges were separated by 60 second intervals. With a positive point, remnant ionization had to be relied upon for initiation; no clearing field was applied, and in Fig. 5.3.1b) successive discharges were separated by about 0.2 seconds. A significant drift may be noticed, especially in the positive point photographs.

Plausible qualitative interpretations are easier in the case of the negative point. Field emission electrons emerging from the wire tip are likely to create Townsend avalanches during the initial oscillating peak; during the initial trough the electrons have insufficient energy to ionize but they drift forward; during the second peak the electrons again acquire enough energy to ionize and hence produce the second bright region, and so on.

The case of the positive point is more difficult; although triggering depended on remnant ions being present in the gap, the delay of 0.2 seconds between each of the 15 discharges should have prevented a stationary equilibrium pattern of ions being set up and governing the second and later stages. The bright patches develop successively from the point against the electron flow and hence a photoionization mechanism must be active. A streamer mechanism cannot, however, be suggested, because of the extraordinary

regularity of the patterns is unlike the random fluctuations observed in the length of the individual streamers (Rice-Evans 1974, Nasser 1971, Loeb 1965).

Quantitative results were not possible as the field in the gap was not known, nor was it open to calculation. The difficulty here lay in the fact that, although some point-to-plane configurations are amenable to field calculation, (cf. Chapter 1, Section 1.4.1), the geometry used in the present case consisted of a sharply terminated stressed electrode which rules out any possibility of a theoretical treatment. Even in the case of a point-to-plane with a hemispherical cap on the point, the field can only be calculated for one ratio of gap distance to point radius at a time, and only along its axial component (Dodd 1950).

The hemispherically capped point geometry was considered because of the possibility of obtaining electric field values in the gap. However, after some trials it had to be abandoned because it was impossible to trigger the discharge at will as was necessary, and work was continued with the thin gold-plated tungsten wire as the point. This permitted complete control of the triggering, although of course the field in the gap was not known. The results presented in this chapter have already been published (Rice-Evans and Franco 1977).

CHAPTER 6

Microdensitometer Studies

6.1 Introduction

The microdensitometer measures the photographic density of photographic films, plates and other transparencies. This photographic density is, in the present studies, related to the light emitted by the discharge which is recorded on film. Over a limited range of light intensity the film responds linearly to this intensity and by using a calibration step-wedge the microdensitometer reading can be used to give directly a measure of the relative light intensity.

The columnar discharges studied in Chapter 5 were analysed with the microdensitometer to obtain some kind of information on the light emitted by the discharge under different pulse arresting conditions. Visually, it appeared that once chopping of the discharge was initiated, the luminosity of the discharge increased. It was thus felt useful to decide accurately whether there was any variation in light emission when the discharge was arrested at several distances from its initiating electrode.

This was carried out at both polarities for the columnar discharge and some of the ringed Lichtenberg figures were also analysed in this way.

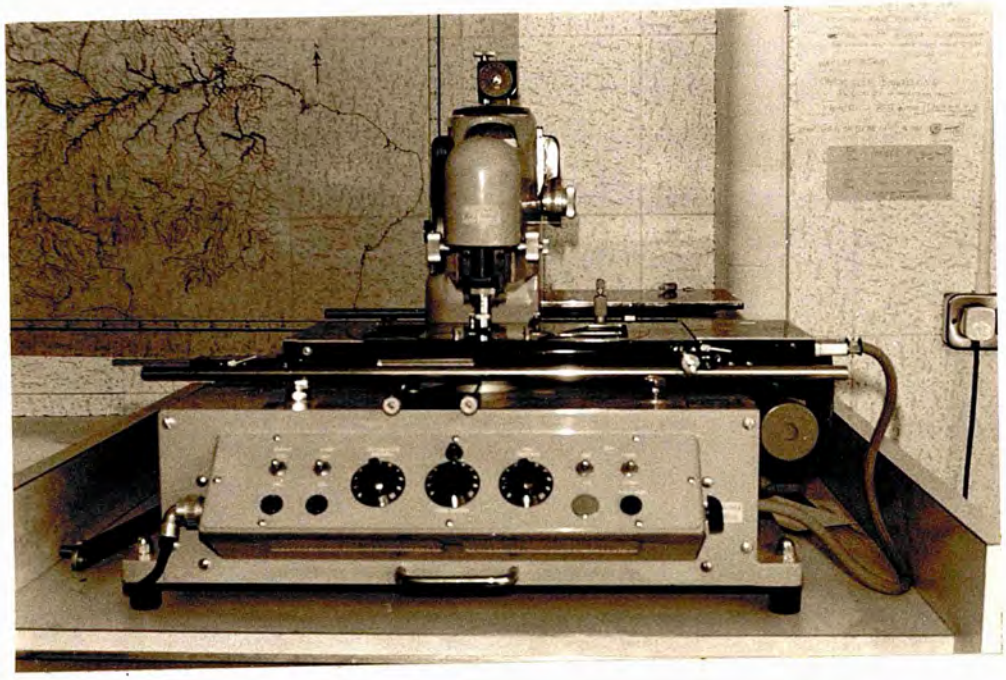

FIG. 6.2.1

The Microdensitometer.

6.2 The Microdensitometer

The microdensitometer used was a Joyce-Loebl automatic recording MKIII C model (Fig. 6.2.1). The principle of operation of this instrument is based on a true double beam light system, in which two beams from a single light source are switched alternately to a single photomultiplier. If the two beams are of a different intensity, a signal is produced by the photomultiplier, which, after amplification, causes a servo motor to move an optical attenuator so as to reduce the intensity difference to zero. In this way a continuous null balancing is obtained, in which the position of an optical attenuator is made to record the density at any particular part of a specimen.

This principle is illustrated in Fig. 6.2.2 where A is the common light source, (B,C,D) indicate one light path and (F,G) the other; H is a synchronous motor with a shutter exposing each beam alternately, J is the plane of the specimen and K the optical wedge.

The position of the optical wedge to which a direct-writing pen is attached is controlled as follows: the signal from the photomultiplier E is fed to the amplifier M, the output of which is applied to the servo motor N. Servo stability and sensitivity control are achieved by applying a feed-back signal, derived from the tacho generator coupled to

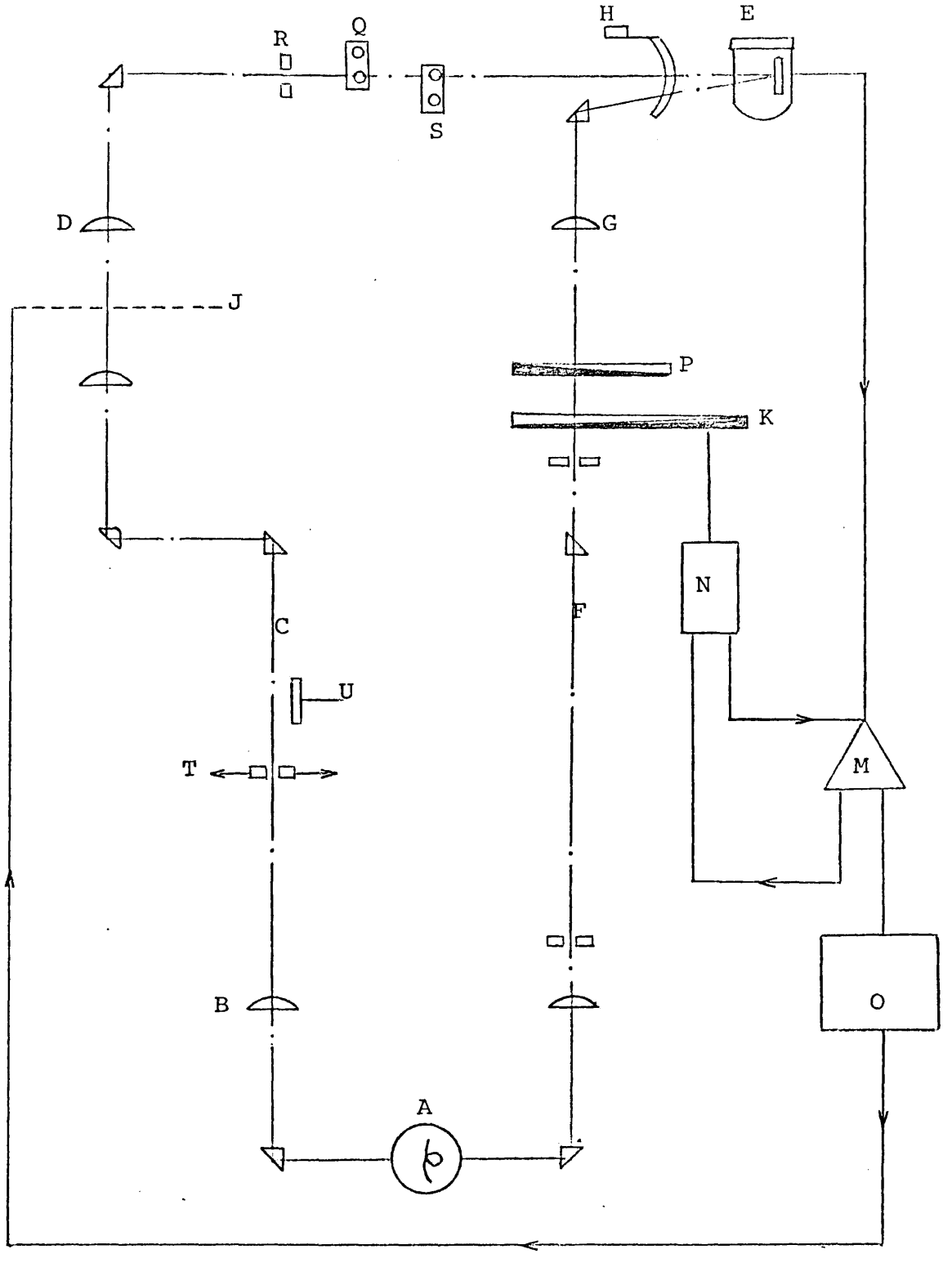

FIG. 6.2.2

Schematic diagram of optical and servo systems of micro-densitometer.

the servo motor N, to the amplifier.

The specimen and record tables are driven by another servo system O at a speed proportional to the rate of change of density. When the rate of change is small, the speed is at its maximum, and vice-versa.

The base line can be set by controlling the position of the optical attenuator and, therefore, the pen is controlled by a manually-operated wedge P in light path (F,G).

The major design features of the instrument are:

a) double beam system of operation

The instrument incorporates a true double beam system in which the two beams arise from a single light source and terminate in a single photoelectric receiver. This makes the instrument almost independent of its own parameters and complete reproducibility of record is possible within the range of densities specified.

b) direct record/specimentable linkage

The mechanical direct linkage between the specimen and record tables ensures complete synchronisation, irrespective of the ratio by which the record is expanded with respect to the specimen. This enables the instrument to be used for accurate measurements of distances

bewteen specimen details. The direct linkage also facilitates identification of specimen details provided a simple routine is followed.

c) direct density measurement

The instrument records density directly and linearly within the range of densities specified. The range of density is related to many other variables of the instrument.

d) visual location of specimen details

The image presented to the aperture is the magnified image. This not only enables a high degree of resolution to be achieved, but also provides a simple means for locating fine detail on the viewing screen. The aperture is continuously variable in both width and height up to a maximum of 3mm and 25mm respectively.

6.3 Microdensitometer Analysis of the Columnar Discharge

6.3.1 The Negative Point Discharge

In the following experiments a point-to-plane gap of 14cm was employed. As before, (Chapter 5), a gold-plated tungsten wire of 10μm diameter was employed as the point to aid triggering. The gas was the usual spark chamber gas, i.e. 70% neon 30% helium at a pressure of 39cmHg.

With the shunting spark gap to limit the discharge duration a series of photographs were obtained which were then subjected to photographic density measurements. This series of photographs consisted of increasing number of exposures superimposed on a single frame from two to just over forty, so that a comparison could be made regarding the increase in photographic density with the emitted light density, and in this manner verify whether a linear relationship applied between these two quantities.

A great deal of care was taken to ensure constant conditions during the photographing, developing and microdensitometer analysis of the film. Photographing was carried out in a completely light tight room with an open shutter camera. The discharges were counted for each exposure both visually and aurally. The method used here was to slowly increase the d.c. supply voltage (at a fixed gap length of the low voltage circuit) until discharge occurred, and then reduce it quickly. In this manner the frequency of the discharge was limited to one at a time, and could easily be counted for each exposure of the film.

As discussed in Chapter 4, over-voltaging of the low voltage circuit spark gap did not affect the pulse shape in any way as this was simply determined by the gap width and the R and C values of the passive devices used in the circuit.

Four films were obtained for the negative polarity point, one for each discharge arresting condition. The first film consisted of a series of photographs of increased number of exposures for the discharges arrested after the first peak of the oscillating pulse; the second film similarly recorded the discharge arrested after two peaks of the voltage pulse, and so on. Film four consisted of the unarrested discharge.

The four HP4 films were developed together at a constant temperature of 20^0 C, and the developer used was Ilford Microphen in a 1+1 dilution. The development time was 15 minutes. In this connection a photographic parameter, the γ of the film, is of importance.

Gamma (γ) is a sensitometric quantity derived from the characteristic curve of photographic emulsions. It is loosely interpreted as a measure of the contrast produced in a negative image, i.e. the ratio of negative contrast to original subject contrast for a given range of tone values. Such a comparison is based on the assumption that the brightness values of the subject tones can be accurately measured and that the corresponding negative densities fall within the straight line portion of the characteristic curve. γ is also often quoted as a yardstick for the degree of development especially when the film manufacturer recom-

mends development times for his material. In this sense it can be said that negatives developed to the same show comparable tone reproduction.

In technical terms γ stands for the slope of the straight line part of the characteristic curve. In the present case the height is the density and the base is the exposure. So γ = density/exposure. γ is important because it indicates how a photographic material will respond to a change in exposure. In a material with a low γ a small change of exposure will produce a small change in density, but the same small change of exposure with a high γ material will produce a much larger change in density.

The γ value of a photographic material is not fixed and can often be varied within wide limits by the method of development and the choice of developer. In general, γ is low for short times of development or if the temperature of the developer is low. As the time of development is increased, values rise until they reach an optimum value which is known as γ_{∞}. The plot of γ against time of development is known as a gamma-time curve; such curves are often plotted for a range of time development.

The type of developer used also affects γ. The highest values are obtained with very alkaline developers. Fine-grain developers will give low figures.

Information on the relationship between γ and development is generally stated in the manufacturers' descriptive literature, but where high accuracy is required such information should not be taken too literally. There may be variations between batches of the material, and the conditions of development, agitation etc. may not be the same.

Because of the above difficulties, the film used for the following experiments was taken from the same large 200ft reel of Mark 5 roll of HP4 Ilford film. This has a speed of 650ASA when developed in Ilford Microphen for 5.5 mins at 20°C giving a γ of 0.55. The speed of the film was increased further by developing for 15 mins at 20°C, the speed then becoming 1250ASA with a contrast gradient of 0.9.

The microdensitometer was calibrated by means of a step-wedge, although it was claimed by the manufacturer that its response should be linear. The calibration curve obtained is shown in Fig. 6.3.1.1. Within the values of photographic densities shown this was indeed highly linear. The plot was obtained by scanning the step-wedge at several points, each step consisting of an increase of 0.15 units and taking an average numerical reading from the microdensitometer. The density was then plotted on the Y axis against the microdensitometer reading on the X axis.

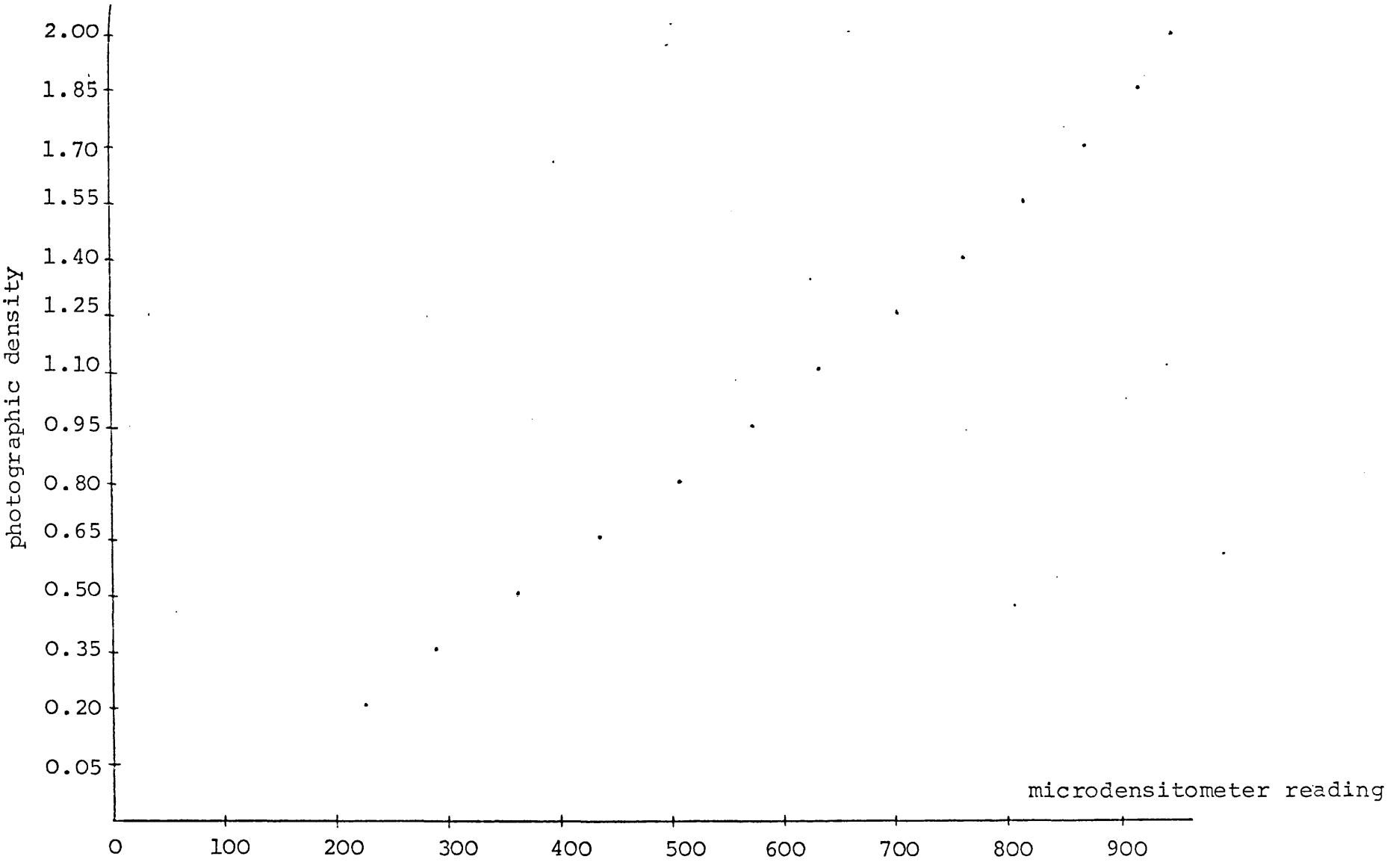

FIG. 6.3.1.1

The calibration curve for the microdensitometer.

After the calibration procedure the film was then analysed frame by frame. The image of the discharge could be aligned on the moving table of the microdensitometer by looking through a viewing screen which showed a projected image of the negative. Typical traces obtained are shown in Fig. 6.3.1.2. The four traces shown correspond to the four stages of arrest of the discharge.

The significant result is that once the discharge has created a bright region, its total light emission is virtually unaffected by its subsequent development towards the plane electrode. Only when the discharge reaches the electrode is there a significant rise in its total brightness. The peak to the left of the highest trace of Fig. 6.3.1.2. is due to the part of the discharge spreading over the dielectric surface of the plane electrode.

6.3.2 The Positive Point Discharge

Microdensitometer traces for the corresponding positive columnar discharge are shown in Fig. 6.3.2.1. These were obtained from four films taken at the same time as the films for the negative polarity. The procedure consisted simply of reversing the polarity of the d.c. supply voltage and photographing the positive discharge under exactly the same conditions as the negative discharge,

FIG. 6.3.1.2

Typical microdensitometer traces for the negative discharge. The four traces shown correspond to the four stages of arrest of the discharge.

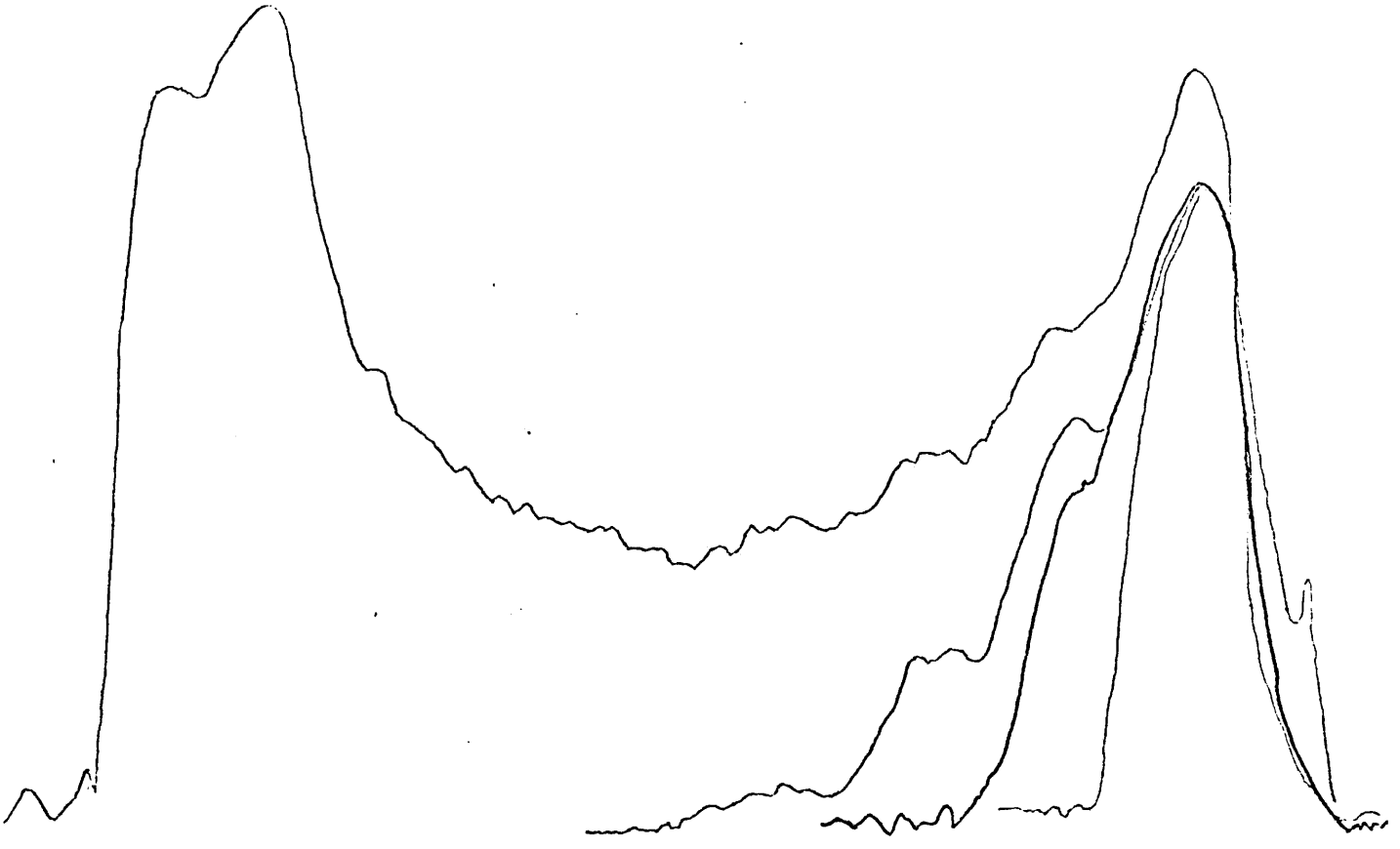

FIG. 6.3.2.1

Typical microdensitometer traces for the positive discharge. The four traces shown correspond to the four stages of arrest of the discharge.

except of course for the pulse sign. This allowed both kinds of discharges to be compared.

Again it is seen that for the first voltage peak (corresponding to the first bright patch of the discharge) there is no increase in brightness even after further development of the discharge into the gap takes place (traces 1, 2, 3). However, after the first dark space is reached this no longer applies and the brightness increases with extended development of the discharge.

The behaviour of the unaffected part of the discharge can best be shown by plotting a graph of photographic density of a fixed point on the first bright region against the number of exposures taken for each case. The point chosen was the peak of the discharge and the graphs obtained for both the positive and negative polarities are shown in Figs. 6.3.2.2 and 6.3.2.3 respectively. These show that in either case the brightness is independent of the subsequent development of the discharge into the gap, except when the discharge reaches the plane electrode for the negative case and the first dark space for the positive case. At the plane an increase in brightness is noted in both cases.

In the positive case the result obtained cannot be explained

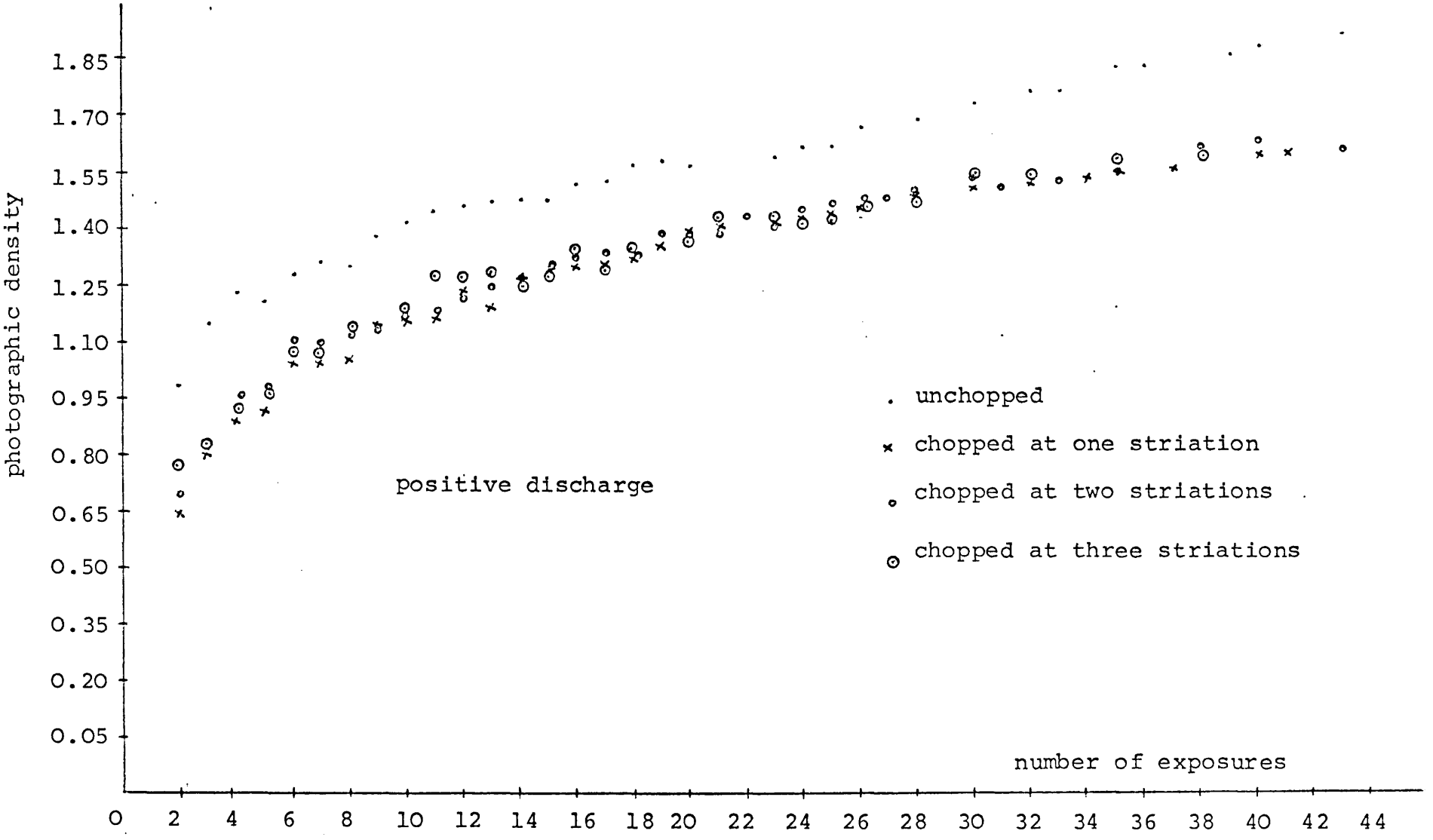

FIG. 6.3.2.2

Photographic density variation of peak for four stages of arrest of the discharge.

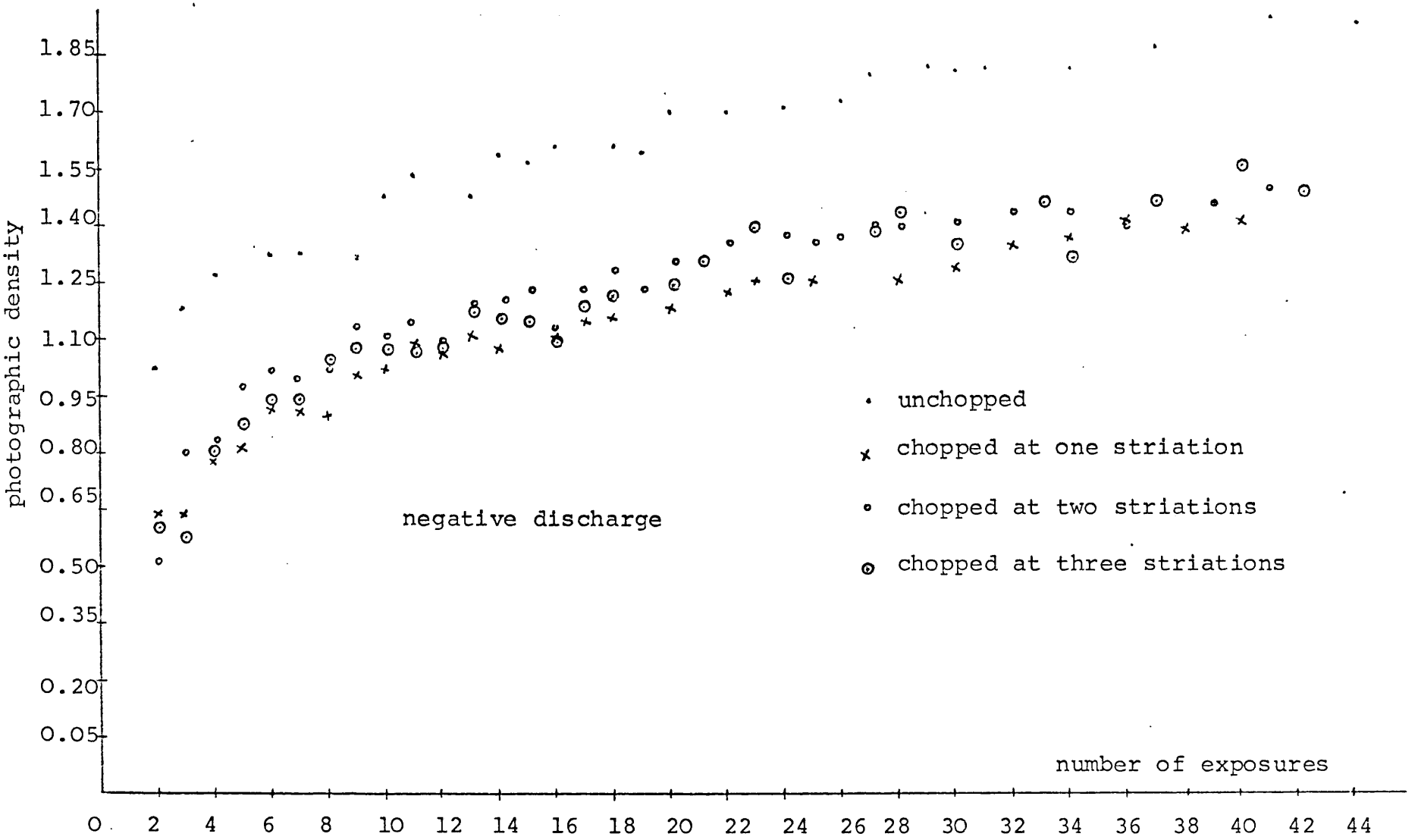

FIG. 6.3.2.3

Photographic density variation of peak for four stages of arrest of the discharge.

by a streamer theory picture. This would require that as avalanches converge into the developing streamer tip the electrons would move up the forming channel and produce 'waves' of ionization which would increase the recorded brightness of the discharge. This appears to be so only up to the first dark space (counted from the point). However, after this it appears that the electrons, if they are indeed collected by the stressed positive electrode, no longer produce any excitation leading to subsequent increase in brightness of the discharge. This observation once again produces doubts about the streamer mechanism being active in the development of the discharge at least in part of its development.

CHAPTER 7

Photomultiplier Analysis of the Columnar Discharge

7.1 The Photomultiplier Arrangement

For these studies a 13-stage 56 AVP photomultiplier was used. The base employed with this photomultiplier is shown in Fig. 7.1.1.

The light from the discharge was focused onto a horizontal slit of 2mm width and 1mm height at the photomultiplier window by means of a 20cm focal length lens mounted on a light-tight cylindrical tube of appropriate length. The whole assembly was electrically screened to avoid any background noise pickup on the oscilloscope trace from the photomultiplier.

The photomultiplier could be moved vertically up and down and made to view the discharge at various points in the gap from the stressed electrode to the grounded electrode.

7.2 Analysis of the Positive and Negative Point Discharges

For these observations a gap of 12.5cm was used with the gas at a pressure of 39cmHg. The discharge was viewed at alternately bright and dark regions from the point electrode towards the plane electrode (Fig. 7.2.1). The

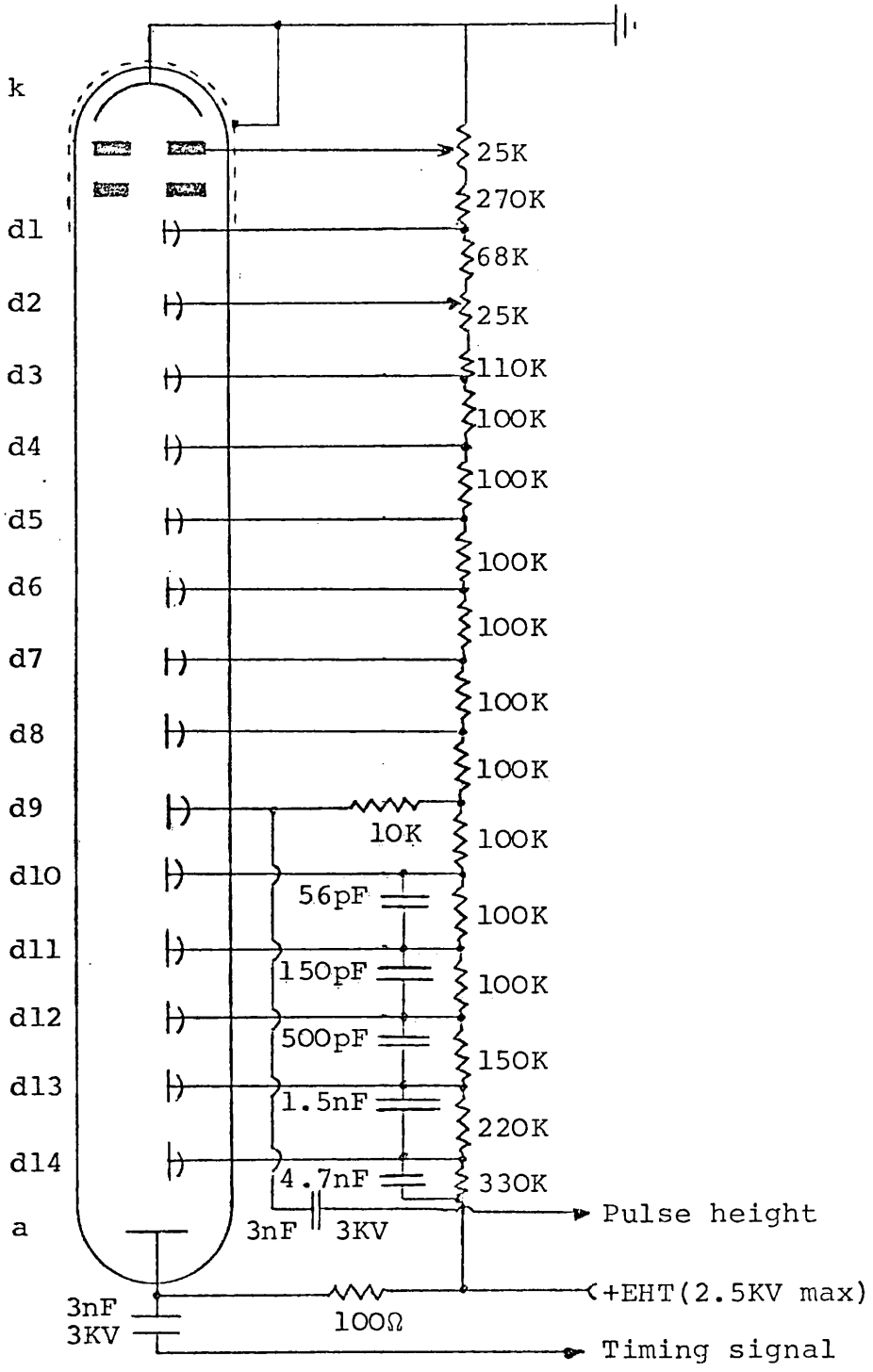

FIG. 7.1.1

The 56 AVP photomultiplier base.

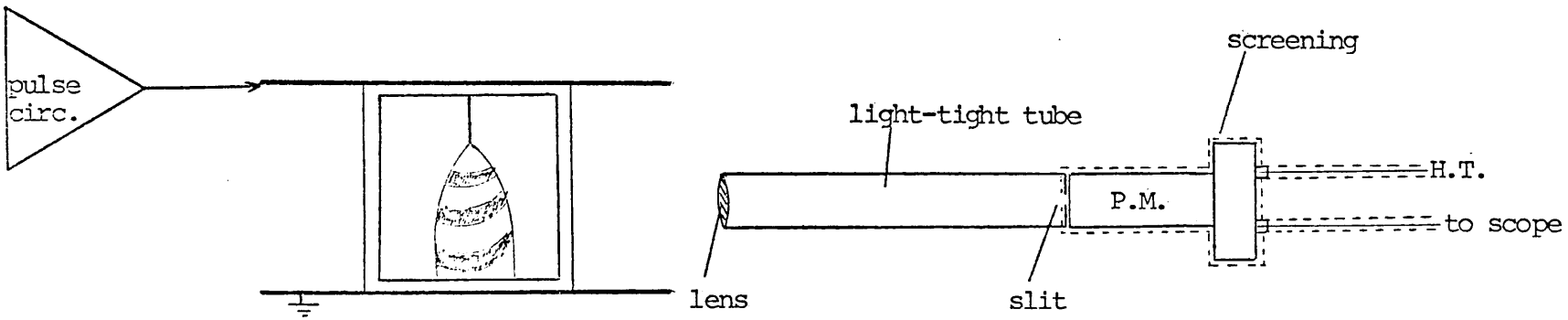

FIG. 7.2.1

The experimental arrangement for the photomultiplier studies.

discharge viewed was the complete (unchopped) discharge and at each bright patch the trace recorded was that which showed the largest pulse; this corresponded approximately to the centre of the bright region. This was easily achieved by moving the photomultiplier up and down over the region and simultaneously observing the size of the pulse on the oscilloscope.

For each polarity the light output at the tip of the point electrode was also recorded and is shown as the first photomultiplier trace (a) in Fig. 7.2.2. The figure shows the voltage pulses applied to the discharge chamber and the corresponding photomultiplier pulses at successively bright and dark regions from the point electrode. After dark space (5) only the pulses from the next three bright regions were recorded. The change of polarity of the stressed electrode was simply effected by a change in polarity of the voltage supply generator to the external circuit, all else remaining fixed for the observation of the discharges at both signs of voltage.

In all the oscilloscope photographs of the photomultiplier pulses the initial high voltage pulse triggered the trace. Each sequence corresponds to about 20 successive sweeps at the same distance from the point electrode. The uniformity in behaviour of successive discharges is remarkable. In

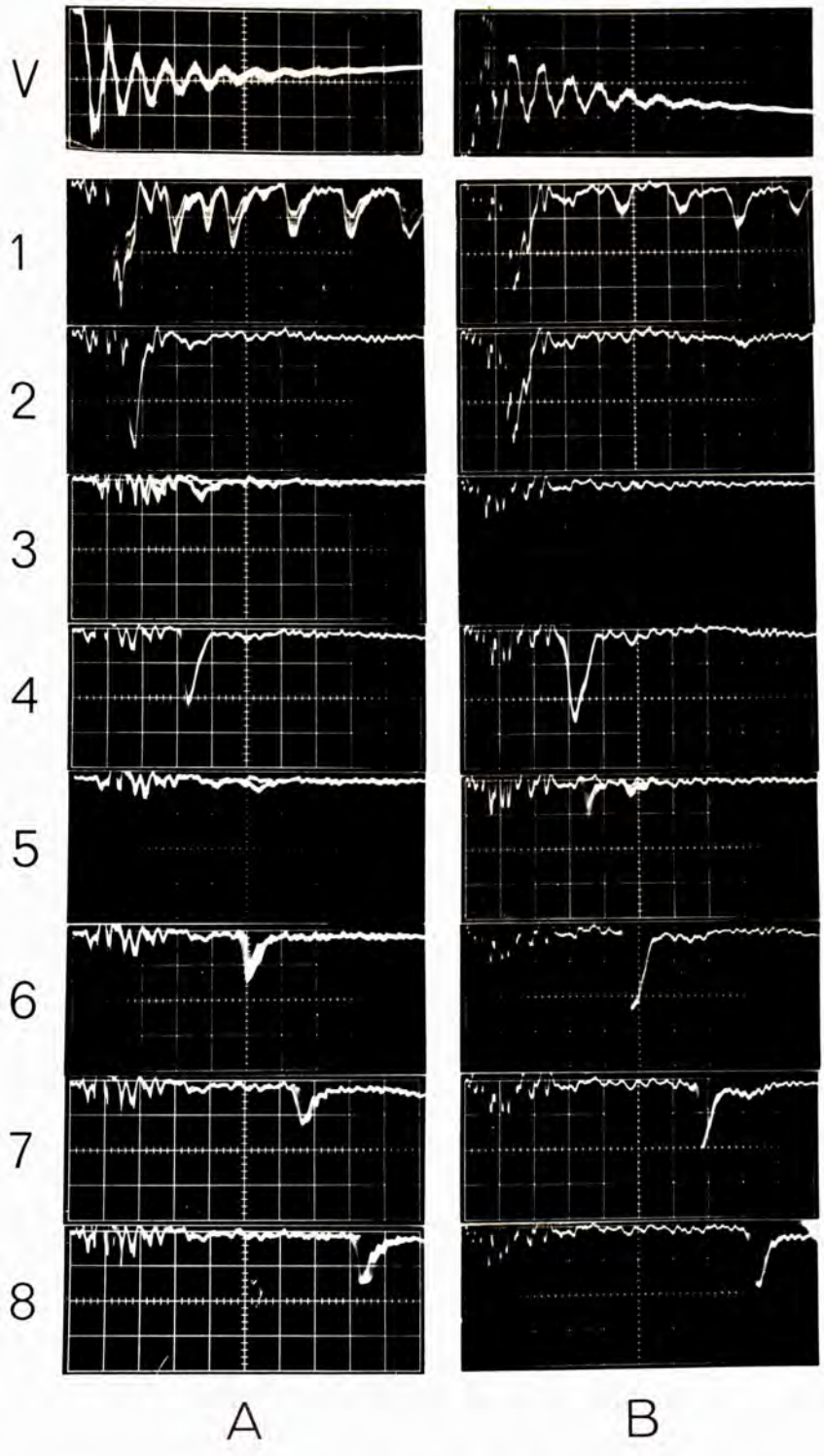

FIG. 7.2.2

The voltage pulses (V) (200ns/div, 5KV/div) and corresponding photomultiplier traces for the columnar discharge (100ns/div, 10V/div). (A)negative, (B) positive.

each case the pulse is seen to grow smaller and progress with time to the right of the initial pulse. It can also be seen that the light output from a luminous region is limited mainly to the period of creation of the region except at the tip of the gold-plated tungsten wire where light is emitted with each peak of the applied voltage pulse.

The previous chapters showed that the discharge developed from the stressed electrode into the gap and that each bright patch corresponded to a peak of the short duration oscillatory pulse. The photomultiplier results show that each luminous region is created independently of previous bright regions and that the intensity of the bright region decreases as the large electrode is approached for both cases of voltage polarity.

For the voltage pulses shown in Fig. 7.2.2 the typical rise times of the negative discharge photomultiplier pulses for the second bright region were of the order of 20nsec decaying in about 60nsec. The positive point discharge showed photomultiplier pulses of rise time of the order of 35nsec and decay time 50nsec. The appearance of the discharges scanned with the photomultiplier are shown in Fig. 7.2.3.

a) b)

FIG. 7.2.3

The columnar discharges analysed with the photomultiplier (p = 39cmHg).

a) negative polarity b) positive polarity

From the photographs obtained (Fig. 7.1.3) and the corresponding oscillographs (Fig. 7.2.2 V) The speeds of propagation of the discharge in the gap for both polarities was obtained. Table 7.2.1 shows these values. In both cases the discharge shows a small decrease in speed from its initial stage, but after that the speed remains constant across the gap.

Table 7.2.1

The Speeds of formation of the Striated Discharge for each Polarity.

Discharge Stage	Negative Point	Positive Point
1st striation	.8 X 10^7cm/s	.6 X 10^7cm/s
2nd striation	.7 X 10^7cm/s	.5 X 10^7cm/s
3rd striation	.6 X 10^7cm/s	.5 X 10^7cm/s
4th striation	.6 X 10^7cm/s	.5 X 10^7cm/s
5th striation	.6 X 10^7cm/s	.5 X 10^7cm/s

For each polarity the distance from the point to the centre of successive dark spaces (corresponding with the pulse troughs) was measured and was then divided (after scaling to actual size) by the corresponding time of voltage application taken from the oscillograph.

As has been discussed (Chapter 5) the field in the gap was not known and correlation of speeds with field amplitude could not be carried out. However, the results are unexpected as the field must certainly decrease from the highly stressed point electrode to the plane, and assuming constant mobility the velocities should also follow this pattern. A plausible explanation would be that the space charge field of the advancing discharge front compensates exactly for the decrease in the applied field in the gap. In this way the decrease in field strength due to the geometrical arrangement would be compensated by the increased space charge field due to increasing ionization charges.

CHAPTER 8

CONCLUSION

The ringed Lichtenberg figures formed at the extremities of a cosmic ray track in the streamer chamber were shown to be due to the oscillations superimposed on the short duration voltage pulse applied to the chamber.

The characteristic 'interference' dark region separating two simultaneously produced figures was used as a basis of a method for measuring the speed of formation of the figures without the actual knowledge of the voltage pulse shape.

It was found that a track-simulating wire placed centrally in the chamber could give rise to the same ringed patterns centred at its extremities. This fact allowed triggering of the chamber to be achieved without the need to wait for a cosmic ray particle to start the discharge. It also permitted the use of the lower voltages and the observation of the voltage pulse on the oscilloscope. A correlation between the voltage pulse and the figure appearance could thus be carried out.

The speeds of formation of the figures at the lower voltages were also measured and they were shown to vary in a linear manner with the applied voltage. The values obtained for these speeds of formation were of the same order of magnitude as those attributed to streamers at similar voltages(Nasser 1971).

The high speeds of formation measured and the characteristic branching observed in the radial channels making up the figures suggest a streamer mechanism must be active in their formation. However, the appearance of the superimposed dark and bright rings could not be reconciled with such a mechanism.

Recent experiments by Brzosko et al (1975, 1976) also put in question the mechanism of streamer formation for a 'creep discharge' at the surface of a dielectric. They studied the flash energy spectra by photon measurements using a photomultiplier technique. The pictures obtained by them for the flashes using a photographic method revealed 'star-like patterns of peculiar design' and different arm (channel) length. These are Lichtenberg figures. The main objective of their 1976 paper was to find relations between the structure of the sample dielectric material and the light characteristics of the surface discharges. They found that the dielectric strongly affected the discharge phenomena.

The important results of their work were the observation of two different discharge phenomena: a) low energy high-intensity "spark" localised around the electrodes, b) high-energy but usually low intensity "sparks" radially distributed around the electrodes in 1cm long channels. They also observed that a) the flash energy was proportional to the channel length b) electric fields 300V above the inception voltage induced a flash energy of about 5MeV, and the channels were 5-10mm long, c) the high energy flashes appeared rapidly in a limited number of channels (about 30) radially distributed about the

electrodes, d) the upper limit of the number of photons emitted in one flash was estimated as about 3×10^6.

They point out that these observations indicate that the streamer mechanism should be rejected, since only 3×10^6 electrons are produced in one discharge. Streamers occur when the number of primary electrons is high enough, usually about 10^8 or more.

The new model advanced by them for high energy discharges assumes that time-dependent external electric fields produce positive and negative poles alternatively (at a distance of 10^{-5}cm) which produce internal electric fields sufficient to give breakdown in air. They consider the distortion of the surface structure of a dielectric as well as crystal dislocations or electric domains to be the sources of the charge poles.

To verify whether the dielectric did indeed play any important role in the formation of the rings the wire inside the chamber was shortened. If the rings observed were associated with any effect caused by the dielectric this new geometry should affect the observed pattern. Quite remarkably the dark rings became dark spaces in the column. No discontinuity was observed in this passage from the surface to the gas volume. The use of a moveable point electrode showed that the rings could be continuously drawn in and up the gas volume as the electrode was moved away from the plane dielectric surface.

The model proposed by Brzosko might be applied to the work

on the ringed Lichtenberg figure on the surface of the dielectric but it cannot be extended to the case of the columnar discharge. It was shown that the dielectric did not play a role in the formation of the rings, and so an explanation based on dielectric properties cannot be suitable.

The ringed Lichtenberg figures were also observed in air, this gas being, in contrastrast with He/Ne, an electronegative gas. The presence of negative ions which are responsible for many effects in discharge phenomena did not affect the present discharge characteristics.

The dark and bright regions of the columnar discharge showed a similar regular appearance to the d.c. glow discharge striations but in contrast with that d.c. equilibrium they they resulted from single field pulses.

They were shown to develop simultaneously with the branches which propagate the plasma channels. This is unlike the way in which d.c. glow discharge striations are believed to be formed. All the theories of these d.c. striations so far put forward start with the assumption that a gas where striatins occur is ionized into a plasma before some sort of instability triggers the oscillations responsible for the striations. The most recent of these theories also takes into account the effect of the large number of neutral particles inevitably present in the volume of the plasma at the usual laboratory temperatures (Pekarek 1961).

The columnar discharges of both polarities studied in chapter 5 and analysed by photomultiplier in chapter 7 propagate into the gap towards the plane electrode with an almost constant speed of about $\cdot 6 \times 10^7$ cm/sec for the negative discharge and $\cdot 5 \times 10^7$ cm/sec for the positive case for an applied voltage pulse of peak magnitude 18KV. These values are smaller than those for the discharge on the surface of the dielectric and the behaviour of the discharge is not similar to that of streamers. The negative 'feathers'of Nasser(1971) showed a large increase in velocity as they approached the anode unlike the almost constant speeds observed for the negative dischage. On the other hand his positive impulse streamers (1968 Nasser) showed a decrease in speed as the plane cathode was approached,whereas the positive discharges studied show an almost constant speed of propagation.

The analysis of the discharge with the microdensitometer also showed that,especially for the negative polarity discharges, once the discharge has created a bright region its total light emission is virtually unaffected by its subsequent development towards the plane electrode. The same is also true for the positive dischage, but only up to the first dark region,subsequent growth of the discharge giving rise to an increase in light intensity of the striations previously formed. This is true for all stages of arrest, but not for the unarrested discharge where a considerable increase in luminosity is apparent from the microdensitometer traces. That is, once the discharge

reaches the plane electrode, the whole channel brightness is increased.

Experience showed that the use of the shunting gap to arrest the discharges was not as satisfactory as had been expected. The fluctuations in the effective discharge times resulted in uncertainties in the microdensitometer measurements and hence their quantitative interpretation. This led to the use of a photomultiplier technique.

The photomultiplier analysis of the discharge showed the remarkable uniformity in behaviour of successive discharges as each C.R.O. trace recorded corresponded to 20 or so successive sweeps at the same distance from the point electrode. This kind of behaviour is very unlike that of streamers which show large statistical variations in light emission and range. The sharp boundaries shown by the rings and striations are also a demonstration of this consistent behaviour of the discharges studied. The luminous regions of the columnar discharge were shown to develop successively from the point electrode and independently of previously created bright regions. It was also shown that the light output from a luminous region is limited mainly to the period of creation of the region except at the tip of the point electrode where light is emitted with each peak of the applied voltage pulse.This is also in contrast with observations on the d.c. discharge striations where the

light is emitted with each peak of the voltage fluctuations (Donahue and Dieke 1951).

The light intensity of regions further away from the point electrode diminished. The photomultiplier traces show that the emission occurs mainly at the edge of the expanding plasma.

In conclusion, this work has shown that discharge plasmas can expand by mechanisms other than conventional avalanches and streamers. The origin of the dark spaces remains unsolved and must await for further study.

ACKNOWLEDGEMENTS

I wish to express my sincere appreciation to my supervisor Dr. P. Rice-Evans for the guidance and help extended by him during the course of this research.

I wish to thank Prof. E.R. Dobbs for his support and Dr. I.A. Hassairi for his help during the early stages of this work.

I should also like to thank Prof. C. Grey-Morgan for his useful comments on this work.

I should also like to thank Messrs. W.A.G. Baldock, F.A. Grimes, A.K. Betts, A. LeMotte, B. Pashley and A. King for their technical assistance.

I am grateful to Bedford College for the financial help extended to me which enabled me to complete this work.

Finally, I must thank my wife Linda for her patience and encouragement, and for typing this manuscript.

References

Abou-Seada, M.S., Ph.D.Thesis, Iowa State Univ. (1970)
Digital Computer Calculation of Corona Thresholds in Non-Uniform Fields

Allen, K.R., Phillips, K., Proc. Roy. Soc. (London) 278 A, 188, (1964)

Ann.Rep. on the Conf. of Elect.Inst.& Diel.Phenomena
National Academy of Sciences, Washington D.C. (1972)

Anstey, F.B., Ph.D.Thesis, Univ.Lond.(Imp.Coll.)(1947)
A Study of the Lichtenberg Figures and an Experimental and Mathematical Investigation of the Surge Generator Used Therein

Armstrong, E.B., Emeleus K.G., Proc.Roy.Irish Acad.A54, 291, (1951)

Bailey, R.A., Emeleus K.G., Proc.Roy.Irish Acad.A57, 53 (1955)

Barnes, B.T., Eros S., J.App.Phys.L1,1275, (1950)

Barnes, B.T., Phys.Rev. 86, No.3, 351, (1952)

Bohm, D., Gross, E.P., Phys.Rev.75, No.12, 1851, (1949)

Boyd, R.L.F., Twiddy, N.D., Nature Lond.173, 633, (1954)

Boyers, D.G., Tiller, W.A., J.App.Phys.44, No.7, 3102 (1973)

Brown, S.C., Introduction to Electrical Discharges in Gases, Wiley, New York, (1966)

Brzosko, J.S. et al, J.Phys.D:App.Phys.V.8, L187 (1975)

Brzosko, J.S. et al, J.Phys.D:App.Phys.V.9, 2369 (1976)

Brzosko, J.S. et al, J.Phys.D:App.Phys.V.10,1583 (1977)

Brzosko, J.S. et al, J.Phys.D:App.Phys.V.10,L155 (1977)

Bulos, F., Odian, A., et al, SLAC Report 74 (1967)

Chanin, L.M., Rork, G.D., Phys.Rev.132, 2547 (1963)

Chapman, S., Cowling, T.G., The Mathematical Theory of Non-Uniform Gases, Cambridge Univ.Press.(1970)

Colli, L. et al, J.App.Phys.25, No.4, 429 (1954)

Cragg, J.D., Meek, J.M., High Voltage Laboratory Technique, London Butterworth Scientific Publications (1954)

Crandall, J.L., Cooper, A.W., Proc.8th Intern.Conf.Phen. Ionized Gases, Springer, Vienna (1967)

Cross, J.D., Srivastava, K.D., App.Phys.Letts.21 No.11, 549 (1972)

Cross, J.D., Sudarshan, T.S., IEEE Transactions on Electrical Insulation V.El - 11, No.2, 63, (1976)

Davidenko, V.A., Dolgoshein, B.A., et al, Soviet Physics GETP 28, 227 (1969)

Davidenko, V.A., Dolgoshein, B.A., et al, Nucl.Phys.75 277 (1969)

Davidenko, V.A., Dogolshein B.A., et al, Soviet Phys.GETP 28, 223, (1969)

Dodd, E.E., Phys.Rev.78, 620L, (1950)

Donahue, T., Dieke, G.H., Phys.Rev.81, 248 (1951)

Druyvesteyn, M., Z.Physik, 73, 33, (1931)

Druyvesteyn, M., Penning F.N.Rev.Mod.Phys.12 102 (1940)

Engel, von, A., Steenbeck, M., Elektrische Gasentladungen, J.Springer, Berling, (1932) V.1

Engel, von, A., Ionized Gases, Oxford Clarendon Press (1955)

Flugge, S., Encycl. of Physics, Springer-Verlag (1956) V.22.

Francis, G., Encycl. of Physics, Springer-Verlag (1956) V.22

Fowler, R.G., Encycl. of Physics, Springer-Verlag (1956)V22

Gabor, D. et al, Nature 176, 916, (1955)

Gabor, D., Brit.J.App.Phys. 2, 209, (1951)

Gallimberti, I., J.Phys.D:App.Phys.5,2179 (1972)

Gill, E.W.B., Phil.Mag.8, 955 (1929)

Goldstein, (1881), cf. Ref.Flugge (1956)

Hasikuni, M., J.of Sci.of the Hiroshima Univ.SER A, 17, No.1, 129, (1953)

Hassairi, I.A., Ph.D.Thesis, Univ.London (1976)
Cosmic Ray Studies with a Streamer Chamber

Hermstein, W., Arch.Elektrotech. 45, 214 (1960)

Hinazumi, H., et al, J.Phys.D:App.Phys. 6, L21 (1973)

Holst, G., Oosterhuis, E., Physica, Haag 1, 78 (1921)

Holst, G., Oosterhuis, E., Phil.Mag. 46, 1117 (1923)

Ieda, M., Sawa, G., et al, IEE Conference Dielectric
Materials Measurements and Applications (1969)

Indraneel, S., Prabhashanker, V., J.Phys.D:App.Phys. 9,
987 (1976)

Kornfeld, M.I., Sov.Phys.Sol.State 17, No.3, 596 (1975)

Kuffel, E., Bera, M.M., Proc.8th Int.Conf.on Phenomena
on Ionized Gases P.191 (1967)

Kuffel, E., Abdullah, M., High Voltage Engineering
Pergamon Press (1970)

Lavoie, L., Parker, S., et al, Rev.Sci.Inst. 35, No.11,
1567 (1964)

Lichtenberg, G.C., Novi.Comment.Gött.8, 168 (1777)

Linder, E.G., Phys.Rev. 49, 753 (1936)

Loeb, L.B., Phys.Rev. 86, 256 (1952)

Loeb, L.B., Phys.Rev. 74, No.2, 210 (1948)

Loeb, L.B., J.App.Phys. 19, 882 (1948)

Loeb, L.B., Dodd, E.E., et al, Rev.Sci.Inst. 21, No.1, 42 (1950)

Loeb, L.B., Leigh, W., Phys.Rev. 51, 149A (1937)

Loeb, L.B., Kip, A.F., J.App.Phys. 10, 142 (1939)

Loeb, L.B., Basic Processes of Gaseous Electronics, Univ. of Calif. Press (1955)

Loeb, L.B., Electrical Coronas, Their Basic Physical Mechanisms, Univ. Calif.Press, Berkeley (1965)

Loh, H.Y., Dieke, G.H., J.Opt.Soc.Americ. 37, 837 (1947)

Lozanskii, E.D., Firsov, O.B., Sov.Phys. GETB, 29, 367, 1567 (1969)

Margenau, H., Phys.Rev. 73, No.4, 326 (1948)

Margenau, H., Phys.Rev. 73, No.4, 297,(1948)

Margenau, H., Phys.Rev. 73, No.4, 309 (1948)

Meek, J.M., Craggs, J.D., Electrical Breakdown of Gases Clarendon Press, Oxford (1953)

Meek, J.M., Craggs, J.D., Electrical Breakdown of Gases Wiley Interscience (1978)

Meek, J.M., Phys.Rev. 57, 722 (1940)

Merril, F.H., Hippel, von, A., J.App.Phys. 10, 873 (1939)

Merril, J.H., Webb, W.H., Phys.Rev. 55, 1191 (1939)

Mishra, S.R., Ph.D.Thesis, Univ.London, Bed.Coll. (1969)

Mitra, S.K., Syam, P., Phil.Mag. 14, 616 (1932)

Morgan, C.G-, Handbook of Vacuum Physics A.H.W. ed. V.2 (1965)

Morgan, G.D., Nature 172, 542 (1953)

Moussiegt, J., Ann.Phys.Paris 4, 593 (1949)

Nasser, E., Arch. Elektrotechn. 44, 157, 168 (1959)

Nasser, E., Loeb, L.B., J.App.Phys. 34, 3340 (1963)

Nasser, E., J.App.Phys. 37, No. 13, 4712 (1966)

Nasser, E., Fundamentals of Gaseous Ionization and Plasma Electronics, Wiley Interscience (1971)

Nasser, E., Heiszler, M., J.App.Phys. 45, No.8, (1974)

Olsen, H.N., Huxford, W.S., Phys.Rev. 87, 922 (1952)

Papoular, R., Electrical Phenomena in Gases, London Iliffe Books Ltd. (1965)

Pardue, L.A., Webb, J.S., Phys.Rev. 32, 946, (1928)

Pekarek, L., Krejci, V., Czech J.Phys. B11, 729 (1961)

Penning, F.M., Electrical Discharges in Gases, Cleaver-Hume Press Ltd., (1957)

Petropoulos, G.M., Phys.Rev. 78, No.3, 250 (1950)

Phelps, C.T., Griffiths, R.F., J.App.Phys. 47, No.7, 2929 (1976)

Pierce, J.R., J.App.Phys. 19, 231 (1948)

Raether, H., Z.Phys. 107, 91 (1937)

Raether, H., Electron Avalanches and Breakdown in Gases Butterworths, London (1964)

Rees, J.A., Electrical Breakdown in Gases, The Macmillan Press Ltd., (1973)

Rice-Evans, P., Mishra, S.R., Nucl.Inst.Meth. 67, 337 (1969)

Rice-Evans, P., Mishra, S.R., J.Phys. E4, 638 (1971)

Rice-Evans, P., Hassairi, I.A., Phys.Letts. 38A, 196 (1972)

Rice-Evans, P., Hassairi, I.A., Nucl.Inst.Meth. 106, 345 (1973)

Rice-Evans, P., Hassairi, I.A., Betts, A.K., Nucl.Inst. Meth, 130, 571 (1975)

Rice-Evans, P., Spark Streamer Proportional and Drift Chambers The Richelieu Press, London (1974)

Rice-Evans, P., Franco, I.J.A., Phys.Letts. 63A, No.3, 291 (1977)

Rogowski, W., Archiv. fur Elektrotechnik 20, 99 (1928)

Rudenko, N.S., Smetanin, V.I., Sov.Phys. GETB, 34, 76 (1972)

Rudenko, N.S., Smetanin, V.I., Sov.Phys. GETB, 36, No. 2, 260 (1973)

Salama, M.M.A., et al, J.App.Phys. 47, No.7, 2915 (1976)

Subertova, S., Czech.J.Phys.B15, 701 (1965)

Thomas, C.H., Duffendach, O.S., Phys.Rev. 35, 72 (1930)

Thomson, J.J., Thomson, G.P., Conduction of Electricity through Gases, Cambridge 3rd Edn. Vol.1 (1928)

Thomson, J.J., Thomson, G.P., Conduction of Electricity through Gases, Cambridge 3rd Edn. Vol.2 (1933)

Tonks, L., Langmuir, I., Phys.Rev. 33, 195 (1929)

Townsend, J.S., Theory of Ionization of Gases by Collision, London Constable (1910)

Townsend, J.S., Electricity in Gases, Oxford, Clarendon Press (1915)

Wagner, K.H., Z.Physic. 186, 466 (1966)

Warren, R., Phys.Rev. 98, 1650, 1658 (1955)

Wilson, O.B., J.Acoustical Soc. Americ. 39, No.6, 1260 (1966)

Wilson, A., Ph.D.Thesis, Strathclyde Univ.(1971) Discharge Breakdown of Solid Dielectrics under Impulse Voltage